Dear Editor,

We were glad to read the positive reviews and the interest shown in our research, and we are grateful for the timely and useful reviews provided. Please find below the detailed response (blue font) to all comments made by the reviewers, in accordance to our responses in the interactive discussion.

Following the comments made by the reviewers we rewrote some segments of the text as shown in the two "track changes" texts below (one for the main text and the other for the supplementary) and detailed here.

The manuscript and supplementary files were uploaded separately in their revised form.

Sincerely,

Moshe Armon, on behalf of all authors.

Anonymous Referee #1

General comments and manuscript summary: In the submitted manuscript, the authors use 24 years of historical radar data to identify historical heavy precipitation events (HPEs) in Israel, based on various threshold criteria. These 41 HPEs are then re-simulated using the WRF model at convection-permitting resolution (1 km grid spacing). Following this, the manuscript is primarily focused on evaluating how realistically the WRF model simulates the precipitation of the 41 HPEs, compared with what the radar shows. In addition to that, the radar data are used to identify common characteristics of HPEs in the study region.

The manuscript is primarily a model evaluation study of high-resolution WRF for eastern Mediterranean HPEs, with some accompanying radar-based climatological analysis. From the scientific/technical perspective, everything seems OK. My comments which follow in the next sections are thus of a technical and minor nature, and the main question I need to answer here as a reviewer is if the paper presents sufficiently “novel concepts, ideas, tools, or data” to justify publication in HESS?

We thank reviewer #1 for acknowledging our scientific and technical work. We hope that our answers and revisions, in part proposed by reviewer #1, result in an improved contribution that justify publication in HESS. The reviewer is highly appreciated for the time and efforts dedicated for improving our manuscript. The additional references suggested by the reviewer will (a) complete the literature review, and (b) further emphasise the advances we made relative to the existing literature. In the revised manuscript we will address the issues raised by the reviewer as detailed below.

The comments made by reviewer #1 helped us understand that we did not emphasise enough the uniqueness of the high-resolution characterisation itself, and we therefore explain it better in the revised manuscript (Lines 75-77). Long, high-resolution rainfall data records (24 yr) are truly scarce, and we therefore think that this characterisation is interesting even on its own. Currently, the characterisation is detailed in section 4.4. To validate the model, each one of the pattern-related parameters we have characterised was also checked using model simulations of the same events.

This manuscript is certainly not the first to evaluate if “the model description of rainfall during HPEs” in a convection-permitting model (CPM) is “credible”, despite the claims of the authors (L62). There is even a study investigating just that with WRF in the eastern Mediterranean (Zittis et al., 2017), which surprisingly wasn’t cited. For other studies asking similar questions in other regions see, for example, Berthou et al. (2018), Brisson et al. (2018), Chan et al. (2014), Chen et al. (2001), Hally et al. (2014), Kendon et al. (2012), Lean et al. (2008); many more CPM evaluation studies can be found – both event-based and climatological. This manuscript represents another contribution to this important topic. I think the publication of the manuscript can be justified on the following grounds: (1) the authors’ event-based approach incorporates an unusually high number of events, which is different to the most common approaches of either continuous multi-year simulations (e.g. Ban et al., 2014) or just a handful of events (e.g. Coppola et al., 2018); (2) the authors incorporate a nice range of temporal and spatial diagnostics which are (to my knowledge) not prevalent in the extant CPM-evaluation literature, presumably because of the rarity of such long radar archives (24 years) with high spatiotemporal resolution as used by the authors; (3) CPM evaluation studies for this region of the world are not well represented in the literature.

We much appreciate the reviewer's view about our contribution. It is true that we are not the first to answer this question ("Is the model description of rainfall during HPEs credible?" [Line 62]), and we have referred in the text to many of the previous studies of the topic, but, to the best of our knowledge, we are the first to systematically do it for all the available HPEs over a 24-year period. Furthermore, there is still much to contribute in this area (in our case, we address specifically **rainfall space-time patterns** during all the available **HPEs** during a period of 24 yr). We do understand that the wording we chose may be misleading, thus we changed it in the revised manuscript, so it will not be read as if we are claiming to be the first to answer this question (L65). We actually did not know the paper you have mentioned (Zittis et al., 2017), and we are glad that you have referred us to it, since it presents a much needed conclusion both about the WRF performance during extreme rainfall events in the eastern Mediterranean and about the need for good precipitation data, even if based on a more limited number (5) of HPEs. Thus, we referred to this paper in the revised manuscript (L58-60).

Specific comments:

1. Structure of results. I wonder would the authors consider that it might make more sense to present some of the results from the characterization of rainfall patterns section (S4.2) at the start of the results section, i.e. before model biases are presented? For example, Section 4.2.1 is based on observations rather than model evaluation. It would seem more logical to me to first present the characteristics of the observed HPEs to readers and then examine if these characteristics are reproduced by the model. Indeed, in your abstract (L13-15) you present the manuscript contents in this order. However, this is for the authors to decide!

We understand the reviewer's point and we thought quite a lot on the best order of steps – first HPEs characteristics from radar and then model skill to reproduce those characteristics (as suggested by the reviewer) or first model skill and then HPEs characteristics as manifested in observations (radar) and model. Our tendency towards the latter approach is due to our understanding that radar observations are not perfect and have their own limitations. Therefore, we prefer to present HPE characteristics from the two sources and to emphasise both agreements and disagreements between them. This comparison follows model skill assessment. We do however agree that some of the HPEs characterisation can be moved to the first part of the results section, specifically those that are not relying on pattern analysis, i.e., seasonality and relation between HPEs at different durations (previously shown in Fig. 8 and 9). Therefore, we made some changes in the structure of the results section: starting with general properties of HPEs (presently in Section 4.1), then model skill (4.2-4.3), following by space-time HPEs characteristics detected from observations and model (4.4). Accordingly, we made small modifications in the introduction section. E.g., in the introduction (line 77) we replaced the word "Then" by "Considering that our observations are based on radar data, they are certainly not perfect. Therefore, we quantified and compared …"

2. Title. It is not really apparent from the title of the manuscript that this is primarily a model evaluation study. I expect your results will be of most interest to readers concerned with the quality of CPM simulations, however I fear that due to the title the manuscript might be overlooked by readers searching for such information and not reach the full audience it deserves. If it was my manuscript, I'd go for a title along the lines of "Heavy precipitation in the eastern Mediterranean and its representation in a convection-permitting model". This is, of course, for the authors to decide!

We agree, but we do want to keep the "characterisation" part, from the reasons stated above. We changed the title to:

"Radar-based characterisation of heavy precipitation in the eastern Mediterranean and its representation in a convection-permitting model".

3. Poorly simulated events. Of the 41 HPEs, you identify two which are simulated particularly poorly and observe that these were characterised by short storm durations (L256-257) and were highly localized (L500-501). You also suggest that the poor simulation may be due to a poorly represented moisture field in the ERA-Interim lateral boundary conditions (L466-467). Have you checked this (if possible)? It would be interesting to know if there was any trace of these precipitation events in (i) the ERA-Interim precipitation fields, or (ii) the coarser resolution WRF domains. If the boundary and initial conditions are inadequate, then there is of course no chance for WRF to well reproduce the event. But this doesn't mean that WRF itself is deficient or is incapable of simulating such events! Maybe WRF could simulate the event using data assimilation techniques beyond the scope of this experiment, or with better boundary conditions.

We agree with the suggestion. We presently show (in the supplementary materials) the results of the coarsest WRF domain. This could possibly give an idea of both the WRF simulated rain fields and of the ERA-Interim input. To have an impression of it, we attach below a preliminary analysis of the rainfall for the first of these two events (event #5; 31/3/93-2/4/93), based on the WRF coarsest domain, to be compared with Fig 8. In contrast to most of the simulated HPEs, in which rainfall was simulated quite well in the innermost WRF domain, this event had almost no rainfall simulated in the inner domain. As the figure below shows, rainfall was not produced by the WRF coarsest domain over the area where it was observed (Fig 8), but rather a few hundred km from there – suggesting that the initial conditions were insufficient to produce rainfall in vicinity of the observed one, regardless to the spatial error of the small-scale (innermost) domain. As the reviewer states, it might have been better simulated using data assimilation, or any other better boundary conditions. However, both are beyond the scope of our manuscript.

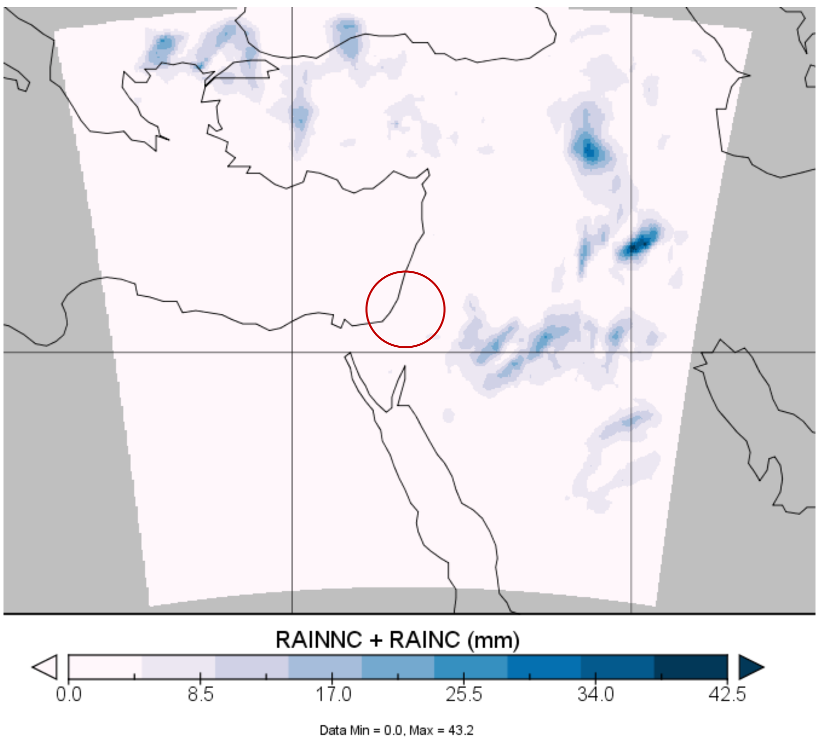

Figure: Rainfall in the coarsest WRF domain during HPE #5 (Table S1) and the approximate range of the Shacham radar (Figure 1).

4. Expectations of CPMs.

My final substantive point is about what we should expect from convection-permitting models, i.e. should we expect them to match radar on a pixel-by-pixel basis? And if they can't do this, does it represent a poor simulation? This is discussed in the introduction of Roberts (2008), where it is argued that the main added value of higher-resolution precipitation forecasts should be seen in area averages – e.g. over a catchment – rather than at specific point locations. I think it's also important to remember that the observed event is also just one possible realisation of the event and WRF will never have perfect initial conditions. You correctly (L469-473) advocate the utility of ensemble simulations for HPEs in the discussion, i.e. as a means of characterizing uncertainty. Similar information to the aforementioned could potentially additionally be presented in the introduction or during the results, as the authors see fit.

The point raised by the reviewer is a crucial one that we want to stress out in the manuscript, and it is actually one of the main points we examine in this manuscript. This is the reason we utilise neighbourhood-based rainfall pattern measures (SAL, FSS), rather than pixel-based indices of success (Fig. 7d, 7f, 9, 10 versus Fig 7e). Moreover, when we compare rainfall patterns, we consider the centre-of-mass of precipitation, Depth-Area-Duration (DAD) curves, and spatial and temporal autocorrelation curves, all of which are not based on point observations. We will better stress this aspect in the revised manuscript. Specifically, we added to the discussion (lines 493-496) the following: "The main added value of convection-permitting models is seen in area averages, rather than over small-scale regions (Roberts, 2008). Therefore, over large catchments (e.g., larger than a few hundred square kilometres, as suggested by the minimal scale presented in Fig. 9), their forecasts are expected to be relatively useful and accurate. Nonetheless, the use of a deterministic convection-permitting model is still unsatisfactory for pinpointing the highest observed rain accumulations…".

5. Data availability. I think that Section 8 about data availability is inadequate. If someone wants to reproduce your results, a bit more than the two non-specific web domains (L517-518) is needed. Is there a specific web page or ftp server where the radar and rain gauge data can be downloaded? If so, please provide the links. If not, then provide more information about how the data can be found. Additionally, what about the WRF model simulations? Will (have) you upload(ed) them to an openaccess server? If so, provide the download link. Or are they available by contacting the corresponding author? Finally, I suggest uploading the WRF namelist.input as an asset when you are resubmitting the manuscript.

We agree with this comment, however not all of the data are owned by us or can be publicly accessed. We added to the revised version of the manuscript the specific domain from which one can download the rain gauge data (https://ims.data.gov.il/). These data are not ours to give, however it is available through this data archive (unfortunately, only in Hebrew). The radar data are also not ours to give. It was provided to us by "EMS-Mekorot projects". However, if needed, corrected and gauge-adjusted data (previously published in (Marra and Morin, 2015)) could be given, in the form of images, through a personal communication with the head of the Hydrometeorology lab in the Hebrew University of Jerusalem, Prof. Efrat Morin (efrat.morin@mail.huji.ac.il).

The size of the simulation results is really big (~4.6 TB), so we prefer not to upload those results to the web. We accept your suggestion, and we added the WRF namelist.input file to the supplementary materials. Using the namelist and the ERA-Interim input files, one will be able to fully reproduce our results.

6. Proof reading. There are a large number of minor grammar errors throughout the text, which are too numerous to list. I therefore suggest a thorough proof reading prior to resubmission.

Accepted. We proof read the manuscript thoroughly.

Minor and technical comments:

- Section 3.2. Could you please also state (i) the number of vertical levels and height of the model top, (ii) if shallow convection is parametrized in the inner nest, (iii) the interpolation method used, i.e. bilinear, nearest-neighbour, conservative, etc. (i) and (ii) could also be added to table 1, if appropriate.

(i) The number of vertical levels is 68, as stated in Table 1 and the top of the model is at 25 hPa., this information is now shown in the manuscript (L129-130) (ii) We use the WRF Tiedtke scheme in the two outer domains (as stated in Table 1) that has a shallow cumulus component, as detailed in (Tiedtke, 1989; Zhang et al., 2011). We detailed this part in the text (L135-136), as it seems not to be clear from Table 1 only. (iii) The interpolation method used is simply nearest-neighbour, and it is now stated clearly in the text (L133). Moreover, as suggested, we intend to add the WRF namelist files, so all of the details of our simulations will be clearer.

- Figure 1. It looks like the domain boundaries have been drawn by simply finding the domain corners and drawing straight lines between them. The lower/upper boundaries of Lambert conformal domains shouldn't have constant latitudes. I think you need to extract the outermost rows/columns from WRF's XLONG and XLAT arrays and use these to plot your domain boundaries.

That's correct. The domains are not plotted with their exact extent. We have corrected this in the revised Figure 1.

- Figure 2. I wonder would it make more sense to compute the %-bias? i.e. instead of bias = WRF/Radar, use bias = 100.*(WRF – Radar)/Radar. With the current formulation the dry biases are lower bounded whereas the wet biases are not upper bounded. With %-bias this would not be the case. I suppose it's not really that big of a deal. The authors can decide for themselves.

This was also mentioned by the other reviewers. We have changed the bias definition into normalised difference (i.e. (WRF-radar)/radar) (Sect. 4.2, Fig. 6c, 7c, 8c).

- Figure 2. Please add "a, b, c, d" labels to the panel plots, to match the text.

We accept this correction, probably intended for Figure 3, and we have applied it in the revised version of the now-named Figure 6.

- L123: Note that it should be possible in WRF to just save precipitation at 10-minute intervals and other variables at a lower frequency, to reduce storage space.

That's correct. Still, after doing this (we actually saved few 2D variables, and not only the precipitation field, however we did not save 3D fields every 10-min), because of the high resolution, the results weigh on average ~112 GB per event.

- L128: I think the reference to "Sect 3.2" is wrong.

Right. This is now corrected to "Sect 3.3" and we added a reference to Table S1 as well (L139).

- L170: The abbreviation "TP" isn't defined anywhere

Correct. We have changed this abbreviation to the full synoptic class name (i.e. "Tropical Plume"; L183 & L185).

- L396-398: It may prove difficult to identify which days to downscale from the GCMs, especially for convective events. There are some papers recently suggesting methods for identifying the best days to downscale (Chan et al., 2018; Meredith et al., 2018; Gómez-Navarro et al., 2019).

This is true, and we now address it in L421-422.

References:

Ban, N., Schmidli, J., Schär, C. (2014). Evaluation of the convection-resolving regional climate modeling approach in decade-long simulations. Journal of Geophysical Research: Atmospheres, 119, 7889–7907.

Berthou, S., Kendon, E. J., Chan, S. C., Ban, N., Leutwyler, D., Schär, C., Fosser, G. (2018). Pan-european climate at convection-permitting scale: A model intercomparison study. Climate Dynamics, 1–25.

Brisson, E., Brendel, C., Herzog, S., Ahrens, B. (2018). Lagrangian evaluation of convective shower characteristics in a convection-permitting model. Meteorologische Zeitschrift, 59-66.

Chan, S., Kendon, E., Fowler, H., Blenkinsop, S, Roberts, N. (2014). Projected increases in summer and winter UK sub-daily precipitation extremes from high-resolution regional climate models. Environmental Research Letters, 9(8), 084019.

Chan, S. C., Kendon, E. J., Roberts, N., Blenkinsop, S., Fowler, H. J. (2018). Largescale predictors for extreme hourly precipitation events in convection-permitting climate simulations. Journal of Climate, 31(6), 2115-2131.

Chen, F., Warner, T. T., Manning, K. (2001). Sensitivity of orographic moist convection to landscape variability: a study of the Buffalo Creek, Colorado, flash flood case of 1996. Journal of the Atmospheric Sciences, 58(21), 3204-3223.

Coppola, E., Sobolowski, S., Pichelli, E., Raffaele, F., Ahrens, B., Anders, I., ... Caldas-Alvarez, A. (2018). A first-of-its-kind multi-model convection permitting ensemble for investigating convective phenomena over Europe and the Mediterranean. Climate Dynamics, 1-32.

Gómez-Navarro, J. J., Raible, C. C., García-Valero, J. A., Messmer, M., Montávez, J. P., Martius, O. (2019). Event selection for dynamical downscaling: a neural network approach for physically-constrained precipitation events. Climate Dynamics, 1-17.

Meredith, E. P., Rust, H. W., Ulbrich, U. (2018). A classification algorithm for selective dynamical downscaling of precipitation extremes. Hydrology and Earth System Sciences, 22(8), 4183-4200.

Kendon, E. J., Roberts, N. M., Senior, C. A., Roberts, M. J. (2012). Realism of rainfall in a very high-resolution regional climate model. Journal of Climate, 25(17), 5791– 5806.

Lean, H. W., Clark, P. A., Dixon, M., Roberts, N. M., Fitch, A., Forbes, R., Halliwell, C. (2008). Characteristics of high-resolution versions of the Met Office Unified Model for forecasting convection over the United Kingdom. Monthly Weather Review, 136(9), 3408-3424.

Roberts, N. (2008). Assessing the spatial and temporal variation in the skill of precipitation forecasts from an NWP model. Meteorological Applications: A journal of forecasting, practical applications, training techniques and modelling, 15(1), 163-169.

Zittis, G., Bruggeman, A., Camera, C., Hadjinicolaou, P., Lelieveld, J. (2017). The added value of convection permitting simulations of extreme precipitation events over the eastern Mediterranean. Atmospheric research, 191, 20-33.

Anonymous Referee #2

The manuscript presents a study focusing on HPEs using weather radar data and convection-permitting numerical simulations. Overall, it is an interesting study that merits publication. In particular, the consideration of a long radar data time series is important, deviating from the common practice of considering a few HPEs. Further, the methodology followed for evaluating model performance is thorough, providing useful insights. I recommend publication subject to minor revisions summarised as follows.

We highly appreciate the reviewer's comments regarding our manuscript. We have addressed all of the comments raised, as detailed below, in the revised version of the manuscript.

Comments

1. Title: I believe that the title of the manuscript is a bit misleading. To my view, the authors focus more on evaluating the WRF model at convection-permitting scales, than providing a study for the characterisation of HPEs in the study region. Hence, I would suggest changing the title of the manuscript, to better reflect the real subject of the presented study.

This idea was also raised by reviewer #1. We understand that we did not focus enough attention to our presentation of HPEs' characterisation, which is unique due to the high resolution rainfall data and the relatively large number of events. We better emphasised this part of the paper in the revised manuscript (L65). Moreover, to better present our paper, we have substituted the previous title with the following one: "Radar-based characterisation of heavy precipitation in the eastern Mediterranean and its representation in a convection-permitting model".

2. Sect. 4.1.2: Two poorly simulated events were identified and some reasoning is provided in the Discussion, mainly focused on the quality of the large-scale driving reanalysis. Therefore, it would be interesting to know if the authors did check the driving ERA-Interim data for these two events, and if so, what can be concluded? Were it really an issue of bad boundary conditions? In addition, what were the results obtained from the coarser resolution domains? Were they equally poor? Such an elaboration would strengthen the authors' claim about the poor model performance.

This is a good point, also raised by reviewer #1. To address it, we included some analyses of the coarser domains in the WRF simulations. It is hard to tell for sure if the boundary conditions are bad, because we do not have better data than the reanalysis, and comparison of other reanalyses or data assimilation techniques are beyond the scope of this manuscript. However, in contrast to most of the model simulations, in which rainfall was quite well simulated, in these two HPEs the innermost domain exhibited almost no rain. At the coarsest model domain, there is no rainfall simulated over the region, but rather only hundreds of km from the observed rain (compare the figure below with Fig 8). Below is a preliminary analysis of rainfall for one of the two events (event #5 in table S1).

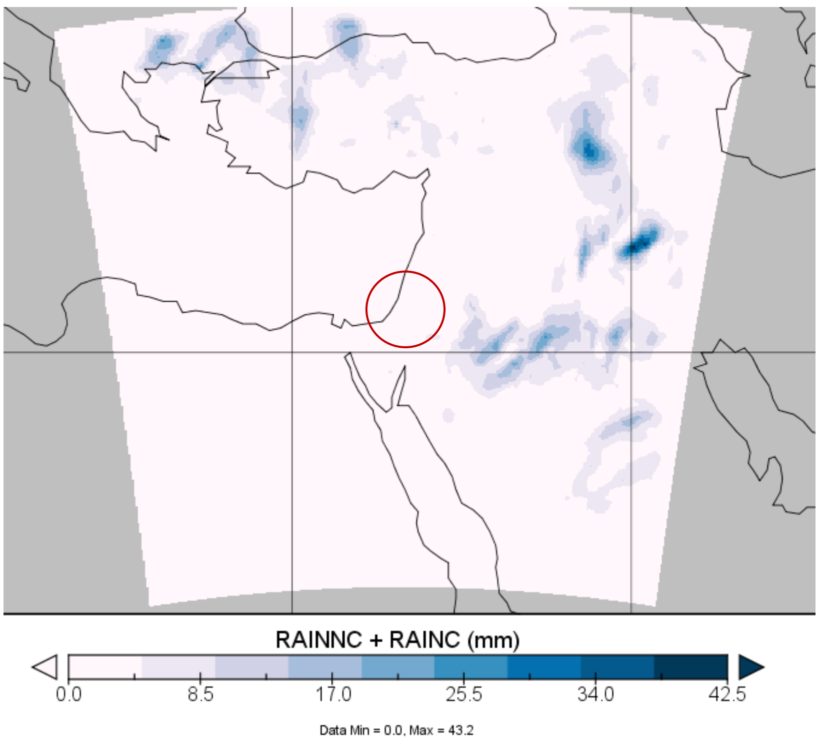

Figure: Rainfall in the coarsest WRF domain during HPE #5 (Table S1) and the approximate range of the Shacham radar (Figure 1).

3. Section 4.2.1 could be moved up, before the presentation of the model evaluation, as it discusses results based on observations.

We understand the reviewer's point and we thought quite a lot on the right order – first HPEs characteristics from radar and then model skill to reproduce those characteristics (as suggested by the reviewer) or first model skill and then HPEs characteristics as manifested in observations (radar) and model. Our tendency towards the latter approach is due to our understanding that radar observations are not perfect and have their own limitations. Therefore, we prefer to present HPEs characteristics from the two sources and to emphasise both agreements and disagreements between them. This comparison follows model skill assessment. We do however agree that some of the HPEs characterisation can be moved to the first part of the result section, specifically those that are not relying on pattern analysis, i.e., seasonality and relation between HPEs at different durations (previously shown in Fig. 8 and 9). Therefore, we made some changes in the structure of the results section: starting with general properties of HPEs (Sect. 4.1), then model skill (4.2-4.3), following by space-time HPEs characteristics detected from observations and model (4.4).

4. Fig.3: Instead of presenting the WRF/RADAR ratio, the authors should consider presenting either the bias (WRF-RADAR) or transform the ratio to %. This would facilitate the interpretation of evaluation results.

Agreed. We have changed our bias definition into normalised difference (i.e. (WRF-radar)/radar) (Sect. 4.2).

5. L123: It would be useful to provide information on the interpolation method? Was it bilinear, bicubic?

The interpolation method we used is simply nearest-neighbour, and it is now stated clearly (L133).

6. Quality of the figures needs improvement for readability.

Thank you for this comment. We reviewed our figures and made them clearer for the revised manuscript. Moreover, we plan to upload the final figures in a vectorised format (wherever possible), so that their quality in any case would be improved.

7. The manuscript text needs a thorough proof-reading for correcting numerous grammar and spelling errors.

Accepted. We proof read the manuscript thoroughly.

Anonymous Referee #3

General comments:

The paper summarizes a comprehensive compilation of heavy precipitation events (HPEs) in the Eastern Mediterranean (EM) based on high-resolution radar data and WRF simulations. This set of events can be representative of the climatology in this area, and is used to quantify the spatio-temporal characteristics of HPE, and the ability to numerically predict the patterns of HPEs. A collection of four diagnostics are used to typify and contrast the radar-based and WRF spatio-temporal precipitation patterns. The events are further classified according to the synoptic situation responsible for the HPEs: namely, Mediterranean cyclone (MC) and active Red Sea trough (ARST). This topic is important as it serves as a benchmark for using numerical weather prediction for flood forecasts, as well as for downscaling of future climate projections. Overall, the presentation is very good, although some excessive text can still be made easier to read, as I suggest in the following. Two major weaknesses of the results and their organization should be fully addressed before the paper can be considered for publication, as detailed in the first two Specific Comments below. Other specific comments should also be clarified.

We thank the reviewer for the comments provided, and for the time and efforts spent in reviewing the manuscript. We have carefully addressed all of the comments and we believe the revised manuscript will benefit from them.

Specific comments:

1. An important distinction is made between HPE under ARST and MC. However, the classification is not maintained throughout the results, having in mind the double goal of the paper: (i) characterize HPE patterns and (ii) evaluate WRF performance. In its current form, the classification is merely mentioned, while referring to previous works on the different spatio-temporal patterns under MC/ARST, but this is not directly shown here, with an exception of Fig. 11a-f. As mentioned in the text, HPE related to ARST is harder for prediction because of the local characteristic convection which dominates the patterns. On the other hand, HPE under MC is characterized by a cold front structure. To enhance the presentation of the results in light of the MC/ARST classification, and to make the discussion and conclusions robust, I suggest to (i) show the spatio-temporal patterns separately for each group (ii) compare the radar/WRF bias between HPE-ARST and HPE-MC. The two aspects can be achieved by reorganization of the presentation of the results, and showing figures such as Fig. 2, 3, 6, 7, 11g and 12 in light of the classification. By doing this, it will be interesting to see if there are consistent differences in the model performance, and substantiate the discussion in Lines 449-458.

We thank the reviewer for raising this point. We agree the distinction between ARST and MC is important both for HPE pattern characterisation and for the ability to forecast the events with a NWP model. Accordingly, we modified some of the figures, as detailed below, to present this distinction, and further detailed it in the results section (L253, L328-330, L342-345, and discussion sections (L419) and in the abstract (L16-17).

Previously Fig. 2 & 3 (presently Fig. 2 & 6): HPE identification is based on specific rainfall thresholds that do not take the classification into account but rather the local quantiles (Sect 3.3). We do not think these thresholds should be defined with classification, since it will reduce their robustness. In addition, the distinction between regions that are better observed by the radar (Fig. 6) would not benefit from synoptic classification. Therefore, synoptic distinction is not relevant for Figs. 2 and 6.

Previously Fig. 6 (presently Fig. 9): Although, in principle, the FSS median and range shown in Fig. 9 for all HPEs can be computed for each synoptic type separately, it should be noted that we deal with only 6 ARST-type HPEs, out of them, two are not well simulated. Since we cannot provide a reliable statistic for ARST type we would not include in Fig. 9 the distinction between the two types. We still, however, referred in the text to some general differences, qualitatively identified, from FSS analysis of the individual HPEs for each type (L328-330).

Previously Fig 7 (presently Fig. 10): We have added the synoptic distinction to the SAL analysis presented in Fig. 10 and in the text discussing these results (L342-345).

Previously Fig. 10 (presently Fig. 4): We have added the synoptic distinction to the figure.

Fig. 11: The DAD analysis is already classified into the two types of synoptic circulation patterns, however, to make a better distinction between rain-fields based on their duration of accumulation and their source (radar-QPE / WRF), we extracted the median curves from each one of the sub figures (a-f) and enlarged them in panel g. We feel that adding a synoptic distinction to this panel, may attract the attention of the reader from the distinction between durations and the source of the rainfall, which was the purpose of panel g.

Fig. 12: We have added the synoptic distinction to the figure and discuss its results (Sect. 4.4.2).

2. Two individual HPE events are shown in more detail. They are important to get a better grasp of the patterns and the model/radar biases and the diagnostics used. It is, however, remaining unclear if the reader should take these results as representative, and if so, of what. It is mentioned that HPE #1 is of MC type, while HPE #5 is ARSTtype. Are they representative of the two types? Since both cases perform badly in terms of the SAL diagnostic, why do you focus on them? As the message of the work is to demonstrate the overall good performance of WRF, I find this confusing, and suggest to also illustrate the point with a case where WRF performs representatively well. I suggest to clarify this issue by explaining the rationale behind choosing to focus on these events. Further, it will make an easier reading to mark the chosen events onto Figs. 6,7,10,11.

The two events shown previously in Figs. 4, 5 (Presently in Figs. 7, 8) are meant to represent one well-simulated event (event #1, shown in Fig. 7) and one poorly-simulated event (#5, Fig. 8). It seems there was a confusion with the two poorly simulated events (#5 and #20, Table S1) discussed later on, but this was not the intension; we have modified the text to better clarify this point (see below). The two events shown in Figs. 7 and 8 are given as an example to show what the model is able (Fig. 7) or unable (Fig. 8) to simulate, and they also exemplify a typical MC and a typical ARST cases. It turns out that it is harder for the model to represent the localised rainfall that often happens during ARSTs. The different performance for the two cases is very clear from the SAL analysis (see figure below).

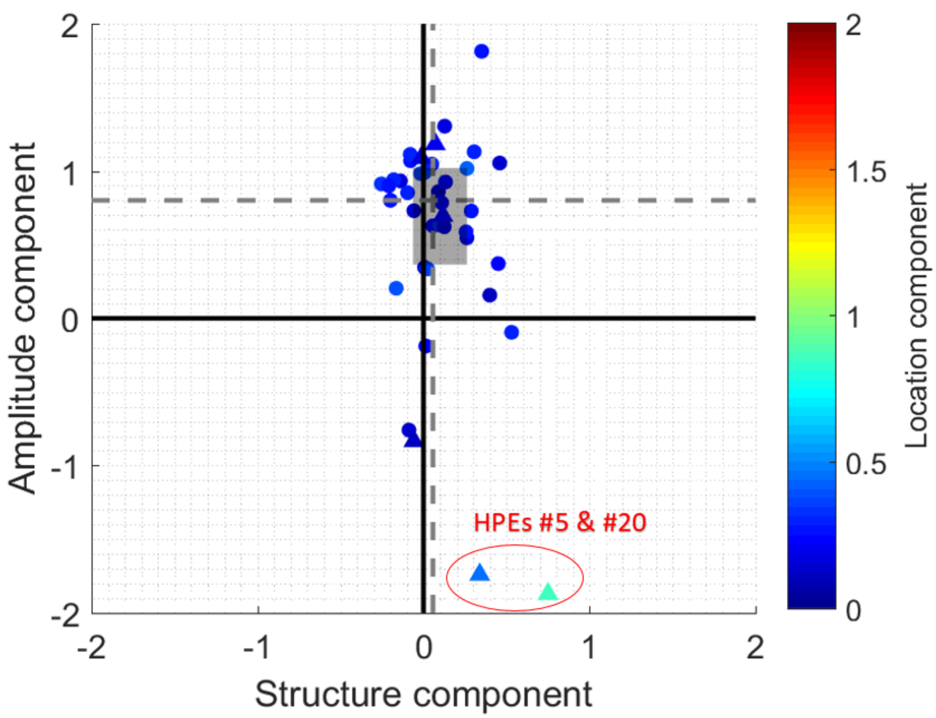

Figure: SAL analysis of the 41 HPEs. MC-type of HPEs denoted with circles and ARST-type with triangles.

In light of your comment, we clarified in the revised manuscript the purpose of the closer look at these two events (Section 4.3): "…localised rainfall. Figure 7 presents, as an example, a well-simulated HPE case (event #1, Table S1). In addition, the distributions of rainfall among pixels were generally well represented (Fig. 7d). At the same time, pixel-based comparisons were deemed inappropriate for such an analysis, as shown in the scatter plot (Fig. 7e). Most of the examined HPEs led to similar observations, with the exception of two HPEs in which the WRF model clearly failed to represent the rainfall patterns. An example of such a poor simulation is given in Fig. 8 (event #5, Table S1).".

3. Table S1 and Fig. 8: How is HPE duration calculated, and what does it mean if an HPE has a 48-h duration but no shorter durations (e.g., HPE #6)? This is confusing and should be clarified. Consequently, the results in Fig. 8 are confusing, and it is not very clear to me what we can learn from this figure.

The term “event duration” in Fig. 5, Table S1 and possibly in other sections of the paper, does not refer to the total duration of the event but rather to the duration according to which it was selected as HPE. We defined HPEs, in Sect 3.3 by “the exceedance of local, quantile-based thresholds over a sufficiently large area… For a set of durations between 1 and 72 hours we defined the threshold as the 99.5th quantile of the non-zero (i.e. >0.1 mm) hourly amounts observed in each radar pixel… we classify as HPEs all time intervals during which at least 1000 pixels (i.e., 1000 km2) exceeded their local threshold”. This is to say that, if enough pixels in the radar archive exceeded their own threshold, for a given examined duration, we defined this event as an HPE for this duration. Obviously, a given event can be selected for several examined durations. Fig. 5 shows that it is hard to separate events according to their duration, i.e. the duration for which rain intensity was exceeded the threshold, because of the above overlapping. However, we see that it is not clear enough. We will have clarified it in the text (L160-161), and moved Fig 5. Earlier (previously it was Fig. 8), to relate also to the details in Sect. 3.3.

4. Section 3.5.4 is difficult to understand, and the description of the 2D autocorrelation field, its ellipticity and orientation in Lines 379-392 is not also not clear when not referring to a figure. Please enhance or clarify these parts, possibly with an illustrative figure, such that the analysis can be standalone without referring to the references.

We agree and make sure the description is clear enough by its own in the revised manuscript. However, we do not want to add a lot of text to describe what was already published (e.g., in Marra and Morin, 2018). Therefore, we added an explanatory figure to the supplementary (SF1).

5. I suggest to move the spatio-temporal characteristics in Fig. 9 and 10 to earlier on in the text, even to when presenting the list of events in Sec. 3.4. This seems more natural to understand the events characteristics before assessing the model performance.

We agree that it seems more natural to talk about the characteristics of events before presenting the model performance. However, our goal is to characterise HPEs and to evaluate model capability in reproducing those characteristics. Therefore, we chose to present the examined characteristics from both radar and model, and thus these analyses come after model performance results. However, accounting for suggestions from all reviewers, we would like the re-order the results section as follows:

a) General properties of HPEs (previously shown e.g., in Fig. 8 and 9), now in Sect 4.1 (and Figs. 3, 4 and 5)
b) Model skill (previously Figs 3-7), now in Sect. 4.2-4.3 (and Figs. 6-10)
c) Comparison of characteristics between the radar-QPE and the model (previously Fig. 10-12), now in Sect. 4.4. (and Figs. 11-12).

Technical corrections:

1. Line 10: add 'spatio-temporal' before 'patterns', and elaborate on what you mean by 'effects'.

Accepted. We have changed this sentence to "Spatiotemporal rainfall patterns govern the hydrological, geomorphological and societal effects of HPEs".

2. Line 78: replace 'getting a' by 'receiving'.

Accepted.

3. Line 101: Add the coordinates of Ben-Gurion airport.

Agreed. We added "31.998N, 34.908E".

4. Line 130: replace 'Other' by 'Additional'.

OK.

5. Section 3.1: add more details about the radar such as: wavelength (The authors mentioned about the C band), radar parameters (reflectivity, doppler, etc). What is the maximum range of the radar observations? We see it very clearly in Fig. 1b, but number will further clarify.

We have added the radar wavelength (5.35 cm), its range (185 km), the fact that it is a non-doppler radar, and that raw radar reflectivity data were translated to QPE using first a fixed Z-R relationship, $Z = 316 \cdot R^{1.5}$, and then into QPE by applying physically based corrections and gauge-based adjustment procedures (see details in Marra and Morin(2015)) (L109-115).

6. Fig. 2: Are the white areas on the eastern side of the circle domain masked out according to the black line in Fig. 3c? If so, this should be mentioned.

Yes. OK, we have added this to the figure caption (L936).

7. Fig. 3: There is no legend of (a), (b), (c) and (d) as mentioned in the caption and text.

Thanks for noting this. We added the legend to the figure.

8. Figs. 3,4,5: a normalized difference (e.g., (WRF-radar)/radar) would make more sense than a ratio WRF/radar, such that the red areas will not distract the attention from more important biases.

Accepted. We have changeed our definition for the bias to be a normalized difference (i.e. ((WRF-radar)/radar)) (Sect. 4.2).

9. Line 210: Section 3.5.3 please add a sentence to motivate the use of the DAD curve.

We agree that a motivation is needed. Therefore, section 3.5.3 starts with a motivation sentence ("Areal rainfall amounts are crucial drivers of the hydrologic response and are important for understanding rainfall structure and triggering mechanisms"). We think that this text is enough for the aims of this manuscript.

10. Fig. 4e: replace the scatter plot by a density plot, to see the details inside the black area.

Accepted. We have replaced it.

11. Fig. 5: add the equivalent Fig. 4d-f to this case.

Panels d-f were added to Fig. 4 to show that even in a well-simulated event, there is a large disagreement on a pixel scale, while the general characteristics (considering all pixels, as in the histogram, or a large neighbourhood, as in the FSS analysis) could still be well simulated. Fig. 5, however, presents a poorly-simulated event and it is not much successful no matter in what perspective we examine it. This is why we did not present further analyses of rainfall patterns. We also think that due to the clarification made in response to the reviewer's 2nd comment this point is now clearer.

12. Line 165: the synoptic classification is based on semi-objective classification by Alpert (2004). This classification is based on parameters such as T, P, U and V at 1000 hPa once per day based on NCEP-NCAR reanalysis with coarse resolution ãA˘U2.5ã ˝ A˘Uˆ ˚ ∘ . The model (WRF) was analyzed with six hourly ERA-Interim reanalysis with 80km horizontal resolution. It is worth mentioning this.

Agreed. We have mentioned it (L177-178).

13. Line 266: greater than 99% of pixels': do you mean to write 'corresponding to less than 1% of the pixels in this HPE'?

Yes. This was our intention, and we have edited the text accordingly (L318-319).

14. Line 278: which bias to you refer to in the square brackets?

It is the bias of the median (inter-event) amplitude score (from the SAL analysis). However, we have explained this better in the revised text (L332).

15. Line 336: missing 'a' after 'are'.

Correct. Thank you for noticing.

16. Line 437: remove 'a' before 'catchments'.

Accepted.

17. Line 490: replace 'weather' by 'numerical weather prediction'.

Accepted.

18. Fig. 11a-f: make the green and blue colors more distinguishable.

OK.

19. Fig. 12: would ‘temporal lag’ be more suitable than ‘temporal distance’?

It is suitable, however we tried to follow the term used in Marra and Morin (2018) that refer to time-distance.

References:

Alpert, P., Osetinsky, I., Ziv, B. and Shafir, H.: Semi-objective classification for daily synoptic systems: Application to the eastern Mediterranean climate change, Int. J. Climatol., 24(8), 1001–1011, doi:10.1002/joc.1036, 2004.

Kendon, E. J., Roberts, N. M., Fowler, H. J., Roberts, M. J., Chan, S. C. and Senior, C. A.: Heavier summer downpours with climate change revealed by weather forecast resolution model, Nat. Clim. Chang., 4(7), 570–576, doi:10.1038/nclimate2258, 2014.

Liu, C., Ikeda, K., Rasmussen, R., Barlage, M., Newman, A. J., Prein, A. F., Chen, F., Chen, L., Clark, M., Dai, A., Dudhia, J., Eidhammer, T., Gochis, D., Gutmann, E., Kurkute, S., Li, Y., Thompson, G. and Yates, D.: Continental-scale convection-permitting modeling of the current and future climate of North America, Clim. Dyn., 49(1–2), 71–95, doi:10.1007/s00382-016-3327-9, 2017.

Marra, F. and Morin, E.: Use of radar QPE for the derivation of Intensity–Duration–Frequency curves in a range of climatic regimes, J. Hydrol., 531, 427–440, doi:10.1016/j.jhydrol.2015.08.064, 2015.

Marra, F. and Morin, E.: Autocorrelation structure of convective rainfall in semiarid-arid climate derived from high-resolution X-Band radar estimates, Atmos. Res., 200(September 2017), 126–138, doi:10.1016/j.atmosres.2017.09.020, 2018.

Tiedtke, M.: A Comprehensive Mass Flux Scheme for Cumulus Parameterization in Large-Scale Models, Mon. Weather Rev., 117(8), 1779–1800, doi:10.1175/1520-0493(1989)117<1779:ACMFSF>2.0.CO;2, 1989.

Zhang, C., Wang, Y. and Hamilton, K.: Improved Representation of Boundary Layer Clouds over the Southeast Pacific in ARW-WRF Using a Modified Tiedtke Cumulus Parameterization Scheme, Mon. Weather Rev., 139(11), 3489–3513, doi:10.1175/MWR-D-10-05091.1, 2011.

Zittis, G., Bruggeman, A., Camera, C., Hadjinicolaou, P. and Lelieveld, J.: The added value of convection permitting simulations of extreme precipitation events over the eastern Mediterranean, Atmos. Res., 191, 20–33, doi:10.1016/j.atmosres.2017.03.002, 2017.

~~Characterising patterns~~Radar-based characterisation of heavy precipitation ~~events~~ in the eastern Mediterranean ~~using a weather radar~~ and its representation in a convection-permitting ~~WRF simulations~~model

Moshe Armon[1], Francesco Marra[1], Yehouda Enzel[1], Dorita Rostkier-Edelstein[2], Efrat Morin[1]

[1]Fredy and Nadine Herrmann Institute of Earth Sciences, the Hebrew University of Jerusalem, Edmond J. Safra Campus, Jerusalem~~,~~ 9190401, Israel

[2] Department of Applied Mathematics, Environmental Sciences Division, IIBR, Ness-Ziona~~,~~ 7410001, Israel

Correspondence to: Moshe Armon (moshe.armon@mail.huji.ac.il)

Formatted: Font: (Default) Times New Roman, 10 pt, Complex Script Font: Times New Roman, 12 pt, (Complex) Arabic (Saudi Arabia), English (United Kingdom)

Abstract. Heavy precipitation events (HPEs) can lead to natural hazards (floods, debris flows) and contribute to water resources. ~~Rainfall~~Spatiotemporal rainfall patterns govern ~~HPEs~~the hydrological, geomorphological and societal effects of HPEs. Thus, a correct characterisation and prediction of rainfall patterns is crucial for coping with ~~HPEs~~these events. Information from rain gauges is generally limited due to the sparseness of the networks, especially in the presence of sharp climatic gradients. Forecasting HPEs depends on the ability of weather models to generate credible rainfall patterns. This paper characterises rainfall patterns during HPEs based on high-resolution weather radar data and evaluates the performance of a high-resolution, convection-permitting~~,~~ Weather Research and Forecasting (WRF) model in simulating these patterns. We identified 41 HPEs in the eastern Mediterranean from a 24-year radar record using local thresholds based on quantiles for different durations, classified these events into two synoptic systems, and ~~we~~ ran model simulations ~~of these events.~~for them. For most durations, HPEs near the coastline ~~are~~were characterised by the highest rain intensities~~,~~; however, for short durations, the highest rain intensities ~~characterise~~were characterised for the inland desert. During the rainy season, the rain field's centre~~-~~ of~~-~~ mass ~~of the rain field~~ progresses from the sea inland. Rainfall during HPEs is highly localised in both ~~in~~ space (<10 km decorrelation distance) and ~~in~~ time (<5 min). WRF model simulations were accurate in generating the structure and location of the rain fields in 39 out of 41 HPEs. However, they showed a positive bias ~~with respect~~relative to the radar estimates and exhibited errors in the spatial location of the heaviest precipitation. Our results indicate that convection-permitting model outputs can provide reliable climatological analyses of heavy precipitation patterns; conversely, flood forecasting requires the use of ensemble simulations to overcome the spatial location errors.

1 Introduction

Heavy precipitation events (HPEs) cause natural hazards such as flash, riverine, and urban floods, landslides and debris flows; ~~at the same time,~~ they also serve as a resource ~~in~~for recharging ground- and surface~~-~~ water reservoirs (e.g., Bogaard and Greco, 2016; Borga et al., 2014; Borga and Morin, 2014; Doswell et al., 1996; Nasta et al., 2018; Raveh-Rubin and Wernli, 2015; Samuels et al., 2009; Taylor et al., 2013; UN-Habitat, 2011). Diverse rainfall patterns during HPEs cause different hydrological responses, thus an accurate representation of rainfall patterns during ~~HPEs~~these events is crucial ~~in~~to detecting and predicting climate~~-~~ change~~-~~ induced precipitation changes (Maraun et al., 2010; Trenberth et al., 2003). In particular, understanding the specific interactions between rainstorms and catchments is critical in small watersheds, where accurate, high spatiotemporal resolution observations and forecasts are required (e.g., Bloschl and Sivapalan, 1995; Cristiano et al., 2017). However, these data may not be available through operational tools, such as rain gauge networks and coarse~~-~~-scale weather models (e.g., commonly used, global or even regional circulation models). High-resolution observation and HPE forecasts thus remain~~ thus~~ a challenge (Borga et al., 2011; Collier, 2007; Doswell et al., 1996).

Rain gauge data can be used to quantify general characteristics of HPEs (such as rain intensity and depth ~~at the~~on a point scale), but~~,~~ their density is generally insufficient to adequately represent the spatial gradients, particularly in the case of sparsely gauged regions, short~~-~~-duration events, and arid climates (Amponsah et al., 2018; Kidd et al., 2017; Morin et al., 2009, 2019). This problem is enhanced in regions characterised by high climatic gradients such as the eastern Mediterranean (EM) (El-Samra et al., 2017; Marra et al., 2017; Marra and Morin, 2015; Morin and Gabella, 2007; Rostkier-Edelstein et al., 2014). Thus, ~~characterising~~a characterisation of HPEs with high resolution in such regions must be supported by other types of records. Remotely~~-~~ sensed precipitation estimates, such as those acquired from weather radars, provide the necessary spatiotemporal resolutions (e.g., 1 km, 5 min) and coverage (regional scale), and have been shown to be useful for analysing specific events (e.g., Borga et al., 2007; Dayan et al., 2001; Krichak et al., 2000; Smith et al., 2001). Where continuous radar records exist, they have been used in climatological studies as well (Belachsen et al., 2017; Bližňák et al., 2018; Peleg et al., 2012; Saltikoff et al., 2019; Smith et al., 2012). However, climatological characterisations of rainfall patterns during HPEs are rare in the literature and often based on rain gauge identification of ~~HPEs~~those events (Panziera et al., 2018; Thorndahl et al., 2014).

High-resolution numerical weather ~~predictions (NWPs)~~prediction (NWP) models allow ~~to simulate~~simulating and ~~forecast~~forecasting HPEs, and ~~represent an~~as added value~~ for~~, enable understanding their past and present patterns, and ~~predicting~~a prediction of possible future behaviours (Cassola et al., 2015; Deng et al., 2015; El-Samra et al., 2017; Kendon et al., 2014; Prein et al., 2015; Rostkier-Edelstein et al., 2014; Yang et al., 2014). In particular, convection-permitting models are increasingly used in weather forecasts, climatological studies and event-based reanalyses (e.g., Ban et al., 2014; Fosser et al., 2014; Hahmann et al., 2010; Khodayar et al., 2016; Prein et al., 2015; Rostkier-edelstein et al., 2015). Such models downscale global or regional NWP models, and ~~allow to directly represent~~provide a direct representation of convective rainfall that, due to its high~~-~~ intensity and local characteristics, often plays a major role in HPEs (e.g., Flaounas et al., 2018). ~~Additionally, they~~In addition, these models can provide ~~3D~~3-D fields of otherwise unmeasurable meteorological variables, thus contributing to our understanding of the dynamics of HPEs. Studies based on high-resolution NWP models commonly focus on specific cases~~, with only a few also examining the climatology of model results, either for determining the atmospheric conditions that trigger HPEs, or understanding the overall rainfall pattern in comparison with~~. For example, Zittis et al. (2017) examined the performance of a high-resolution NWP model during five HPEs in the EM, and identified large discrepancies between grid- and gauge-based precipitation datasets, making it hard to validate the model. Only a few studies have examined the climatology of model results, to either determine the atmospheric conditions that trigger HPEs, or understand the overall rainfall pattern in comparison to observational records (e.g., Flaounas et al., 2019; Kendon et al., 2014; Khodayar et al., 2018). Commonly, climate change studies based on high-resolution NWP models characterise the expected changes in precipitation, focusing on rainfall intensity or frequency, or some derived index (e.g., Ban et al., 2014; Hochman et al., 2018a; Schär et al., 2016; Westra et al., 2014).

A basic question, however, remains ~~unanswered: Is~~open: To what degree is the model description of rainfall during HPEs credible? Moreover, the model's ability to reproduce rainfall patterns can differ among synoptic types. To answer this question, both a realistic spatiotemporal representation of rainfall during HPEs and a large number of observed HPEs, triggered by various synoptic systems, are necessary. In this paper, we present a successful step in this direction based on a corrected and calibrated~~,~~ 24-year~~-~~-long record of weather radar data recently developed for the EM, and found to adequately represent extreme precipitation events (Marra and Morin, 2015). As an essential step in understanding and quantifying rainfall-generating processes involved in HPEs, and as a basis for a future study that ~~includes~~will include downscaling of climate change projections to understand changes in rainfall patterns, here we aim ~~here~~ to (~~a~~i) systematically characterise high-resolution rainfall patterns during HPEs in the hydroclimatically-heterogeneous EM, and (~~b~~ii) assess the capabilities of a regional convection-permitting weather model to simulate these patterns. To ~~do so~~this aim, we identified ~~41~~all HPEs embedded in the radar record~~,~~ (41 events), and simulated them using a convection-permitting ~~weather research~~Weather Research and ~~forecasting~~Forecasting (WRF) model (Skamarock et al., 2008). ~~Then~~This long and consistent high-resolution dataset is unique, and is therefore interesting both for examining HPE climatology, and as a basis for convection-permitting model evaluation. Considering that our observations are based on radar data, they are certainly not perfect. Therefore, we quantified and compared several rainfall characteristics~~, and compared simulated rain fields to~~ from both radar estimates and simulated rainfall to evaluate the model's ability ~~of the model~~ to reproduce the rainfall patterns and to obtain climatological characteristics of HPEs.

The paper is structured as follows: Section 2 describes the study region. The radar and ~~the~~ weather model data are explained in Sect. 3.1~~-~~ and 3.2, respectively. Identification and synoptic classification of HPEs are presented in Sect. 3.3 and ~~Sect.~~ 3.4, respectively. The methods used in evaluating model performance ~~is~~are presented in Sect. 3.5. Section 4 presents the results of the evaluation and characterisation of rainfall patterns during HPEs. Section 5 provides a discussion and a summary of the study, and Sect. 6 concludes.

2 Study region

This study focuses on the EM region, where Mediterranean climate (with parts of it ~~getting a~~receiving mean annual precipitation >1000 mm year^{-1}) drops to hyperarid (<50 mm year^{-1}) over a short distance (Goldreich, 2012) (Fig. 1). Precipitation is dominated by rainfall, and occurs mainly between October and May, with summer months (June ~~-~~–September) being essentially dry (Kushnir et al., 2017). Most of this rainfall is associated ~~to~~with cold north-westerly flows ~~at~~in the rear part of Mediterranean Cyclones (MCs). These MCs pass above the warm water of the Mediterranean Sea, absorbing moisture and precipitating it over the EM region (Alpert et al., 2004; Alpert and Shay-EL, 1994; Armon et al., 2019; Saaroni et al., 2010; Ziv et al., 2015). High surface water temperature favours high~~-~~-intensity rainfall and floods, most commonly at the beginning of the rainy season and near the sea. ~~While~~As the MCs move inland and towards the desert, a substantial amount of the moisture is lost, and rainfall occurrence and amounts are greatly reduced (Enzel et al., 2008). ~~In this arid region HPEs are associated not only to MCs (Armon et al., 2018; Kahana et al., 2002),~~

~~but also to the Active Red Sea Trough (ARST~~In this arid region, HPEs are associated not only with MCs (Kahana et al., 2002), but also with Active Red Sea Troughs (ARSTs) (Ashbel, 1938; Krichak et al., 1997; De Vries et al., 2013) and, more rarely, ~~to~~with Tropical Plumes (Armon et al., 2018; Rubin et al., 2007; Tubi et al., 2017). Commonly, rainfall during ARSTs is of a spotty nature, ~~could~~can reach far into the desert, and ~~could have~~can be of very high ~~intensities~~intensity (Armon et al., 2018; Sharon, 1972). Conversely, during Tropical Plumes, rainfall is widespread ~~and can simultaneously cover~~, potentially covering most of the region simultaneously with moderate intensities. Desert HPEs frequently result in large and sometimes devastating flash floods (e.g., Armon et al., 2018; Dayan and Morin, 2006; Farhan and Anbar, 2014; Kahana et al., 2002; Saaroni et al., 2014; Seager et al., 2014).

Projections for precipitation in the EM indicate a substantial decrease in annual rainfall amounts (Giorgi and Lionello, 2008); however, the importance of credible HPE simulations stems from, among others, ~~from~~ opposing trends that may appear between number and intensity of HPEs generated by different synoptic conditions (Alpert et al., 2002; Hochman et al., 2018a, 2019; Marra et al., 2019); for example, based on Dead Sea ~~sedimentologic~~sedimentological data, it ~~was~~has been suggested that when ~~MCs~~MC frequency is reduced, i.e., there is a regional drought, the frequency of HPEs generated by ~~ARST~~ARSTs may increase (Ahlborn et al., 2018).

3 Methodology and data

3.1 Weather radar data

The weather radar data used in this study consist of 24 hydrological years (September~~-~~–August~~)~~), between 1990~~-~~–1991 and 2013~~-~~–2014, observed by the Electrical Mechanical Services (EMS/Shacham) non-Doppler C-band weather radar~~,~~ (5.35 cm), located at Ben~~-~~ Gurion Airport (Fig. ~~1). Radar~~1; 31.998°N, 34.908°E). Its effective range is ~185 km. Raw radar reflectivity data were translated to quantitative precipitation estimates (~~QPE) were produced~~QPEs) by initially using a fixed Z–R relationship ($Z = 316 \cdot R^{1.5}$) and then applying physically based corrections and gauge-based adjustment procedures (see details in Marra and Morin, 2015)~~, and were available~~. These produced QPEs at 1~~-~~-km^2, ~5-min resolutions. Examining the radar QPE and comparing it with rain gauges at hourly and yearly resolution yielded a root mean square error of 1.4~~-~~–3.2 mm h^{-1} and 13~~-~~–220 mm ~~y~~year^{-1}, respectively, and a bias of 0.8~~-~~–1.1 (hourly) and 0.9~~-~~–1.1 (yearly) (Marra and Morin, 2015). This archive ~~was~~has been previously used for a series of studies focusing on high~~-~~-intensity precipitation, ~~such as~~including precipitation frequency analysis (Marra et al., 2017; Marra and Morin, 2015), floods (Rinat et al., 2018; Zoccatelli et al., 2019), and characterisation of convective rain cells (Belachsen et al., 2017; Peleg et al., 2018). ~~Few~~A few issues potentially affecting the QPE should be mentioned. The radar was turned off during the dry season and, for technical reasons, sometimes during the wet season; thus, a few severe storms were missed and are not included in the archive. ~~There is a~~A long-term decline in the availability and quality of ~~the~~ radar data ~~that~~ might have decreased the number of high~~-~~-quality archived HPEs ~~during~~over the years, mainly since 2010. Since we ~~do~~did not aim ~~at providing~~to provide a *complete* climatology, these aspects ~~are~~were not expected to influence the results of the study. Due to technical reasons, the radar products were not always available at their intended temporal resolution (~5 min) and longer gaps may exist between consecutive radar scans. Gaps of <20 min between consecutive radar scans were linearly interpolated to recreate the 5-min resolution; gaps of >20 min were treated as missing data. Due to the uneven spatial distribution of the rain gauges, adjustment procedures may inadequately represent the south-easternmost areas covered by the radar, where the gauge network is ~~the sparsest~~most sparse. Finally, due to overshooting of the radar beam, precipitation occurring east of the Dead Sea (Fig. 1) is generally underestimated.

3.2 WRF model configuration

The WRF model was configured using three~~,~~ 1-way nested domains, ~~at~~with a 1:5 resolution ratio between them (Fig. ~~1).~~1) and 68 vertical levels (model top is at 25 hPa). The inner domain (~~551X551~~551 x 551 pixels) ~~is~~was set at a 1 km^2 horizontal resolution, to be comparable with the radar data. To comply with the Courant–Friedrichs–Lewy numerical stability criterion, model time steps ~~at~~in the innermost domain ~~are~~were 4~~-~~–8 ~~seconds~~s (Warner, 2011)~~, however~~. However, to spare computer storage, outputs were saved at 10~~-~~-min intervals. When analysed, the WRF grid was interpolated using nearest-neighbour interpolation from a Lambert projection grid to a similar~~ size~~-sized grid on ~~Transverse~~a transverse Mercator projection, as in the radar archive. It is important to note that a 1 km^2 spatial resolution enables ~~to~~ explicitly ~~resolve~~resolving convection, without the use of parametrisation (e.g., Prein et al., 2015). ~~The model input data are six~~The two outer domains used the WRF Tiedtke scheme for the parametrisation of convection (Tiedtke, 1989; Zhang et al., 2011a). The model input data were 6-hourly ERA-Interim reanalyses, at ~80 km horizontal resolution and with 60 vertical levels, including sea surface temperature, along with basic meteorological parameters (Dee et al., 2011). The model was used to simulate the HPEs identified in the radar archive (Sect 3.~~2~~3; Table S1). Each simulation started 24 h prior to the beginning of the event, rounded down to the previous 6 h, and ~~ended~~stopped with the ~~HPE~~ ending of the HPE, rounded up to the next 6 h. Therefore, the spin-up period of each simulation ~~is~~was at least 24 h. ~~Other~~Additional model settings, presented in Table 1, were selected because they are considered suitable for convection-permitting simulations (e.g., Romine et al., 2013; Schwartz et al., 2015).

3.3 ~~HPEs~~HPE identification

HPEs have various definitions in different research fields and geographical regions. For example, climatologically, HPEs are commonly associated ~~to~~with a specific time interval (i.e~~.~~., sub-daily to a number of consecutive days) during which precipitation depth surpasses a threshold representing a predefined quantile (e.g., 95^{th} or 99^{th}), or a high, but constant~~,~~ intensity (e.g., 10, 20, or 50 mm day^{-1}) (e.g., Drobinski et al., 2014; Nuissier et al., 2011; Westra et al., 2014; Zhang et al., 2011b). On the other hand, hydrological definitions usually focus on the resulting flood. In general, a good definition of a HPE should also include the areal dimension, ~~in order~~ to ~~consider~~enable considering hydrological and social impacts (Easterling et al., 2000).

Here we define HPEs by the exceedance of local, quantile-based thresholds over a sufficiently large area. The decision to set local thresholds ~~is~~was due to the sharp climatic gradient characterising the study area. To decrease the computational ~~efforts~~effort and guarantee adequate temporal sampling, the HPE identification was based on a radar database comprising ~~the~~ hourly intervals ~~in~~for which at least 60% of the expected radar scans are available (Marra et al., 2017). For a set of durations between 1 and 72 ~~hours~~h, we defined the threshold as the 99.5^{th} quantile of the non-zero (i.e. >0.1 mm) hourly amounts observed in each radar pixel. Depending on duration and location, these are equivalent to annual return periods of roughly 2~~-~~–10 years (Fig. 2). To account for the spatial scale, we ~~classify as~~

~~HPEs~~classified all time intervals during which at least 1000 pixels (i.e., 1000 km^2) ~~exceeded~~exceed their local threshold as HPEs. Jointly, these thresholds (99.5% for each pixel, and aggregation of 1000 pixels for an event) settle the trade-off between having too many (or too few) events and accounting for HPEs that are too local (or only including the most widespread rainstorms). These selected thresholds ~~allow to analyse~~enable analysing a reasonable number of diverse HPEs, with some ~~HPEs~~ being quite local and others more widespread. It should be noted that storms typically last longer than the duration for which they are selected as HPEs. Moreover, the same storm can be identified as a HPE for multiple durations.

The selection procedure yielded 76~~-~~–98 individual events for each of the examined durations, summing ~~up~~ to 120 when overlaps between durations ~~are~~were included. Similar to Marra and Morin (2015), storms were separated by at least 24 ~~hours~~h with <100 pixels displaying rainfall of >0.1 mm. Since the ERA-Interim data are available ~~on a~~at 6~~-~~ h resolution, ~~too short~~ rainstorms that were too short (<12 h) were excluded from the analysis. Storms longer than 144 h were excluded to avoid major changes in sea surface temperature during events. In addition, events were discarded manually when the radar data ~~was~~were abundantly contaminated by ground clutter due to anomalous propagation, or ~~in case~~when other data~~-~~-quality issues were observed. The final list of HPEs ~~consists~~consisted of 41 independent events lasting on average 3.4~~±~~ ± 1.6 days (Table S1).

For each of these events, a filter was used to remove pixels with residual ground clutter. Pixels in which the probability of rain detection (POD, i.e., the fraction of time in which the pixel exceeds 0.1 mm h^{-1}) exceeds 10% and is larger than 1.9 times the average POD of the surrounding area (25 × 25 km) were removed. The extent of the explored area and of the ratio were chosen subjectively ~~chosen~~ after examining ranges between 1~~-~~ and 3 (for the ratio) and 5~~-~~ and 50 km (for the areal extent). Additional areas known to be persistently contaminated by ground echoes (from our experience and earlier studies) were masked out manually (e.g., the circular area near the radar). Together, these procedures excluded ~0.5% of the radar pixels.

3.4 Synoptic classification

We classified the HPEs into two classes representing the most common rainy synoptic circulation patterns prevailing in the region: MC and ARST. To do so, we ~~rely~~relied on the semi-objective synoptic classification by Alpert et al. (2004), based on daily (at 12 UTC) meteorological fields at the 1000 hPa pressure level~~.~~ from the NCEP/NCAR reanalysis (2.5° spatial resolution). We classified a HPE as a MC if one of the following conditions occurred: (~~1) the majority~~i) most of the days comprising the HPE were considered, according to Alpert et al. (2004), as days with either a MC or a high-pressure system following a MC; (~~2~~ii) one of the days during the HPE was a MC and none of them was an ARST. Similarly, we classified a HPE as an ARST if (~~1) the majority~~i) most of its days were classified as ARST according to Alpert et al. (2004), or (~~2~~ii) one of its days was an ARST and none of them was a MC. The abovementioned ~~TP~~Tropical Plume synoptic pattern (Rubin et al., 2007; Tubi et al., 2017) is not ~~a~~ part of our classification because of ~~the~~its low frequency and because ~~they do~~it does not appear in~~ a~~ near sea level pressure meteorological fields. Specifically, one HPE (#41; Table S1) was characterised, during its 5-day duration, first by the prevalence of ~~TP~~a Tropical Plume (Armon et al., 2018) and then by a MC; it was classified here as a MC. Despite the simplification, these two classes ~~were~~have been recently shown to exhibit distinct characteristics of~~ the~~ rainfall intensity distribution (Marra et al., 2019). Indeed, 85% and 15% of HPEs were classified as MCs and ARSTs, respectively (Table S1), reasonably following the expected proportions of the two synoptic circulation patterns (Goldreich et al., 2004; Saaroni et al., 2010).

3.5 Evaluation of simulated rain fields

Inaccurate initial conditions in the presence of non-linear precipitation~~-~~-generation processes, together with the presence of atmospheric instabilities, may limit the atmospheric predictability and, consequently, ~~the~~ modelling skills (Anthes et al., 1985). Moreover, increasing the model resolution may pose difficulties in a pixel-by-pixel evaluation of the forecasts (e.g., Davis et al., 2006; Mass et al., 2002). Approaches that are more suitable for high-resolution rainfall fields range from simple visual comparisons to more sophisticated, object-oriented or filtering methods capable of representing spatiotemporal properties of the fields (e.g., Davis et al., 2006; Gilleland et al., 2009; Roberts and Lean, 2008). In this study, we applied visual comparisons and several numerical measures ~~for comparing~~to compare the ~~radar~~ observed radar QPE with the WRF-derived rain field.

3.5.1 Fractions ~~skill score~~Skill Score

To evaluate rainfall accumulation ~~at~~for different neighbourhood sizes (namely, spatial scales), we ~~use~~used the method suggested by Roberts and Lean (2008). The methodology includes a conversion of the continuous rain field to a binary field based on the exceedance of a given rain~~-~~-depth threshold. The fraction of model-output positive pixels (i.e~~.~~., pixels that have exceeded the threshold) within a certain neighbourhood size is then compared with the matching fraction from the radar~~-~~ QPE, through the ~~fractions skill score~~Fractions Skill Score (FSS) statistic (Supplementary material [S1]). When the forecast is perfect and unbiased, i.e., when an equal number of observed (in our case, radar) and forecasted (WRF) pixels exceed the threshold, ~~the~~ FSS~~=~~ = 1. If there is a bias, the FSS ~~would~~will tend asymptotically to a lower value. To quantitatively evaluate the model's ability to predict the observed rainfall above the selected threshold, within a close-enough distance, the uniform FSS (halfway between a random forecast and a perfect skill forecast, yielding a hit rate of 0.5; [S1]) is also calculated. An FSS ~~score~~that is larger than the uniform FSS is considered skilful. It is important to note that if the FSS exceeds the uniform FSS ~~at~~on too large a spatial scale ~~that is too large~~, the forecast might still be skilful, but it is not useful. We applied the FSS method to the cumulative rain field, comparing the radar ~~QPE~~QPEs and WRF rainfall output (Sect. 4.~~1.1~~3).

3.5.2 Structure~~-~~–amplitude~~-~~–location ~~(SAL)~~ analysis

To evaluate the characteristics of the WRF precipitation ~~forecasts~~forecast errors, we used the object-oriented structure~~-~~–amplitude~~-~~–location (SAL) analysis (Wernli et al., 2008) (Supplementary material [S2]). As in the FSS analysis, it was applied to the cumulative rain field. The SAL analysis splits the rain field into three distinct components and yields a skill score for the forecast of each of them; in each of the components, a zero score indicates a perfect forecast. The amplitude component (A) expresses the ~~model~~model's over/underestimation of the total rainfall for a specific rainstorm (with $A \in [-2,2]$, and $A = 1$ or $A = -1$ indicating over and underestimation by a factor of 3, respectively). The location component ($L \in [0,2]$) sums the differences between modelled and observed (~~a~~i) centre of mass of

Formatted: Font: (Default) Times New Roman, 10 pt, Italic, Complex Script Font: Times New Roman, 12 pt, (Complex) Arabic (Saudi Arabia), English (United Kingdom) precipitation and (~~b~~ii) average distance between the centre of mass and the location of precipitation objects that constitute the rain field (i.e., connected regions in which the cumulative rainfall exceeds 1/15 of the maximal cumulated value; Wernli et al., 2008). The structure component ($S \in [-2,2]$) quantifies the tendency of the forecasted precipitation objects to be either too smooth (positive values) or too noisy (negative values) ~~with respect~~relative to the observations.

3.5.3 Depth~~-~~–area~~-~~–duration curves

Areal rainfall amounts are crucial drivers of the ~~hydrologic~~hydrological response and are important for understanding rainfall structure and triggering mechanisms (e.g., Armon et al., 2018; Durrans et al., 2002; Kalma and Franks, 2003; Zepeda-Arce et al., 2000). To quantify and compare observed and simulated areal rainfall amounts, we used depth~~-~~–area~~-~~–duration (DAD) curves, which represent the areal extent ~~in~~for which given rainfall depths over given durations are exceeded (Zepeda-Arce et al., 2000).

3.5.4 Autocorrelation structure of rain fields

High-intensity, small-scale convective rain cells are among the main factors generating flash~~-~~ floods in small, mountainous and desert catchments (e.g., Armon et al., 2018; Doswell et al., 1996; Merz and Blöschl, 2003), and their fine spatiotemporal structure directly affects the potential of rain-gauge monitoring (Marra and Morin, 2018). To analyse the convective rain structure, we computed, from both the observed radar~~-~~ QPE and ~~from~~ the WRF output, the spatial autocorrelation structure of the maps containing convective elements using the methodology presented by Marra and Morin (2018)~~.~~ (an example is given in supplementary Fig. 1 [SF1]). We interpolated the radar ~~QPE~~ QPEs to 10-min ~~time~~ intervals to match the ~~model~~model's temporal resolution, and defined as convective rainfall fields all ~~the~~ rain maps in which at least one convective rain cell, defined as a connected region ≥3 km^2 with rain intensity exceeding 10 mm h^{-1} and including at least one pixel exceeding 25 mm h^{-1}, is observed (Marra and Morin, 2018). We computed the 2-D spatial autocorrelation function of the convective fields following the method in Nerini et al. (2017). A three-parameter exponential function (Eq. 1) was fitted to the 2-D spatial autocorrelation to quantify the correlation distance:

$$r(h) = ae^{-\left(\frac{h}{b}\right)^{c}}, \qquad (1)$$

Formatted: Right, Line spacing: 1.5 lines

where h is the lag distance, b is the correlation distance (the distance ~~in~~at which the correlation drops to $r = e^{-1}$), and a and c are the nugget and shape parameters of the curve, respectively. ~~Eq.~~Equation 1 results in an approximation of the 1-D autocorrelation function of convective rain fields. Spatial heterogeneity of the ~~of the~~ autocorrelation field is quantified by calculating the deviation of the 2-D autocorrelation field from isotropy, following the approach in Marra and Morin (2018). To that end, we defined the ellipticity of the 2-D autocorrelation as the ratio of the minor to major axis of the (approximated) ellipse encompassing the $r = e^{-1}$ region of the spatial autocorrelation field~~.~~ (Fig. SF1). The temporal autocorrelation is computed by converting the 2-D spatial domain to a 1-D array and adopting time as the second dimension, as proposed by Marra and Morin (2018). It is worth noting that the computed temporal correlation distance neglects advection (Eulerian perspective), and is therefore shorter than the correlation distance ~~one would obtain~~obtained in a Lagrangian perspective.

4~~.~~ Results

4.1 ~~Model skill~~Quasi-climatology of HPEs

~~4.1.1 Bias~~

~~Figure 3 shows~~Of the ~~rainfall accumulated throughout all HPEs as estimated by the weather radar, modelled by the WRF, and measured by rain gauges (Fig. 3a, b and d, respectively). The bias, defined here as the ratio between WRF rainfall and radar QPE, is shown in Fig. 3c. In 69% of the studied region, the bias lies between 3 and 1/3 while some areas show a strong positive bias (Fig. 3c). The three stations highlighted in the figure (the values shown for radar and WRF represent the average of the 9 pixels surrounding the gauge locations) show how this large bias is mostly caused by radar underestimation. In fact, these areas are generally located far from the radar or in the eastern portion of the radar coverage, where radar QPE suffers from range degradation and beam overshooting due to the presence of mountains. In other areas, the bias seems related to residual beam blockages. Bias smaller than 1 is also apparent in regions with ground clutters, and some spatial inconsistencies related to the interpolation of a few fully blocked beams can also be noticed. To avoid this radar estimation inaccuracies interfering with our results, hereinafter we focus only on the areas in which the bias lies between 3 and 1/3 (Fig. 3c).~~

~~4.1.2 Visual, neighbourhood and object-based evaluation of WRF model forecasts~~

~~Visual comparison of observed (radar) and simulated (WRF) rainfall fields yielded mostly (subjectively) good results in terms of the spatial rainfall patterns, such as widespread vs. localised rainfall (e.g., Fig. 4a-c, in which the first HPE in the list in Table S1 is shown). The spatial frequency is also generally well represented (Fig. 4d). At the same time, pixel-based comparisons are deemed inappropriate for such an analysis, as shown in the scatter plot (Fig 4e). These observations are true for most of the examined~~41 identified HPEs, ~~with the exception of two HPEs in which the WRF model clearly failed in representing the rainfall patters (e.g., one example in Fig. 5). Both these poorly simulated HPEs were characterised by relatively short total storm durations (1.7 and 2 days) just exceeding the durations that defined them as HPEs (6 h and 3-24 h, respectively). Synoptically they are classified as ARSTs, a system generally characterised by local, short living convection associated with localised rainfall triggering mechanism (Armon et al., 2018). Mesoscale models (e.g., WRF) skill is poorer in simulating this type of events, mainly due to their short predictability and stochastic nature (see e.g., Yano et al., 2018). Although a deeper understanding of these aspects can be beneficial for improving future simulations, it falls beyond the scope of this study and will need future dedicated research efforts.~~

~~The FSS of the first HPE (Fig. 4f) further manifests the accuracy of the simulated rainfall fields. The forecast has a larger FSS than the uniform FSS for all cumulative rainfall ≤50 mm, even at the model resolution (1 km). For larger cumulative rainfall (but <125 mm), the FSS is still higher than the uniform FSS, when spatially averaged (e.g., 40 km~~

~~averaging for cumulative rain of 100 mm). Only for the higher rainfall amounts, e.g., 125 mm, greater than 99% of pixels in this HPE, the model forecast is unskilled, i.e., the uniform FSS outperforms the WRF forecast FSS.~~

~~During EM rainstorms, cumulative rainfall values are distributed unevenly in space, and extremely high rainfall depths are embedded within the larger aerial coverage of lower rainfall depths (e.g., Armon et al., 2018; Dayan and Morin, 2006; Morin et al., 2007). Forecasting the spatial distribution (location and spatial frequency) of low cumulative rainfall is thus easier than forecasting the distribution of the high end of cumulative rainfall, even when averaging is conducted over large scales. The minimal scale (Roberts and Lean, 2008) at which the FSS of the model's forecast is higher than the uniform FSS was calculated for cumulative rainfall of 1–200 mm, for all of the identified HPEs (Fig. 6). This allows estimating the minimal scales for skilful forecasts for various cumulative rain depths. For example, the original model resolution yields a skilful forecast for cumulative rainfall depths of <25 mm in 50% of the HPEs (Fig. 6). The figure also shows that cumulative rainfall exceeding 45 mm, in most of the cases, are skilfully forecasted only at relatively large spatial scale (tens of kilometres).~~

~~The SAL analysis (Fig. 7) shows a good performance of the model, except for a substantial positive amplitude bias (inter-event amplitude component median = 0.80 [i.e. bias of 2.3, as defined above], interquartile range = 0.37–1.02). Two events stand out with a bias smaller than one; these are the abovementioned poorly simulated HPEs. The structure component is well modelled in most cases, showing the ability of the WRF to accurately generate precipitation objects (0.06 and −0.06 to +0.26, median and interquartile range, respectively). This is particularly important in regions and events where rainfall is generated through both convective and stratiform processes, or when intense rainfall is embedded within a larger-scale low intensity precipitation (Wernli et al., 2009).~~

~~Relatively low values of the location component (0.25 and 0.18–0.31, median and interquartile range, respectively) demonstrate the high capability of the model to spatially distribute precipitation objects. Medially, 34% of this component is composed of the error in the centre of mass location (i.e., a median error of 30 km in the location of the centre of mass), and the rest is from the average location of each precipitation object. Namely, the model prediction of the centre of mass of the rain field is quite satisfying, but the prediction of individual precipitation objects is poorer. Standing out with high location values (0.46 and 0.85) are the same two challenging HPEs, in which the model was unable to simulate the rainfall in a satisfying manner, yielding biases smaller than one and large spatial inconsistency with respect to observations (see above, e.g., Fig. 5).~~

~~The overall positive bias, seen in the amplitude component (Fig. 7), could result both from underestimation of the radar QPE or overestimation of the WRF simulations. Possible reasons leading to radar underestimation were discussed above, and may contribute to this bias even after the most severely biased regions have been masked. However, this positive bias still needs to be taken into account when addressing the actual cumulative rainfall amounts predicted by the model.~~

~~The overall good representation of precipitation objects implies that precipitation processes generated by the model represent actual processes and rainfall characteristics (Wernli et al., 2009).~~

~~4.2 Characterisation of rainfall patterns~~

~~4.2.1 General properties of HPEs~~

~~According to the definition applied in this study, a given event can be considered as HPE for more than one duration. This could happen when the thresholds associated with the selected durations (Sect. 3.3) are exceeded either at the same location or when they are exceeded in different regions. The durations associated with each HPE are listed in Table S1. The co-occurrence of each HPE-duration with the rest of the examined durations is shown on Fig. 8; these co-occurrence values are similar to values determined in the Alps by Panziera et al. (2018). For example, 79% of the HPEs at 24 h duration are also HPEs at 72 h duration. Fig. 8 indicates that there is a high dependency (i.e. co-occurrence) of the short-duration HPEs (3-12 h). Similarly, there is a high dependence within the long duration (24-72 h) HPEs. Nevertheless, even the shortest duration HPEs examined here, show a rather high co-occurrence with longest duration HPEs (probabilities in all cases ≥ 0.5).~~

35 occurred during MC synoptic prevalence and the rest during ARST prevalence. Despite the dependence of the identification ~~of HPEs depended~~ on the quality and availability of the radar data ~~and only 41 HPEs were available after quality check, this~~, our analysis can be considered ~~as "semi~~"quasi-climatological", as the selected HPEs do not exhibit obvious biases with respect to the rain climatology ~~of HPEs: (a)~~in the region: (i) their seasonality ~~is following~~follows the seasonal pattern of EM rainy days (Fig. ~~9~~3), although HPEs occur more frequently ~~during~~at the beginning of the winter, presumably due to the high sea surface temperatures; (~~b~~ii) HPEs are identified throughout the radar archive (with zero to seven HPEs per year); (~~c~~iii) the frequency of the prevailing synoptic circulation patterns during HPEs (Table S1) resembles the frequency observed ~~during~~on rainy days (Marra et al., 2019); and (~~d~~iv) HPEs characterised by ARST prevalence are common only during the transition seasons (Fig. ~~9~~3) (e.g., De Vries et al., 2013).

For most durations, rain amounts defining the HPEs are larger near the Mediterranean coast, extending a few kilometres off- and on-shore (Fig. 2). This resembles the observed pattern of high rain intensities near the coast, rather than inland (Karklinsky and Morin, 2006; Peleg and Morin, 2012; Sharon and Kutiel, 1986), also reported for extreme precipitation quantiles observed from both weather radar and satellite sensors (Marra et al., 2017). In contrast, short durations (<12 h) exhibit the highest rain intensities in the arid portions of the region. The frequency of rain in the arid areas is lower than in the rest of the region (Goldreich, 2012); thus, the 99.5% quantiles are based on fewer data. ~~Yet~~Nevertheless, the reported higher extreme rain amounts for shorter durations are in agreement with previous studies, which showed that highly localised convective rainfall is more common during HPEs in the desert than in other ~~climate~~climatic environments in the EM (Marra et al., 2017; Marra and Morin, 2015; Sharon, 1972). In the mountains, the opposite case is ~~the opposite~~seen; rainfall is produced more significantly through stratiform (or shallow convection) processes~~,~~ and~~,~~ therefore, rain amounts for short durations are relatively lower (Sharon and Kutiel, 1986). For the longer durations, rain intensities in the mountains are comparable to the intensities near the coast, probably resulting ~~probably~~ from the tendency of rain to persist in orography-affected regions (e.g., Panziera et al., 2015; Tarolli et al., 2012).

Affected by higher rain intensities, the centre of mass of the precipitation field for ~~all~~ each one of the HPEs is located near the EM coastline (Fig. ~~10~~4). Nevertheless, a seasonal pattern appears, with a general landward shift of the centre of mass during the rainy season (Fig. ~~10~~4). This is caused by land~~-~~–sea differential heating and heat capacities, and resembles the seasonal pattern of rain intensities in the EM (Goldreich, 1994; Sharon and Kutiel, 1986). In fact, this points out the observed preference of convective clouds to form above high-temperature surfaces, i.e., the sea surface or nearby coastal plains in autumn or early winter, and farther inland in the spring. The exact location of the centre of mass depends on the radar's ability ~~of the radar~~ to produce accurate ~~QPE~~QPEs over the region. Due to the range degradation typical ~~to~~of radar rainfall estimates, the centre of mass is biased towards the radar location. This is also confirmed ~~also~~ by the WRF results, showing a more widespread distribution of the centres of mass. In terms of seasonality, the simulated centres of mass exhibit a similar, even if slightly less obvious, landward pattern.

According to the definition applied in this study, a given event can be considered a HPE for more than one duration. This can happen when the thresholds associated with the selected durations (Sect. 3.3) are exceeded either at the same location, or when they are exceeded in different regions. The durations associated with each HPE are listed in Table S1. The co-occurrence of each HPE duration with the rest of the examined durations is shown in Fig. 5; these co-occurrence values are similar to values determined in the Alps by Panziera et al. (2018). For example, 79% of the HPEs at 24 h duration are also HPEs at 72 h duration. Figure 5 indicates a high dependence (i.e., co-occurrence) of the short-duration HPEs (3–12 h). Similarly, there is a high dependence within the long duration (24–72 h) HPEs. Nevertheless, even the shortest duration HPEs examined here show a rather high co-occurrence with the longest duration HPEs (probabilities in all cases ≥ 0.5).

4.2 Bias

Figure 6 shows the rainfall accumulated during all HPEs as estimated by the weather radar, modelled by the WRF, and measured by rain gauges (Fig. 6a, b and d, respectively). Bias, defined herein as the normalised difference between WRF rainfall and radar QPE ($\frac{WRF-radar}{radar}$), in percent, is shown in Fig. 6c. In 69% of the studied region, the bias lies between +200% and -67%, while some areas show a strong positive bias (Fig. 6c). The three stations highlighted in the figure (the values shown for radar and WRF represent the average of the 9 pixels surrounding the gauge locations) show how this large bias is mostly caused by radar underestimation. In fact, these areas are generally located far from the radar or in the eastern portion of the radar coverage, where radar QPE suffers from range degradation and beam overshoot due to the presence of mountains. In other areas, the bias seems related to residual beam blockages. Underestimation (bias < 0) is also apparent in regions with ground clutter, and some spatial inconsistencies related to the interpolation of a few fully blocked beams can also be noticed. To avoid interference of these radar estimation inaccuracies with our results, we focus only on the areas in which the bias lies between +200% and -67% (Fig. 6c).

4.3 Visual, neighbourhood and object-based evaluation of WRF model simulations

Visual comparison of observed (radar) and simulated (WRF) rainfall fields yielded mostly (subjectively) good results in terms of the spatial rainfall patterns, such as widespread vs. localised rainfall~~.~~. Figure 7 presents, as an example, a well-simulated HPE case (event #1, Table S1). In addition, the distributions of rainfall among pixels were generally well represented (Fig. 7d). At the same time, pixel-based comparisons were deemed inappropriate for such an analysis, as shown in the scatter plot (Fig. 7e). Most of the examined HPEs led to similar observations, with the exception of two HPEs in which the WRF model clearly failed to represent the rainfall patterns. An example of such a poor simulation is given in Fig. 8 (event #5, Table S1). Both of these poorly simulated HPEs were characterised by relatively short total storm durations (1.7 and 2 days), just exceeding the durations that defined them as HPEs (6 h and 3–24 h, respectively). Synoptically, they were classified as ARSTs, a system generally characterised by local, short-lived convection associated with a localised rainfall-triggering mechanism (Armon et al., 2018). The skill of mesoscale models (e.g., WRF) is poorer in simulating these types of events, mainly due to their short predictability and stochastic nature (see e.g., Yano et al., 2018). Although a deeper understanding of these aspects can be beneficial for improving future simulations, it falls outside the scope of this study and requires future dedicated research efforts.

The FSS of the first HPE (Fig. 7f) further manifests the accuracy of the simulated rainfall fields. The forecast has a larger FSS than the uniform FSS for all cumulative rainfall ≤50 mm, even at the model resolution (1 km). For larger cumulative rainfall (but <125 mm), the FSS is still higher than the uniform FSS, when spatially averaged (e.g., 40 km averaging for cumulative rain of 100 mm). It is only for the higher rainfall amounts, e.g., 125 mm, corresponding to less than 1% of the pixels in this HPE, that the model forecast is unskilled, i.e., the uniform FSS outperforms the WRF forecast FSS.

During EM rainstorms, cumulative rainfall values are distributed unevenly in space, and extremely high rainfall depths are embedded within the larger aerial coverage of lower rainfall depths (e.g., Armon et al., 2018; Dayan and Morin, 2006; Morin et al., 2007). Forecasting the spatial distribution (location and spatial frequency) of low cumulative rainfall is thus easier than forecasting the distribution of the high end of cumulative rainfall, even when averaging is conducted over large scales. The minimal scale (Roberts and Lean, 2008) at which the FSS of the model's forecast is higher than the uniform FSS was calculated for cumulative rainfall of 1–200 mm, for all of the identified HPEs (Fig. 9). This allows estimating the minimal scales for skilful forecasts for various cumulative rain depths. For example, the original model resolution yielded a skilful forecast for cumulative rainfall depths of <25 mm in 50% of the HPEs (Fig. 9). The figure also shows that cumulative rainfall exceeding 45 mm, in most cases, is skilfully forecasted only on a relatively large spatial scale (tens of kilometres). During ARSTs, the minimal scale was much higher than during MCs (not shown); however, it is important to remember that two of these HPEs were poorly simulated.

The SAL analysis (Fig. 10) showed good performance of the model, except for a substantial positive amplitude bias (inter-event amplitude component median = 0.80 [i.e. bias of 130%, as defined in Sect. 4.2], interquartile range = 0.37–1.02). Two events stood out with a bias smaller than zero; these were the abovementioned poorly simulated HPEs. The structure component was well modelled in most cases, showing the ability of the WRF to accurately generate precipitation objects (0.06 and -0.06 to +0.26, median and interquartile range, respectively). This is particularly important in regions and events where rainfall is generated through both convective and stratiform processes, or when intense rainfall is embedded within larger-scale low-intensity precipitation (Wernli et al., 2009). Relatively low values of the location component (0.25 and 0.18–0.31, median and interquartile range, respectively) demonstrate the model's high capability to spatially distribute precipitation objects. Medially, 34% of this component is composed of the error in the centre of mass location (i.e., a median error of 30 km in the location of the centre of mass), and the rest is from the average location of each precipitation object. Namely, the model prediction of the centre of mass of the rain field is quite satisfying, but the prediction of individual precipitation objects is poorer. Standing out with high location values (0.46 and 0.85) are the same two challenging ARST-type HPEs for which the model was unable to simulate the rainfall in a satisfying manner, yielding biases smaller than zero and large spatial inconsistency with respect to observations (see above, e.g., Fig. 8).

The overall positive bias seen in the amplitude component (Fig. 10) could result from underestimation of the radar QPE or overestimation of the WRF simulation. Possible reasons leading to radar underestimation were discussed above, and may contribute to this bias even after the most severely biased regions have been masked. However, this positive bias still needs to be considered when addressing the actual cumulative rainfall amounts predicted by the model.

The overall good representation of precipitation objects implies that precipitation processes generated by the model represent actual processes and rainfall characteristics (Wernli et al., 2009).

4.4 Characterisation of rainfall patterns

4.4.1 Areal rainfall

W~~e show in~~Figure ~~Fig.~~ 11 shows the depth-~~are~~area-duration (DAD) curves obtained from all ~~the~~ 41 HPEs for durations of 30 min, 6 h and 24 h from radar ~~QPE~~QPEs (Fig. 11a, c, and e, respectively) and WRF (Fig. 11b, d, and f, respectively). A major increase in cumulative rainfall with increased ~~durations~~duration is observed for both ~~for~~ the radar and ~~for the~~ WRF curves (Fig. 11g): e.g., based on the radar, an area of 10^3 km^2 is medially covered by 9 mm for a duration of 0.5 h, which increases to 35 mm and 60 mm for 6 and 24 h, respectively (corresponding values from the WRF-derived rainfall are 4, 25 and 50 mm). This increase could be explained by either ~~by~~ continuous rainfall~~,~~ or ~~by~~ frequent arrival of rain cells into the region. The latter increases the wet area and the cumulative rainfall in areas that have already experienced rainfall, and is a major characteristic of HPEs in the EM (e.g., Armon et al., 2018, 2019; Sharon, 1972). Furthermore, over the longer durations, this causes DAD curves for different events to be more similar to one another (e.g., Fig. 11e~~,~~ and f).

The inter-event spread and the difference in the DAD curves for MC and ARST (Fig. 11a~~-~~–f~~),~~) illustrate the various types of HPEs identified here. These types range between rainstorms exhibiting only a minimal increase in rainfall area ~~through~~with time, i.e~~.~~., almost all of the rainfall precipitates during a short period, and rainstorms composed of many rain cells passing through the same area, or long-lasting rainstorms. These results confirm previous findings by Armon et al. ~~(2018),~~(2018) based on a more limited number of events: HPEs classified as ARSTs (Table S1) tend to be of higher rain intensities for smaller regions and shorter periods than HPEs classified as MCs. MCs only exhibit higher rain intensities over larger regions and for longer durations.

~~I~~It is important to note the difference between radar~~-~~ QPE- and WRF-derived rainfall DAD curves. Higher rain values in the radar~~-~~ QPE over the range of smaller areas is the most obvious difference (Fig. 11g). Although these higher values may, at ~~a~~ first ~~sight, point out~~glance, indicate that the WRF is unable to reproduce the high-intensity rainfall of the HPEs in the EM, it should be ~~reminded~~remembered that at short durations, high~~-~~-intensity radar QPEs can be of lower accuracy due to contamination from residual ground clutter or hail. This may affect ~~more selectively~~ the QPEs of the smaller areas~~.~~ more selectively. For instance, for one of the HPEs, an area >100 km^2 has a rain amount ≥100 mm in 0.5 h (Fig. 11a), a value that exceeds the 200-~~yr~~year return period for the area (Morin et al., 2009). Other notable differences are some ARST-classified HPEs with WRF-derived DAD curves (Fig. 11b, d, and f~~),~~) consisting of the two WRF-unresolved HPEs mentioned above, and yielding a median ARST curve that is much lower than the radar-derived ~~curve~~one.

The reported differences between WRF- and radar-derived curves result in an overall greater area-over-threshold radar curves for the high~~-~~-rainfall thresholds, especially for the short durations. For long durations and low rainfall thresholds, the WRF area is larger (Fig. 11), reflecting the positive bias that is probably related to radar range degradation and beam ~~overshooting~~overshoot.

4.4.2~~.3~~ Autocorrelation structure of convective rainfall

HPEs in the EM are commonly composed of highly localised convective rain cells. This is well ~~shown by~~reflected in the sharp decrease of the 1-D autocorrelation describing the convective rain fields (Fig. 12a and b) obtained using all of the convective rain fields throughout the 41 HPEs (n~~=11731~~ = 11,731 snapshots for radar and n~~=14323~~ = 14,323 for WRF). The median decorrelation distance (defined as the distance in which the correlation drops to $r = e^{-1}$, i.e., ~~the~~ parameter b of the 1-D exponential fit [Eq. 1]) of all convective rain snapshots from the radar data is ~~~~~9 km ~~(~~~(7 km using the WRF~~-~~-derived rainfall) and ranges between 3 and 23 km (for the 10% and 90% quantiles, respectively; 2 and 20 km using WRF). The median decorrelation distance during ARSTs is shorter than during MCs, as obtained from both the radar (7 km and 10 km, respectively for ARSTs and MCs) and the WRF (5 km and 7 km, respectively). These values are comparable ~~with~~to previously reported observations (e.g., Ciach and Krajewski, 2006; Morin et al., 2003; Peleg and Morin, 2012; Villarini et al., 2008) and are somewhat larger than the reported values for the south-eastern part of the area by Marra and Morin (2018). However, it ~~must~~should be noted that Marra and Morin (2018) examined 1-min rainfall fields versus the 10-min fields examined here.

The median of the temporal decorrelation distance (Fig. 12c and d) ~~is~~was ~4 min (~14 min for the WRF~~)~~), and it ~~ranges~~ranged between <1 and 19 min (10% and 90% quantiles, respectively; 3 and 29 min using WRF). Despite agreeing with the results of Marra and Morin (2018), the exact temporal decorrelation distance is somewhat dubious, since it is shorter than the time~~-~~ step used for its calculation (10 min). For this reason, we do not report the small differences that exist between the two synoptic systems. The larger temporal correlation in the WRF-derived rainfall is expected, because radar QPE suffers from temporal inconsistencies (e.g., when a convective cell passes through a region with beam blockages). Nevertheless, such a short temporal decorrelation confirms the local and spotty nature of rainfall characterising HPEs in the region.

The declining pattern of the 1-D autocorrelation overlooks the 2-D spatial heterogeneity of the autocorrelation field. The ellipticity of the 2-D autocorrelation yielded a median value of 0.56 (0.~~58 for the WRF~~62 and 0.54 in ARST- and MC-type events, respectively), with a range of 0.33~~-~~–0.80 (10~~%-~~% –90% quantiles~~;~~). WRF-derived ellipticity values were almost the same: 0.58 (0.68 and 0.68 in ARST- and MC-type events, respectively), with a range of 0.33~~-~~–0.79 ~~using WRF).~~. These autocorrelation ellipses in the radar data were oriented 13° anti-clockwise from the ~~E-W~~east-west axis (median value~~) and 25~~; 7° and 14° for ARST- and MC-types, respectively) and 22° for the WRF ellipses~~, similarly~~ (10° and 24° for ARST- and MC-types, respectively). These values are similar to the orientation of radar rain cells ~~orientation~~ in the eastern part of the region (Belachsen et al., 2017), but somewhat different from the orientation of

Formatted: Font: (Default) Times New Roman, 10 pt, Italic, Complex Script Font: Times New Roman, 12 pt, (Complex) Arabic (Saudi Arabia), English (United Kingdom)

~~the~~ autocorrelation fields from the south-eastern part of the region (Marra and Morin, 2018). ~~This orientation represents~~Orientations found in the present analysis cover the ~~general alignment of rain cells during a HPE, accounting for cells during~~entire evolution of HPEs and thus include both south-west (mainly at the beginning of the ~~event (which probably tend to~~storm) and north-west (mainly at the ~~SW direction) and during its~~ end ~~(shifting towards NW).~~of the storm) alignments of rain cells. Therefore, they are oriented more anti-clockwise than the autocorrelation fields from the south-eastern part of the region (Marra and Morin, 2018), which commonly represents rainfall ~~during~~at the end of a rainstorm (Armon et al., 2019). Moreover, Marra and Morin (2018) examined 1-min snapshots while here, advection can play a role in the examined 10-min time interval. Finally, Marra and Morin (2018) analysed only 11 events, thus, inter-event variance may still play a large role in their results. The high agreement between modelled and observed rain field ellipticity and orientation also ~~demonstrate~~demonstrates the high skill of the WRF simulations ~~to~~in accurately ~~represent~~representing convection in the region and~~,~~ thus, ~~reproduce~~reproducing rain-cell properties.

5~~.~~ Discussion and summary

~~This work characterises rainfall patterns during 41 HPEs in the EM and evaluates the ability of a high-resolution WRF model to properly simulate their cumulative rain field, and their spatiotemporal behaviour, with a specific emphasis to their convective component. If this effort is successful it will open the way to downscaling of global climate projections into induced changes in rainfall patterns at a regional scale during HPEs, including the understanding of the strengths and weaknesses of the regional results.~~

T~~o overcome the diverse climatology of the EM, we identified HPEs using a~~This work characterises rainfall patterns during 41 HPEs in the EM and evaluates the ability of a high-resolution WRF model to properly simulate their cumulative rain field and spatiotemporal behaviour, with a specific emphasis on their convective component and the prevailing synoptic system. A successful outcome will open the way to downscaling global climate projections to induced changes in rainfall patterns on a regional scale during HPEs, with an understanding of the strengths and weaknesses of the regional results. However, it is important to note that identification of HPEs in global climate models constitutes yet another challenge (see discussions e.g. in Chan et al., 2018; Gómez-Navarro et al., 2019; Meredith et al., 2018).

To overcome the diverse climatology of the EM, we identified HPEs using pixel-based weather radar climatology. We used a uniquely long, quality-controlled and gauge-adjusted~~,~~ high-resolution weather radar archive to characterise the rainfall patterns. A convection-permitting high-resolution WRF model configuration was used to simulate the same HPEs and the results of this modelling effort were compared to the radar ~~QPE~~QPEs. For most of the 41 HPEs, model simulations ~~resulted in~~gave valuable results: using the ~~Fractions Skill Score~~FSS we ~~determine~~determined that (~~a~~i) WRF simulations are highly accurate for cumulative rainfall <25 mm (Fig. ~~6~~9; Sect. 4.~~1.2), (b) accumulations~~3), (ii) accumulation of >45 mm ~~produce~~produces variable results among different cases (Figs. ~~4, 5~~7, 8 and ~~6~~9; Sect. ~~4.1.2). I.e.,~~4.3). In other words, skilful results are gained if the model output is averaged over at least a few tens of kilometres. ~~Structure-Amplitude-Location~~SAL analysis of cumulative rainfall ~~shows~~showed that rainfall location and structure ~~are~~were correctly reproduced by the model and ~~is~~were similar to the ~~observed by the~~ weather radar data observations in 39 out of the 41 HPEs. Conversely, rainfall amplitude ~~is~~was highly (positively~~)~~) biased, with some of the bias likely ~~explained by~~due to radar underestimation; however, a model positive bias cannot be excluded.

In general, rain amounts forming HPEs are higher near the EM coastline with the ~~exceptions~~exception of (~~a~~i) short durations, for which the highest rain amounts are observed in the desert regions, and (~~b~~ii) the longer-duration HPEs, for which mountainous rain amounts are comparable to ~~the ones at~~those on the coast. Identified HPEs ~~occur~~occurred during the wet season (October~~-~~–April), ~~and,~~ primarily~~,~~ in November~~-~~–February. Their centre~~-~~ of~~-~~ mass ~~is~~was close to the Mediterranean coastline and ~~shifts~~shifted landward during the season. We analysed the areal distribution of rainfall at various durations, the autocorrelation structure of the convective rainfall fields and ~~depth-area-duration~~DAD curves, ~~obtaining~~to obtain quantitative information on the characteristics of the rainfall fields, ~~on~~ the ability of the WRF model to simulate them, and ~~on~~ the ~~processed~~processes generating them, such as the aggregation of small and short~~ living~~-lived rain cells to produce a HPE.

5.1 Spatial distribution of rain~~-~~ intensity thresholds defining HPEs

High~~-~~ intensity ~~thresholds~~ threshold-forming HPEs near the Mediterranean Sea (Fig. 2) are expected, because of its warm surface waters and high moisture fluxes~~, and~~; they are also apparent in other regions of the Mediterranean (e.g., Dayan et al., 2015; Ivatek-Šahdan et al., 2018; Khodayar et al., 2018; Pastor et al., 2002; Peleg et al., 2018; Tarolli et al., 2012). High rain intensities in the desert are somewhat more intriguing. For example, Warner (2004) mentioned that there are hither and tither observations of whether rain intensities in the desert ~~are~~being higher than in non-desert regions. An opposing trend between mean annual rainfall and short-duration rain intensities was also described by Sharon and Kutiel (1986) using rain gauges, and by Marra and Morin (2015) using both rain gauges and weather radar. This trend is related to the higher surface temperatures in desert regions, ~~that~~which may enhance convective activity (e.g., Peleg et al., 2018), ~~associated~~as well as to a deeper boundary layer (e.g., Gamo, 1996; Marsham et al., 2013) and ~~to~~ the ~~prevailing~~prevalence of rainfall from ~~ARSTs~~ARST circulation patterns, which generally cause higher rain intensities (Armon et al., 2018; Nicholson, 2011; Sharon and Kutiel, 1986; De Vries et al., 2013). Such a sharp spatial change in the climatology of the rain intensities defining HPEs ~~may~~can only be captured using high-resolution, high -spatiotemporal~~-~~ coverage data (such as the radar~~-~~ QPE presented here), and reproduced by high-resolution, convection-permitting models.

5.2 Multiple~~-~~ duration HPEs and their relation to flash floods

Mediterranean-climate, and~~,~~ even more~~,~~ so desert~~-~~ climate HPEs, can produce rain amounts of the same order of magnitude ~~of~~as the mean annual rainfall (e.g., Nicholson, 2011; Schick, 1988; Tarolli et al., 2012). Frequent co-occurrence of short- and long~~-~~ duration HPEs is thus to be expected, and dividing events into short versus long duration ~~HPEs~~ is not straightforward. However, our dataset comprises events ~~of~~with different characteristics: local and intense, as well as widespread; rainfall~~-~~ triggering mechanisms and potential ~~hydrologic~~hydrological impact can be quite different.

Zoccatelli et al. (2019) observed a relatively high correlation between rain depths over ~~a~~ catchments and unit peak discharge in catchment areas ranging between 13~~-~~ and 1232 km^2 ~~of~~in Mediterranean and desert environments in the

EM. In arid and semi-arid catchments, a high correlation was reported between the ~~storm~~storm's rain core, defined as the largest hourly intensity over a 9~~ ~~-km^2 area in the catchment, and the unit peak discharge. Floods in Mediterranean catchments were accompanied by larger rain depths (~52 mm) over longer durations (~1 day), compared to the desert catchments (~14 mm, ~7 h). Comparison of these values with the DAD curves in Fig. 11~~, show~~ shows that a portion of the ~~here~~HPEs analysed ~~HPEs~~here are prone to produce floods in smaller catchments and in ~~the ~~desert regions, while others could generate floods in larger catchments and in ~~the ~~Mediterranean climate ~~region~~regions. Specifically, the convective part of the rainstorm is known to generate the highest-magnitude floods, even ~~at the~~in Mediterranean climate areas (e.g., Rinat et al., 2018; Tarolli et al., 2012). The short spatiotemporal autocorrelation distances observed for the convective rain fields highlight, once again, the spottiness of HPE rainfall~~ of HPEs~~ in the EM region (Sharon, 1972), and ~~was~~were well-simulated by the WRF model (Fig. 12).

5.3 Identification and characterisation of HPEs using weather radar and high-resolution weather model

ARST synoptic circulation is often associated ~~to~~with flash floods in the desert part of the region (Ashbel, 1938; Kahana et al., 2002; Krichak et al., 1997), and its rainfall is commonly caused by mesoscale triggering of convection (Armon et al., 2018) and is therefore less predictable (e.g., Keil et al., 2014), as evident from this study as well (e.g., Fig. ~~.~~10-11). ARSTs are also characterised by smaller rain field autocorrelation distance (Fig. 12). It is thus crucial for future studies to understand the reasons for the poor modelling results observed ~~in two (of 41)~~with 2 of these ~~HPEs.~~41 HPEs. This is evident in the coarser model domains as well (SF2). Possible aspects to be inspected include the adopted parametrisation schemes (Table 1~~)~~)), but~~,~~ since we used~~ a~~ convection-permitting resolution, problems could arise from other issues. In particular, since errors in the moisture field tend to propagate ~~fast~~rapidly, the correct amount of moisture ~~should~~must be entered ~~to~~into the model in the correct location to properly reproduce rainfall ~~at~~on the mesoscale (e.g., Rostkier-Edelstein et al., 2014; Zhang et al., 2007). In this study, we used ERA-Interim reanalysis data (~80 km horizontal resolution), which may not be accurate enough to resolve some conditions, but is ~~at~~on the same scale as outputs of global climate ~~model~~models. Future studies should consider using higher~~-~~-resolution input data, such as the newly released ERA5 data (Hersbach, 2016).

Nonetheless, the autocorrelation structure of the rain fields was well simulated (Sect. 4.4.2). This suggests that even if an event is less predictable, some of the rainfall characteristics can still be simulated. This result is encouraging in terms of the use of convection-permitting models, e.g., in nowcasting, because it means that wind patterns (determining orientation and ellipticity) are well forecasted.

The use of a long record of radar ~~QPE~~QPEs enabled us to provide a high-resolution ~~semi~~quasi-climatological characterisation of the rainfall patterns during HPEs with a resolution and spatial coverage that cannot be achieved using rain gauges. However, rainfall characteristics could not be adequately retrieved in regions suffering from radar data~~ -~~-acquisition problems. ~~Despite this~~Nevertheless, the ~~resulted~~resultant skill of the WRF rainfall fields ~~support~~supports its use for representing HPEs in regions that are not well covered by radars. Since the analyses were performed in a region exhibiting a strong climatic gradient, we suggest that similar results ~~should ~~be obtained in other parts of the world, at least in areas characterised by similar climates.

N~~onetheless, the use of a deterministic convection-permitting model is still unsatisfactory in pinpointing the highest observed rain accumulations.~~The main added value of convection-permitting models is seen in area averages, rather than over small-scale regions (Roberts, 2008). Therefore, over large catchments (e.g., larger than a few hundred square kilometres, as suggested by the minimal scale presented in Fig. 9), their forecasts are expected to be relatively useful and accurate. Nonetheless, the use of a deterministic convection-permitting model is still unsatisfactory for pinpointing the highest observed rain accumulations. Although such models are becoming more common in weather and climate forecasting and research (Prein et al., 2015), they are still not adequate for short-term hydrological applications, such as flash~~-~~ flood predictions. The structure of the high cumulative ~~rain~~rainfall is predicted quite well. However, it still suffers from a positive bias, and is not exactly well located (e.g., Figs. ~~6~~9 and ~~7~~10). In order to provide better flood predictions, especially for small catchments and for flash flood generation controlled by infiltration-excess, there is a need for more structured approaches, such as ensemble forecasts and data assimilation of meteorological observations (e.g., Diomede et al., 2014; Gustafsson et al., 2018; Hamill et al., 2008; Rostkier-Edelstein et al., 2014). These would provide probabilistic (rather than deterministic) information, and could therefore account for the uncertainty characterising the location in high-resolution models (e.g., Alfieri et al., 2012; Vincendon et al., 2011).

Characterisation of rainfall patterns during HPEs has ~~a~~ special significance in the EM: on the one hand, the region suffers from a severe water shortage~~ and,~~; on the other~~ hand,~~, it is prone to devastating floods. Both are predicted to worsen in response to climate change (e.g., Alpert et al., 2002; Kelley et al., 2015; Sowers et al., 2010). Modelling could help ~~understanding~~understand the effects of climate change on these two aspects but, before assessing the projections for a change in rainfall patterns induced by climate change, we need to consider what aspects of these patterns are still not well~~-~~captured by weather models~~ at present. These aspects will thus be~~, posing a challenge ~~in~~for future predictions. For example, we showed here that rainfall during ARSTs is less adequately forecasted. These ARST HPEs are ~~notably~~ known to cause flash floods~~,~~ and, as ARSTs might be occurring more frequently due to global warming (Hochman et al., 2018b), this low predictability should be addressed.

The work presented ~~above~~herein is a step towards better understanding~~ of~~ rainfall patterns during HPEs in the EM, and we are currently extending the research to relate specific rainfall patterns ~~and~~to atmospheric conditions at ~~a~~ high-resolution, and to analyse how the predicted climate change will affect the ~~same~~ rainfall characteristics ~~we~~ outlined ~~above. An additional~~in this paper. Another research direction worth following ~~is to combine~~would involve combining our procedures with satellite-based climatology. However, to date, satellite products present ~~insufficient~~ temporal (≥ 0.5 h, mostly ≥~~ ~~3 h) and spatial (≥~~ ~~0.04°, mostly ≥~~ ~~0.25°) resolutions (e.g., Ashouri et al., 2015; Gehne et al., 2016) that are insufficient to adequately sample the fine~~-~~scale properties of convective rainfall fields, particularly in arid areas.

6~~.~~ Conclusions

This study presents the identification of HPEs using a weather radar. These HPEs were then simulated using a high-resolution ~~weather~~NWP model and evaluated, focusing on the spatiotemporal patterns of the rainfall fields. The main conclusions of this characterisation and evaluation are~~ summarised below~~:

- HPEs in the EM are common between October and April, and their occurrences are focused in November ~~-~~– February. ~~HPEs~~The HPEs' centre of mass is located near the Mediterranean coastline and moves landward during the rainy season.
- For most storm durations, the rain amounts forming HPEs (i.e., larger than 99.5% of all rainy hours) are higher near the Mediterranean coast. For short durations, the highest HPE rain amounts are located in the desert, and for long durations, mountainous and coastal regions exhibit similar values.
- ~~H~~PEs consist of small convective rain cells (spatial and temporal decorrelation of ~9 km and ~4 min, respectively) that form a highly variable rainy area over short durations. The size of the rainy region increases with duration and becomes more ~~homogenous~~homogeneous between events.
- C~~onvection~~A convection-permitting high-resolution WRF model can simulate most HPEs, apart from some of the shortest, most localised storms, associated mainly with ARSTs.
- Rainfall structure is well simulated. Nevertheless, it is slightly less variable than the observed ~~one~~structure, and is characterised by a significant positive bias in ~~the~~ rain volume. This can be, at least partially, attributed to radar underestimations.
- The location of rainfall is generally predicted properly, with the exception of the highest rainfall amounts: the minimal scale for forecasting total rainfall depths >25 mm is highly variable between events, and increases significantly for rainfall depths >45 mm.

U~~sing~~Use of a high-resolution weather model that can reproduce rainfall patterns ~~in times of~~during HPEs is of great importance in predicting the hydrometeorology of flood-producing rainstorms. However, these must be elaborated~~,~~ using, e.g.~~.~~,, ensemble runs of the model. Convection-permitting models may also help ~~in assessing~~assess changes in precipitation induced by climate change, although if ~~those~~they are composed of HPEs that are less~~-~~ skilfully predicted in present, they should be examined ~~cautiously~~with caution.

7~~.~~ Author ~~contribution~~contributions

MA and EM ~~conceptualise~~conceptualised this work. Data curation and formal analysis were performed by MA and FM. Funding ~~acquisition~~ was ~~made~~acquired by EM, YE, FM and DRE. ~~Supervision by~~ EM and YE~~.~~ supervised the work. MA wrote the original draft of this paper, which was reviewed and edited by all authors.

8~~.~~ Data availability

Rain gauge data were provided and pre-processed by the Israel Meteorological Service (~~www.ims.gov.il).~~https://ims.data.gov.il/; freely available in Hebrew only). Shacham radar data were provided by EMS-Mekorot projects (www.emsmekorotprojects.com)~~. ERA-Interim data were downloaded from the Research Data Archive at the National Center for Atmospheric Research, Computational and Information Systems Laboratory: European Centre for Medium-Range Weather Forecasts, 2012, updated monthly. ERA-Interim Project, Single Parameter 6-Hourly Surface Analysis and Surface Forecast Time Series: https://doi.org/10.5065/D64747WN. WRF namelist files are available upon request from the corresponding author.~~

). Corrected and gauge-adjusted data (Marra and Morin, 2015) are available in the form of images, through personal communication with the head of the Hydrometeorology lab at the Hebrew University of Jerusalem, Prof. Efrat Morin (efrat.morin@mail.huji.ac.il). ERA-Interim data were downloaded from the Research Data Archive at the National Center for Atmospheric Research, Computational and Information Systems Laboratory: European Centre for Medium-Range Weather Forecasts, 2012, updated monthly: ERA-Interim Project, Single Parameter 6-Hourly Surface Analysis and Surface Forecast Time Series (https://doi.org/10.5065/D64747WN). The WRF namelist.input file can be found in the supplementary data.

9~~.~~ Competing interests

The authors declare that they have no conflict of interest.

10~~.~~ Acknowledgments

This study is a contribution to the PALEX project "Paleohydrology and Extreme Floods from the Dead Sea ICDP Core", funded by the DFG (~~Grant~~grant no. BR2208/13-1/-2). It is also partially funded by the Israel Science Foundation (1069/18), the NSF–BSF (BSF 2016953), the Israel Ministry of Science and Technology (grant no. 61792), the Advanced School for Environmental Studies at the Hebrew University of Jerusalem, and the Israel Water Authority, and is a contribution to the HyMeX program. The authors thank Prof. Pinhas Alpert for the updated synoptic classification data.

11 References

Ahlborn, M., Armon, M., Ben Dor, Y., Neugebauer, I., Schwab, M. J., Tjallingii, R., Shoqeir, J. H., Morin, E., Enzel, Y. and Brauer, A.: Increased frequency of torrential rainstorms during a regional late Holocene eastern Mediterranean drought, Quat. Res., 89(2), 425–431, doi:10.1017/qua.2018.9, 2018.

Alfieri, L., Thielen, J. and Pappenberger, F.: Ensemble hydro-meteorological simulation for flash flood early detection in southern Switzerland, J. Hydrol., 424–425, 143–153, doi:10.1016/j.jhydrol.2011.12.038, 2012.

Alpert, P. and Shay-EL, Y.: The moisture Source for the Winter Cyclones in the Eastern Mediterranean, Isr. Meteorol. Res. Pap., 5, 20–27, 1994.

Alpert, P., Ben-Gai, T., Baharad, A., Benjamini, Y., Yekutieli, D., Colacino, M., Diodato, L., Ramis, C., Homar, V., Romero, R., Michaelides, S. and Manes, A.: The paradoxical increase of Mediterranean extreme daily rainfall in spite of decrease in total values, Geophys. Res. Lett., 29(11), 1536, doi:10.1029/2001GL013554, 2002.

Alpert, P., Osetinsky, I., Ziv, B. and Shafir, H.: Semi-objective classification for daily synoptic systems: Application to the eastern Mediterranean climate change, Int. J. Climatol., 24(8), 1001–1011, doi:10.1002/joc.1036, 2004.

Amponsah, W., Ayral, P. A., Boudevillain, B., Bouvier, C., Braud, I., Brunet, P., Delrieu, G., Didon-Lescot, J. F., Gaume, E., Lebouc, L., Marchi, L., Marra, F., Morin, E., Nord, G., Payrastre, O., Zoccatelli, D. and M., B.: Integrated high-resolution dataset of high intensity Euro-Mediterranean flash floods, Accept. Publ. Earth Syst. Sci. Data, 2018.

Anthes, R. A., Kuo, Y.-H., Baumhefner, D. P., Errico, R. M. and Bettge, T. W.: Predictability of Mesoscale Atmospheric Motions, Adv. Geophys., 28, 159–202, doi:10.1016/S0065-2687(08)60188-0, 1985.

Armon, M., Dente, E., Smith, J. A., Enzel, Y. and Morin, E.: Synoptic-scale control over modern rainfall and flood patterns in the Levant drylands with implications for past climates, J. Hydrometeorol., 19(6), 1077–1096, doi:10.1175/JHM-D-18-0013.1, 2018.

Armon, M., Morin, E. and Enzel, Y.: Overview of modern atmospheric patterns controlling rainfall and floods into the Dead Sea: Implications for the lake's sedimentology and paleohydrology, Quat. Sci. Rev., 216, 58–73, doi:10.1016/j.quascirev.2019.06.005, 2019.

Ashbel, D.: Great floods in Sinai Peninsula, Palestine, Syria and the Syrian Desert, and the influence of the Red Sea on their formation, Q. J. R. Meteorol. Soc., 64(277), 635–639, 1938.

Ashouri, H., Hsu, K. L., Sorooshian, S., Braithwaite, D. K., Knapp, K. R., Cecil, L. D., Nelson, B. R. and Prat, O. P.: PERSIANN-CDR: Daily precipitation climate data record from multisatellite observations for hydrological and climate studies, Bull. Am. Meteorol. Soc., 96(1), 69–83, doi:10.1175/BAMS-D-13-00068.1, 2015.

Ban, N., Schmidli, J. and Schär, C.: Evaluation of the convection-resolving regional climate modeling approach in decade-long simulations, J. Geophys. Res., 119(13), 7889–7907, doi:10.1002/2014JD021478, 2014.

Belachsen, I., Marra, F., Peleg, N. and Morin, E.: Convective rainfall in a dry climate: Relations with synoptic systems and flash-flood generation in the Dead Sea region, Hydrol. Earth Syst. Sci., 21(10), 5165–5180, doi:10.5194/hess-21-5165-2017, 2017.

Bližňák, V., Kašpar, M. and Müller, M.: Radar-based summer precipitation climatology of the Czech Republic, Int. J. Climatol., 38(2), 677–691, doi:10.1002/joc.5202, 2018.

Bloschl, G. and Sivapalan, M.: Scale Issues in Hydrological Modelling: a Review, Hydrol. Process., 9, 251–2901 [online] Available from: papers2://publication/uuid/EB5C42FF-17C4-4FF1-8216-E985A0ED7C96, 1995.

Bogaard, T. A. and Greco, R.: Landslide hydrology: from hydrology to pore pressure, Wiley Interdiscip. Rev. Water, 3(3), 439–459, doi:10.1002/wat2.1126, 2016.

Borga, M. and Morin, E.: Characteristics of Flash Flood Regimes in the Mediterranean Region, in Storminess and Environmental Change Climate Forcing and Responses in the Mediterranean Region, edited by N. Diodato and G. Bellocchi, pp. 65–76, Springer Netherlands, Dordrecht., 2014.

Borga, M., Boscolo, P., Zanon, F. and Sangati, M.: Hydrometeorological Analysis of the 29 August 2003 Flash Flood in the Eastern Italian Alps, J. Hydrometeorol., 8(5), 1049–1067, doi:10.1175/JHM593.1, 2007.

Borga, M., Anagnostou, E. N., Blöschl, G. and Creutin, J. D.: Flash flood forecasting, warning and risk management: The HYDRATE project, Environ. Sci. Policy, 14(7), 834–844, doi:10.1016/j.envsci.2011.05.017, 2011.

Borga, M., Stoffel, M., Marchi, L., Marra, F. and Jakob, M.: Hydrogeomorphic response to extreme rainfall in headwater systems: Flash floods and debris flows, J. Hydrol., 518(PB), 194–205, doi:10.1016/j.jhydrol.2014.05.022, 2014.

Cassola, F., Ferrari, F. and Mazzino, A.: Numerical simulations of Mediterranean heavy precipitation events with the WRF model: A verification exercise using different approaches, Atmos. Res., 164–165, 210–225, doi:10.1016/j.atmosres.2015.05.010, 2015.

Chan, S. C., Kendon, E. J., Roberts, N., Blenkinsop, S. and Fowler, H. J.: Large-scale predictors for extreme hourly precipitation events in convection-permitting climate simulations, J. Clim., 31(6), 2115–2131, doi:10.1175/JCLI-D-17-0404.1, 2018.

Ciach, G. J. and Krajewski, W. F.: Analysis and modeling of spatial correlation structure in small-scale rainfall in Central Oklahoma, Adv. Water Resour., 29(10), 1450–1463, doi:10.1016/j.advwatres.2005.11.003, 2006.

Collier, C. G.: Flash flood forecasting: What are the limits of predictability?, Q. J. R. Meteorol. Soc., 133(622), 3–23, doi:10.1002/qj.29, 2007.

Cristiano, E., ten Veldhuis, M.-C. and van de Giesen, N.: Spatial and temporal variability of rainfall and their effects on hydrological response in urban areas -- a review, Hydrol. Earth Syst. Sci., 21(7), 3859–3878, doi:10.5194/hess-21-3859-2017, 2017.

Davis, C., Brown, B. and Bullock, R.: Object-Based Verification of Precipitation Forecasts. Part I: Methodology and Application to Mesoscale Rain Areas, Mon. Weather Rev., 134(7), 1772–1784, doi:10.1175/MWR3145.1, 2006.

Dayan, U. and Morin, E.: Flash flood – producing rainstorms over the Dead Sea: A review, New Front. Dead Sea Paleoenviron. Res. Geol. Soc. Am. Spec. Pap., 401(04), 53–62, doi:10.1130/2006.2401(04)., 2006.

Dayan, U., Ziv, B., Margalit, A., Morin, E. and Sharon, D.: A severe autumn storm over the Middle-East: Synoptic and mesoscale convection analysis, Theor. Appl. Climatol., 69(1–2), 103–122, doi:10.1007/s007040170038, 2001.

Dayan, U., Nissen, K. and Ulbrich, U.: Review Article: Atmospheric conditions inducing extreme precipitation over the eastern and western Mediterranean, Nat. Hazards Earth Syst. Sci., 15(11), 2525–2544, doi:10.5194/nhess-15-2525-2015, 2015.

Dee, D. P., Uppala, S. M., Simmons, A. J., Berrisford, P., Poli, P., Kobayashi, S., Andrae, U., Balmaseda, M. A., Balsamo, G., Bauer, P., Bechtold, P., Beljaars, A. C. M., van de Berg, L., Bidlot, J., Bormann, N., Delsol, C., Dragani, R., Fuentes, M., Geer, A. J., Haimberger, L., Healy, S. B., Hersbach, H., Hólm, E. V., Isaksen, L., Kållberg, P., Köhler, M., Matricardi, M., McNally, A. P., Monge-Sanz, B. M., Morcrette, J.-J., Park, B.-K., Peubey, C., de Rosnay, P., Tavolato, C., Thépaut, J.-N. and Vitart, F.: The ERA-Interim reanalysis: configuration and performance of the data assimilation system, Q. J. R. Meteorol. Soc., 137(656), 553–597, doi:10.1002/qj.828, 2011.

Deng, L., McCabe, M. F., Stenchikov, G., Evans, J. P. and Kucera, P. a.: Simulation of Flash-Flood-Producing Storm Events in Saudi Arabia Using the Weather Research and Forecasting Model, J. Hydrometeorol., 16(2), 615–630, doi:10.1175/JHM-D-14-0126.1, 2015.

Diomede, T., Marsigli, C., Montani, A., Nerozzi, F. and Paccagnella, T.: Calibration of limited-area ensemble precipitation forecasts for hydrological predictions, Mon. Weather Rev., 142(6), 2176–2197, doi:10.1175/MWR-D-13-00071.1, 2014.

Doswell, C. A., Brooks, H. E. and Maddox, R. A.: Flash Flood Forecasting: An Ingredients-Based Methodology, Weather Forecast., 11(December 96), 560–581, doi:10.1175/1520-0434(1996)011<0560:FFFAIB>2.0.CO;2, 1996.

Drobinski, P., Ducrocq, V., Alpert, P., Anagnostou, E., Béranger, K., Borga, M., Braud, I., Chanzy, A., Davolio, S., Delrieu, G., Estournel, C., Boubrahmi, N. F., Font, J., Grubišić, V., Gualdi, S., Homar, V., Ivančan-Picek, B., Kottmeier, C., Kotroni, V., Lagouvardos, K., Lionello, P., Llasat, M. C., Ludwig, W., Lutoff, C., Mariotti, A., Richard, E., Romero, R., Rotunno, R., Roussot, O., Ruin, I., Somot, S., Taupier-Letage, I., Tintore, J., Uijlenhoet, R. and

Wernli, H.: HyMeX: A 10-Year Multidisciplinary Program on the Mediterranean Water Cycle, Bull. Am. Meteorol. Soc., 95(7), 1063–1082, doi:10.1175/BAMS-D-12-00242.1, 2014.

Durrans, S. R., Julian, L. T. and Yekta, M.: Estimation of Depth-Area Relationships using Radar-Rainfall Data, J. Hydrol. Eng., 7(5), 356–367, doi:10.1061/(ASCE)1084-0699(2002)7:5(356), 2002.

Easterling, D. R., Evans, J. L., Groisman, P. Y., Karl, T. R., Kunkel, K. E. and Ambenje, P.: Observed variability and trends in extreme climate events: A brief review, Bull. Am. Meteorol. Soc., 81(3), 417–425, doi:10.1175/1520-0477(2000)081<0417:OVATIE>2.3.CO;2, 2000.

El-Samra, R., Bou-Zeid, E. and El-Fadel, M.: To what extent does high-resolution dynamical downscaling improve the representation of climatic extremes over an orographically complex terrain?, Theor. Appl. Climatol., doi:10.1007/s00704-017-2273-8, 2017.

Enzel, Y., Amit, R., Dayan, U., Crouvi, O., Kahana, R., Ziv, B. and Sharon, D.: The climatic and physiographic controls of the eastern Mediterranean over the late Pleistocene climates in the southern Levant and its neighboring deserts, Glob. Planet. Change, 60, 165–192, doi:10.1016/j.gloplacha.2007.02.003, 2008.

Farhan, Y. and Anbar, A.: Fragile Landscape : Impact and Consequences of May 2014 Flash-flood Disaster in the Aqaba Area, Southern Jordan, Res. J. Environ. Earth Sci., 6(9), 451–465, 2014.

Flaounas, E., Kotroni, V., Lagouvardos, K., Gray, S. L., Rysman, J. F. and Claud, C.: Heavy rainfall in Mediterranean cyclones. Part I: contribution of deep convection and warm conveyor belt, Clim. Dyn., 50(7–8), 2935–2949, doi:10.1007/s00382-017-3783-x, 2018.

Flaounas, E., Fita, L., Lagouvardos, K. and Kotroni, V.: Heavy rainfall in Mediterranean cyclones, Part II: Water budget, precipitation efficiency and remote water sources, Clim. Dyn., 0(0), 0, doi:10.1007/s00382-019-04639-x, 2019.

Fosser, G., Khodayar, S. and Berg, P.: Benefit of convection permitting climate model simulations in the representation of convective precipitation, Clim. Dyn., 44(1–2), 45–60, doi:10.1007/s00382-014-2242-1, 2014.

Gamo, M.: Thickness of the dry convection and large-scale subsidence above deserts, Boundary-Layer Meteorol., 79(3), 265–278, doi:10.1007/BF00119441, 1996.

Gehne, M., Hamill, T. M., Kiladis, G. N. and Trenberth, K. E.: Comparison of global precipitation estimates across a range of temporal and spatial scales, J. Clim., 29(21), 7773–7795, doi:10.1175/JCLI-D-15-0618.1, 2016.

Gilleland, E., Ahijevych, D., Brown, B. G., Casati, B. and Ebert, E. E.: Intercomparison of Spatial Forecast Verification Methods, Weather Forecast., 24(5), 1416–1430, doi:10.1175/2009WAF2222269.1, 2009.

Giorgi, F. and Lionello, P.: Climate change projections for the Mediterranean region, Glob. Planet. Change, 63(2–3), 90–104, doi:10.1016/j.gloplacha.2007.09.005, 2008.

Goldreich, Y.: The spatial distribution of annual rainfall in Israel - a review, Theor. Appl. Climatol., 50(1–2), 45–59, doi:10.1007/BF00864902, 1994.

Goldreich, Y.: The climate of Israel: observation, research and application, Springer Science & Business Media., 2012.

Goldreich, Y., Mozes, H. and Rosenfeld, D.: Radar analysis of cloud systems and their rainfall yield in Israel, Isr. J. Earth Sci., 53(2), 63–76, doi:10.1560/G68K-30MN-D5V0-KUHU, 2004.

Gómez-Navarro, J. J., Raible, C. C., García-Valero, J. A., Messmer, M., Montávez, J. P. and Martius, O.: Event selection for dynamical downscaling: a neural network approach for physically-constrained precipitation events, Clim. Dyn., doi:10.1007/s00382-019-04818-w, 2019.

Gustafsson, N., Janjić, T., Schraff, C., Leuenberger, D., Weissmann, M., Reich, H., Brousseau, P., Montmerle, T., Wattrelot, E., Bučánek, A., Mile, M., Hamdi, R., Lindskog, M., Barkmeijer, J., Dahlbom, M., Macpherson, B., Ballard, S., Inverarity, G., Carley, J., Alexander, C., Dowell, D., Liu, S., Ikuta, Y. and Fujita, T.: Survey of data assimilation methods for convective-scale numerical weather prediction at operational centres, Q. J. R. Meteorol. Soc., 144(713), 1218–1256, doi:10.1002/qj.3179, 2018.

Hahmann, A. N., Rostkier-Edelstein, D., Warner, T. T., Vandenberghe, F., Liu, Y., Babarsky, R. and Swerdlin, S. P.: A reanalysis system for the generation of mesoscale climatographies, J. Appl. Meteorol. Climatol., 49(5), 954–972, doi:10.1175/2009JAMC2351.1, 2010.

Hamill, T. M., Hagedorn, R. and Whitaker, J. S.: Probabilistic forecast calibration using ECMWF and GFS ensemble reforecasts. Part II: Precipitation, Mon. Weather Rev., 136(7), 2620–2632, doi:10.1175/2007MWR2411.1, 2008.

Hersbach, H.: The ERA5 Atmospheric Reanalysis., AGU Fall Meet. Abstr., 2016.

Hochman, A., Mercogliano, P., Alpert, P., Saaroni, H. and Bucchignani, E.: High-resolution projection of climate change and extremity over Israel using COSMO-CLM, Int. J. Climatol., (January), 1–12, doi:10.1002/joc.5714, 2018a.

Hochman, A., Harpaz, T., Saaroni, H. and Alpert, P.: The seasons' length in 21st century CMIP5 projections over the eastern Mediterranean, Int. J. Climatol., (December 2017), 1–11, doi:10.1002/joc.5448, 2018b.

Hochman, A., Kunin, P., Alpert, P., Harpaz, T., Saaroni, H. and Rostkier-edelstein, D.: Statistical downscaling of seasonal precipitation over Israel for the 21st century, using CMIP5 projections, Int. J. Climatol., in rev., 2019.

Iacono, M. J., Delamere, J. S., Mlawer, E. J., Shephard, M. W., Clough, S. A. and Collins, W. D.: Radiative forcing by long-lived greenhouse gases: Calculations with the AER radiative transfer models, J. Geophys. Res. Atmos., 113(D13), doi:10.1029/2008JD009944, 2008.

Israel, A. of: The new Atlas of Israel: the national atlas, Survey of Israel ; The Hebrew University of Jerusalem, Jerusalem., 2011.

Ivatek-Šahdan, S., Stanešić, A., Tudor, M., Odak Plenković, I. and Janeković, I.: Impact of SST on heavy rainfall events on eastern Adriatic during SOP1 of HyMeX, Atmos. Res., 200(September 2017), 36–59, doi:10.1016/j.atmosres.2017.09.019, 2018.

Janjić, Z. I.: The Step-Mountain Eta Coordinate Model: Further Developments of the Convection, Viscous Sublayer, and Turbulence Closure Schemes, Mon. Weather Rev., 122(5), 927–945, doi:10.1175/1520-0493(1994)122<0927:TSMECM>2.0.CO;2, 1994.

Kahana, R., Ziv, B., Enzel, Y. and Dayan, U.: Synoptic climatology of major floods in the Negev Desert, Israel, Int. J. Climatol., 22(7), 867–882, doi:10.1002/joc.766, 2002.

Kalma, J. D. and Franks, S. W.: Rainfall in arid and semi-arid regions, in Understanding Water in a Dry Environment, edited by I. Simmers, pp. 15–64, Taylor & Francis., 2003.

Karklinsky, M. and Morin, E.: Spatial characteristics of radar-derived convective rain cells over southern Israel, Meteorol. Zeitschrift, 15(5), 513–520, doi:10.1127/0941-2948/2006/0153, 2006.

Keil, C., Heinlein, F. and Craig, G. C.: The convective adjustment time-scale as indicator of predictability of

convective precipitation, Q. J. R. Meteorol. Soc., 140(679), 480–490, doi:10.1002/qj.2143, 2014.
Kelley, C. P., Mohtadi, S., Cane, M. A., Seager, R. and Kushnir, Y.: Climate change in the Fertile Crescent and implications of the recent Syrian drought, Proc. Natl. Acad. Sci., 112(11), 3241–3246, doi:10.1073/pnas.1421533112, 2015.
Kendon, E. J., Roberts, N. M., Fowler, H. J., Roberts, M. J., Chan, S. C. and Senior, C. A.: Heavier summer downpours with climate change revealed by weather forecast resolution model, Nat. Clim. Chang., 4(7), 570–576, doi:10.1038/nclimate2258, 2014.
Khodayar, S., Fosser, G., Berthou, S., Davolio, S., Drobinski, P., Ducrocq, V., Ferretti, R., Nuret, M., Pichelli, E., Richard, E. and Bock, O.: A seamless weather–climate multi-model intercomparison on the representation of a high impact weather event in the western Mediterranean: HyMeX IOP12, Q. J. R. Meteorol. Soc., 142(April 2015), 433–452, doi:10.1002/qj.2700, 2016.
Khodayar, S., Kalthoff, N. and Kottmeier, C.: Atmospheric conditions associated with heavy precipitation events in comparison to seasonal means in the western mediterranean region, Clim. Dyn., 51(3), 951–967, doi:10.1007/s00382-016-3058-y, 2018.
Kidd, C., Becker, A., Huffman, G. J., Muller, C. L., Joe, P., Skofronick-Jackson, G. and Kirschbaum, D. B.: So, how much of the Earth's surface is covered by rain gauges?, Bull. Am. Meteorol. Soc., 98(1), 69–78, doi:10.1175/BAMS-D-14-00283.1, 2017.
Krichak, S. O., Alpert, P. and Krishnamurti, T. N.: Interaction of topography and tropospheric flow - A possible generator for the Red Sea Trough?, Meteorol. Atmos. Phys., 63(3–4), 149–158, doi:10.1007/BF01027381, 1997.
Krichak, S. O., Tsidulko, M. and Alpert, P.: November 2, 1994, severe storms in the southeastern Mediterranean, Atmos. Res., 53(1–3), 45–62, doi:10.1016/S0169-8095(99)00045-9, 2000.
Kushnir, Y., Dayan, U., Ziv, B., Morin, E. and Enzel, Y.: Climate of the Levant: phenomena and mechanisms, in Quaternary of the Levant: environments, climate change, and humans, edited by Y. Enzel and B.-Y. Ofer, pp. 31–44, Cambridge University Press, Cambridge, UK., 2017.
Maraun, D., Wetterhall, F., Chandler, R. E., Kendon, E. J., Widmann, M., Brienen, S., Rust, H. W., Sauter, T., Themeßl, M., Venema, V. K. C., Chun, K. P., Goodess, C. M., Jones, R. G., Onof, C., Vrac, M. and Thiele-Eich, I.: Precipitation downscaling under climate change: Recent developements to bridge the gap between dynamical models and the end user, Rev. Geophys., 48(2009RG000314), 1–38, doi:10.1029/2009RG000314.1.INTRODUCTION, 2010.
Marra, F. and Morin, E.: Use of radar QPE for the derivation of Intensity–Duration–Frequency curves in a range of climatic regimes, J. Hydrol., 531, 427–440, doi:10.1016/j.jhydrol.2015.08.064, 2015.
Marra, F. and Morin, E.: Autocorrelation structure of convective rainfall in semiarid-arid climate derived from high-resolution X-Band radar estimates, Atmos. Res., 200(September 2017), 126–138, doi:10.1016/j.atmosres.2017.09.020, 2018.
Marra, F., Morin, E., Peleg, N., Mei, Y. and Anagnostou, E. N.: Intensity-duration-frequency curves from remote sensing rainfall estimates: comparing satellite and weather radar over the eastern Mediterranean, Hydrol. Earth Syst. Sci., 21(5), 2389–2404, doi:10.5194/hess-21-2389-2017, 2017.
Marra, F., Zoccatelli, D., Armon, M. and Morin, E.: A simplified MEV formulation to model extremes emerging from

multiple nonstationary underlying processes, Adv. Water Resour., 127(March), 280–290, doi:10.1016/j.advwatres.2019.04.002, 2019.

Marsham, J. H., Hobby, M., Allen, C. J. T., Banks, J. R., Bart, M., Brooks, B. J., Cavazos-Guerra, C., Engelstaedter, S., Gascoyne, M., Lima, A. R., Martins, J. V, McQuaid, J. B., O'Leary, A., Ouchene, B., Ouladichir, A., Parker, D. J., Saci, A., Salah-Ferroudj, M., Todd, M. C. and Washington, R.: Meteorology and dust in the central Sahara: Observations from Fennec supersite-1 during the June 2011 Intensive Observation Period, J. Geophys. Res. Atmos., 118(10), 4069–4089, doi:10.1002/jgrd.50211, 2013.

Mass, C. F., Ovens, D., Westrick, K. and Colle, B. A.: Does Increasing Horizontal Resolution Produce More Skillful Forecasts?, Bull. Am. Meteorol. Soc., 83(3), 407–430, doi:10.1175/1520-0477(2002)083<0407:DIHRPM>2.3.CO;2, 2002.

Meredith, E. P., Rust, H. W. and Ulbrich, U.: A classification algorithm for selective dynamical downscaling of precipitation extremes, Hydrol. Earth Syst. Sci., 22(8), 4183–4200, doi:10.5194/hess-22-4183-2018, 2018.

Merz, R. and Blöschl, G.: A process typology of regional floods, Water Resour. Res., 39(12), 1–20, doi:10.1029/2002WR001952, 2003.

Morin, E. and Gabella, M.: Radar-based quantitative precipitation estimation over Mediterranean and dry climate regimes, J. Geophys. Res., 112(D20), D20108, doi:10.1029/2006JD008206, 2007.

Morin, E., Krajewski, W. F., Goodrich, D. C., Gao, X. and Sorooshian, S.: Estimating Rainfall Intensities from Weather Radar Data: The Scale-Dependency Problem, J. Hydrometeorol., 4(5), 782–797, doi:10.1175/1525-7541(2003)004<0782:ERIFWR>2.0.CO;2, 2003.

Morin, E., Harats, N., Jacoby, Y., Arbel, S., Getker, M., Arazi, A., Grodek, T., Ziv, B. and Dayan, U.: Studying the extremes: hydrometeorological investigation of a flood-causing rainstorm over Israel, Adv. Geosci., 12, 107–114, doi:10.5194/adgeo-12-107-2007, 2007.

Morin, E., Jacoby, Y., Navon, S. and Bet-Halachmi, E.: Towards flash-flood prediction in the dry Dead Sea region utilizing radar rainfall information, Adv. Water Resour., 32(7), 1066–1076, doi:10.1016/j.advwatres.2008.11.011, 2009.

Morin, E., Marra, F. and Armon, M.: Dryland Precipitation Climatology from Satellite Observations, in Satellite Precipitation Measurement, edited by V. Levizzani, C. Kidd, D. Kirschbaum, C. Kummerow, and F. J. Turk, Springer., 2019.

Nasta, P., Adane, Z., Lock, N., Houston, A. and Gates, J. B.: Links between episodic groundwater recharge rates and rainfall events classified according to stratiform-convective storm scoring: A plot-scale study in eastern Nebraska, Agric. For. Meteorol., 259(February), 154–161, doi:10.1016/j.agrformet.2018.05.003, 2018.

Nerini, D., Besic, N., Sideris, I., Germann, U. and Foresti, L.: A non-stationary stochastic ensemble generator for radar rainfall fields based on the short-space Fourier transform, Hydrol. Earth Syst. Sci., 21(6), 2777–2797, doi:10.5194/hess-21-2777-2017, 2017.

Nicholson, S. E.: Dryland climatology, Cambridge University Press, New York., 2011.

Nuissier, O., Joly, B., Joly, A., Ducrocq, V. and Arbogast, P.: A statistical downscaling to identify the large-scale circulation patterns associated with heavy precipitation events over southern France, Q. J. R. Meteorol. Soc., 137(660), 1812–1827, doi:10.1002/qj.866, 2011.

Panziera, L., James, C. N. and Germann, U.: Mesoscale organization and structure of orographic precipitation producing flash floods in the Lago Maggiore region, Q. J. R. Meteorol. Soc., 141(686), 224–248, doi:10.1002/qj.2351, 2015.

Panziera, L., Gabella, M., Germann, U. and Martius, O.: A 12-year radar-based climatology of daily and sub-daily extreme precipitation over the Swiss Alps, Int. J. Climatol., 38(10), 3749–3769, doi:10.1002/joc.5528, 2018.

Pastor, F., Estrela, M. J., Peñarrocha, D. and Millán, M. M.: Torrential Rains on the Spanish Mediterranean Coast: Modeling the Effects of the Sea Surface Temperature, J. Appl. Meteorol., 40(7), 1180–1195, doi:10.1175/1520-0450(2001)040<1180:trotsm>2.0.co;2, 2002.

Peleg, N. and Morin, E.: Convective rain cells: Radar-derived spatiotemporal characteristics and synoptic patterns over the eastern Mediterranean, J. Geophys. Res. Atmos., 117(15), 1–17, doi:10.1029/2011JD017353, 2012.

Peleg, N., Morin, E., Gvirtzman, H. and Enzel, Y.: Rainfall, spring discharge and past human occupancy in the Eastern Mediterranean, Clim. Change, 112(3–4), 769–789, doi:10.1007/s10584-011-0232-4, 2012.

Peleg, N., Marra, F., Fatichi, S., Molnar, P., Morin, E., Sharma, A. and Burlando, P.: Intensification of convective rain cells at warmer temperatures observed from high-resolution weather radar data, J. Hydrometeorol., JHM-D-17-0158.1, doi:10.1175/JHM-D-17-0158.1, 2018.

Prein, A. F., Langhans, W., Fosser, G., Ferrone, A., Ban, N., Goergen, K., Keller, M., Tölle, M., Gutjahr, O., Feser, F., Brisson, E., Kollet, S., Schmidli, J., Van Lipzig, N. P. M. and Leung, R.: A review on regional convection-permitting climate modeling: Demonstrations, prospects, and challenges, Rev. Geophys., 53(2), 323–361, doi:10.1002/2014RG000475, 2015.

Raveh-Rubin, S. and Wernli, H.: Large-scale wind and precipitation extremes in the Mediterranean: a climatological analysis for 1979-2012, Q. J. R. Meteorol. Soc., (June 2013), n/a-n/a, doi:10.1002/qj.2531, 2015.

Rinat, Y., Marra, F., Zoccatelli, D. and Morin, E.: Controls of flash flood peak discharge in Mediterranean basins and the special role of runoff-contributing areas, J. Hydrol., 565(April), 846–860, doi:10.1016/j.jhydrol.2018.08.055, 2018.

Roberts, N.: Assessing the spatial and temporal variation in the skill of precipitation forecasts from an NWP model, in Meteorological Applications, vol. 15, pp. 163–169., 2008.

Roberts, N. M. and Lean, H. W.: Scale-Selective Verification of Rainfall Accumulations from High-Resolution Forecasts of Convective Events, Mon. Weather Rev., 136(1), 78–97, doi:10.1175/2007MWR2123.1, 2008.

Romine, G. S., Schwartz, C. S., Snyder, C., Anderson, J. L. and Weisman, M. L.: Model Bias in a Continuously Cycled Assimilation System and Its Influence on Convection-Permitting Forecasts, Mon. Weather Rev., 141(4), 1263–1284, doi:10.1175/MWR-D-12-00112.1, 2013.

Rostkier-edelstein, D., Kunin, P., Hopson, T. M. and Givati, A.: Statistical downscaling of seasonal precipitation in Israel, Int. J. Climatol., doi:10.1002/joc.4368, 2015.

Rostkier-Edelstein, D., Liu, Y., Wu, W., Kunin, P., Givati, A. and Ge, M.: Towards a high-resolution climatography of seasonal precipitation over Israel, Int. J. Climatol., 34(6), 1964–1979, doi:10.1002/joc.3814, 2014.

Rubin, S., Ziv, B. and Paldor, N.: Tropical Plumes over Eastern North Africa as a Source of Rain in the Middle East, Mon. Weather Rev., 135(12), 4135–4148, doi:10.1175/2007MWR1919.1, 2007.

Saaroni, H., Halfon, N., Ziv, B., Alpert, P. and Kutiel, H.: Links between the rainfall regime in Israel and location and intensity of Cyprus lows, Int. J. Climatol., 30(7), 1014–1025, doi:10.1002/joc.1912, 2010.

Saaroni, H., Ziv, B., Lempert, J., Gazit, Y. and Morin, E.: Prolonged dry spells in the Levant region: Climatologic-synoptic analysis, Int. J. Climatol., 2236(September 2014), 2223–2236, doi:10.1002/joc.4143, 2014.

Saltikoff, E., Friedrich, K., Soderholm, J., Lengfeld, K., Nelson, B., Becker, A., Hollmann, R., Urban, B., Heistermann, M. and Tassone, C.: An overview of using weather radar for climatological studies: Successes, challenges and potential., Bull. Am. Meteorol. Soc., doi:10.1175/bams-d-18-0166.1, 2019.

Samuels, R., Rimmer, A. and Alpert, P.: Effect of extreme rainfall events on the water resources of the Jordan River, J. Hydrol., 375(3–4), 513–523, doi:10.1016/j.jhydrol.2009.07.001, 2009.

Schär, C., Ban, N., Fischer, E. M., Rajczak, J., Schmidli, J., Frei, C., Giorgi, F., Karl, T. R., Kendon, E. J., Tank, A. M. G. K., O'Gorman, P. A., Sillmann, J., Zhang, X. and Zwiers, F. W.: Percentile indices for assessing changes in heavy precipitation events, Clim. Change, 137(1–2), 201–216, doi:10.1007/s10584-016-1669-2, 2016.

Schick, A. P.: Hydrologic aspects of floods in extreme arid environments, in Flood geomorphology, edited by V. R. Baker, R. C. Kochel, and P. C. Patton, pp. 189–203, John Wiley and Sons, New York., 1988.

Schwartz, C. S., Romine, G. S., Sobash, R. A., Fossell, K. R. and Weisman, M. L.: NCAR's Experimental Real-Time Convection-Allowing Ensemble Prediction System, Weather Forecast., 30(6), 1645–1654, doi:10.1175/WAF-D-15-0103.1, 2015.

Seager, R., Liu, H., Henderson, N., Simpson, I., Kelley, C., Shaw, T., Kushnir, Y. and Ting, M.: Causes of increasing aridification of the mediterranean region in response to rising greenhouse gases, J. Clim., 27(12), 4655–4676, doi:10.1175/JCLI-D-13-00446.1, 2014.

Sharon, D.: The spottiness of rainfall in a desert area, J. Hydrol., 17(3), 161–175, doi:10.1016/0022-1694(72)90002-9, 1972.

Sharon, D. and Kutiel, H.: The distribution of rainfall intensity in Israel, its regional and seasonal variations and its climatological evaluation, J. Climatol., 6(3), 277–291, doi:10.1002/joc.3370060304, 1986.

Skamarock, W. C., Klemp, J. B., Dudhia, J., Gill, D. O., Barker, D. M., Duda, M. G., Huang, X. Y., Wang, W. and Powers, J. G.: A Description of the Advanced Research WRF Version 3, , 113, doi:10.5065/D68S4MVH, 2008.

Smith, J. a., Baeck, M. L., Zhang, Y. and Doswell, C. a.: Extreme Rainfall and Flooding from Supercell Thunderstorms, J. Hydrometeorol., 2(5), 469–489, doi:10.1175/1525-7541(2001)002<0469:ERAFFS>2.0.CO;2, 2001.

Smith, J. A., Baeck, M. L., Villarini, G., Welty, C., Miller, A. J. and Krajewski, W. F.: Analyses of a long-term, high-resolution radar rainfall data set for the Baltimore metropolitan region, Water Resour. Res., 48(4), 1–14, doi:10.1029/2011WR010641, 2012.

Sowers, J., Vengosh, A. and Weinthal, E.: Climate change, water resources, and the politics of adaptation in the Middle East and North Africa, Clim. Change, 104(3–4), 599–627, doi:10.1007/s10584-010-9835-4, 2010.

Tarolli, P., Borga, M., Morin, E. and Delrieu, G.: Analysis of flash flood regimes in the North-Western and South-Eastern Mediterranean regions, Nat. Hazards Earth Syst. Sci., 12(5), 1255–1265, doi:10.5194/nhess-12-1255-2012, 2012.

Taylor, R. G., Todd, M. C., Kongola, L., Maurice, L., Nahozya, E., Sanga, H. and Macdonald, A. M.: Evidence of the dependence of groundwater resources on extreme rainfall in East Africa, Nat. Clim. Chang., 3(4), 374–378, doi:10.1038/nclimate1731, 2013.

Tewari, M., Chen, F., Wang, W., Dudhia, J., LeMone, M. A., Mitchell, K., Ek, M., Gayno, G., Wegiel, J. and Cuenca, R. H.: Implementation and verification of the unified NOAH land surface model in the WRF model (Formerly Paper Number 17.5), in 20th Conference on Weather Analysis and Forecasting/16th Conference on Numerical Weather Prediction, pp. 11–15., 2004.

Thompson, G., Field, P. R., Rasmussen, R. M. and Hall, W. D.: Explicit Forecasts of Winter Precipitation Using an Improved Bulk Microphysics Scheme. Part II: Implementation of a New Snow Parameterization, Mon. Weather Rev., 136(12), 5095–5115, doi:10.1175/2008MWR2387.1, 2008.

Thorndahl, S., Smith, J. A., Baeck, M. L. and Krajewski, W. F.: Analyses of the temporal and spatial structures of heavy rainfall from a catalog of high-resolution radar rainfall fields, Atmos. Res., 144, 111–125, doi:10.1016/j.atmosres.2014.03.013, 2014.

Tiedtke, M.: A Comprehensive Mass Flux Scheme for Cumulus Parameterization in Large-Scale Models, Mon. Weather Rev., 117(8), 1779–1800, doi:10.1175/1520-0493(1989)117<1779:ACMFSF>2.0.CO;2, 1989.

Trenberth, K. E., Dai, A., Rasmussen, R. M. and Parsons, D. B.: The changing character of precipitation, Bull. Am. Meteorol. Soc., 84(9), 1205-1217+1161, doi:10.1175/BAMS-84-9-1205, 2003.

Tubi, A., Dayan, U. and Lensky, I. M.: Moisture transport by tropical plumes over the Middle East: a 30-year climatology, Q. J. R. Meteorol. Soc., 143(709), 3165–3176, doi:10.1002/qj.3170, 2017.

UN-Habitat: Cities and Climate Change: Global Report on Human Settlements 2011, Earthscan, London & Washington, DC. [online] Available from: http://books.google.com/books?hl=en&lr=&id=GZG5x6SbeSAC&oi=fnd&pg=PA91&dq=Cities+and+Climate+Change&ots=adeiArrg6X&sig=9TeIo2HeRHPqS1KwBKsvkC78Afg (Accessed 3 January 2015), 2011.

Villarini, G., Mandapaka, P. V., Krajewski, W. F. and Moore, R. J.: Rainfall and sampling uncertainties: A rain gauge perspective, J. Geophys. Res. Atmos., 113(11), 1–12, doi:10.1029/2007JD009214, 2008.

Vincendon, B., Ducrocq, V., Nuissier, O. and Vié, B.: Perturbation of convection-permitting NWP forecasts for flash-flood ensemble forecasting, Nat. Hazards Earth Syst. Sci., 11(5), 1529–1544, doi:10.5194/nhess-11-1529-2011, 2011.

De Vries, A. J., Tyrlis, E., Edry, D., Krichak, S. O., Steil, B. and Lelieveld, J.: Extreme precipitation events in the Middle East: Dynamics of the Active Red Sea Trough, J. Geophys. Res. Atmos., 118(13), 7087–7108, doi:10.1002/jgrd.50569, 2013.

Warner, T. T.: Desert Meteorology, Cambridge University Press, New York., 2004.

Warner, T. T.: Numerical Weather and Climate Prediction., 2011.

Wernli, H., Paulat, M., Hagen, M. and Frei, C.: SAL—A Novel Quality Measure for the Verification of Quantitative Precipitation Forecasts, Mon. Weather Rev., 136(11), 4470–4487, doi:10.1175/2008MWR2415.1, 2008.

Wernli, H., Hofmann, C. and Zimmer, M.: Spatial Forecast Verification Methods Intercomparison Project: Application of the SAL Technique, Weather Forecast., 24(6), 1472–1484, doi:10.1175/2009WAF2222271.1, 2009.

Westra, S., Fowler, H. J., Evans, J. P., Alexander, L. V., Berg, P., Johnson, F., Kendon, E. J., Lenderink, G. and Roberts, N. M.: Future changes to the intensity and frequency of short-duration extreme rainfall, Rev. Geophys., 52, 522–555, doi:10.1002/2014RG000464, 2014.

Yang, L., Smith, J. A., Baeck, M. L., Bou-Zeid, E., Jessup, S. M., Tian, F. and Hu, H.: Impact of Urbanization on Heavy Convective Precipitation under Strong Large-Scale Forcing: A Case Study over the Milwaukee–Lake Michigan Region, J. Hydrometeorol., 15(1), 261–278, doi:10.1175/JHM-D-13-020.1, 2014.

Yano, J. I. I., Ziemian´ski, Mi. Z., Cullen, Mi., Termonia, Pi., Onvlee, J., Bengtsson, L., Carrassi, A., Davy, R., Deluca, A., Gray, S. L., Homar, V., Köhler, M. I., Krichak, S., Michaelides, S., Phillips, V. T. J., Soares, P. M. M. and Wyszogrodzki, A. A.: Scientific challenges of convective-scale numerical weather prediction, Bull. Am. Meteorol. Soc., 99(4), 699–710, doi:10.1175/BAMS-D-17-0125.1, 2018.

Zepeda-Arce, J., Foufoula-Georgiou, E. and Droegemeier, K. K.: Space-time rainfall organization and its role in validating quantitative precipitation forecasts, J. Geophys. Res. Atmos., 105(D8), 10129–10146, doi:10.1029/1999JD901087, 2000.

Zhang, C., Wang, Y. and Hamilton, K.: Improved Representation of Boundary Layer Clouds over the Southeast Pacific in ARW-WRF Using a Modified Tiedtke Cumulus Parameterization Scheme, Mon. Weather Rev., 139(11), 3489–3513, doi:10.1175/MWR-D-10-05091.1, 2011a.

Zhang, F., Bei, N., Rotunno, R., Snyder, C. and Epifanio, C. C.: Mesoscale Predictability of Moist Baroclinic Waves: Convection-Permitting Experiments and Multistage Error Growth Dynamics, J. Atmos. Sci., 64(10), 3579–3594, doi:10.1175/JAS4028.1, 2007.

Zhang, X., Alexander, L., Hegerl, G. C., Jones, P., Tank, A. K., Peterson, T. C., Trewin, B. and Zwiers, F. W.: Indices for monitoring changes in extremes based on daily temperature and precipitation data, Wiley Interdiscip. Rev. Clim. Chang., 2(6), 851–870, doi:10.1002/wcc.147, 2011b.

Zittis, G., Bruggeman, A., Camera, C., Hadjinicolaou, P. and Lelieveld, J.: The added value of convection permitting simulations of extreme precipitation events over the eastern Mediterranean, Atmos. Res., 191, 20–33, doi:10.1016/j.atmosres.2017.03.002, 2017.

Ziv, B., Harpaz, T., Saaroni, H. and Blender, R.: A new methodology for identifying daughter cyclogenesis: application for the Mediterranean Basin, Int. J. Climatol., n/a-n/a, doi:10.1002/joc.4250, 2015.

Zoccatelli, D., Marra, F., Armon, M., Rinat, Y., Smith, J. A. and Morin, E.: Contrasting rainfall-runoff characteristics of floods in Desert and Mediterranean basins, Hydrol. Earth Syst. Sci. Discuss., 12, 2665–2678, doi:https://doi.org/10.5194/hess-23-2665-2019, 2019.

12 Figures and tables

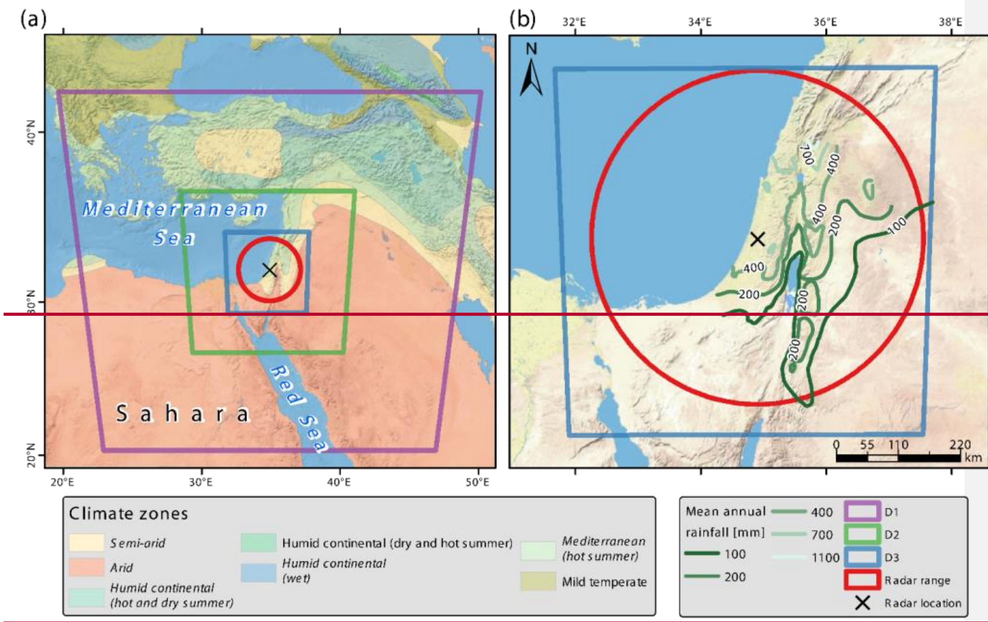

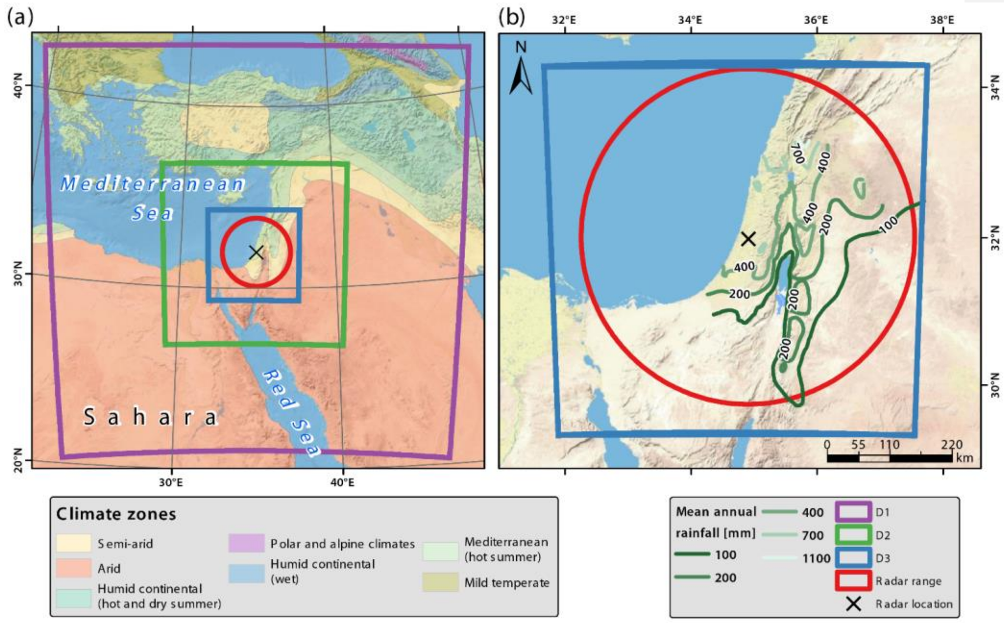

Figure ~~1:~~1: Study region. (a) ~~climate~~Climate zones in the eastern Mediterranean, three nested domains used in the weather model (D1-3; purple, green and blue) and the radar domain (red). (b) ~~mean~~Mean annual rainfall isohyets, radar and innermost model domains. Climatic classification is from the Atlas of Israel (2011)**. Basemap source: U.S. National Park Service.**

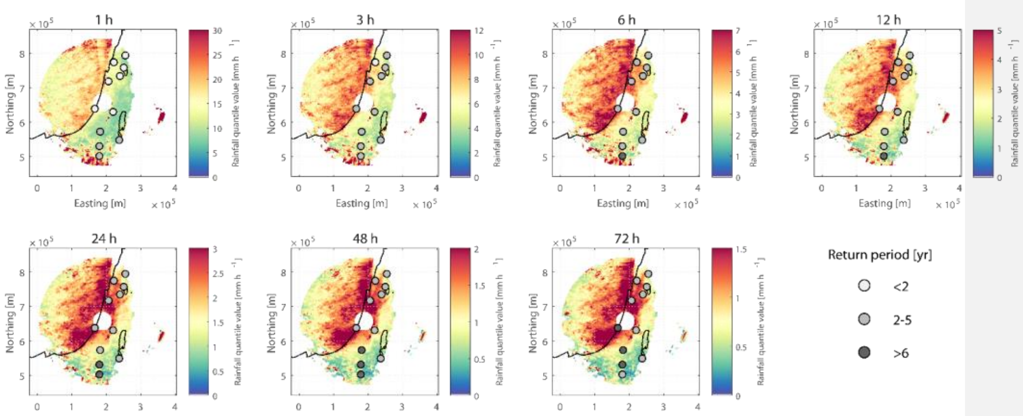

~~F~~igure ~~2:~~2: The 99.5% rain intensity quantile of each radar pixel for durations of 1 h (top-left) to 72 h (bottom-right). Notice change in colour scale between different durations. Also shown are annual return periods of the rain ~~-~~intensity threshold averaged over ~~nine~~9 pixels around 11 locations (generalised extreme value fit of the rain gauge annual maxima series, using the method of ~~the~~ probability ~~-~~weighted moments, with records of at least 44 ~~year~~ years). These computed annual return

periods range between 1.8 and 10.4 ~~yr.~~years. White areas found mostly to the east of the radar were masked out according to the black line in Fig. 6c (Sect. 4.2).

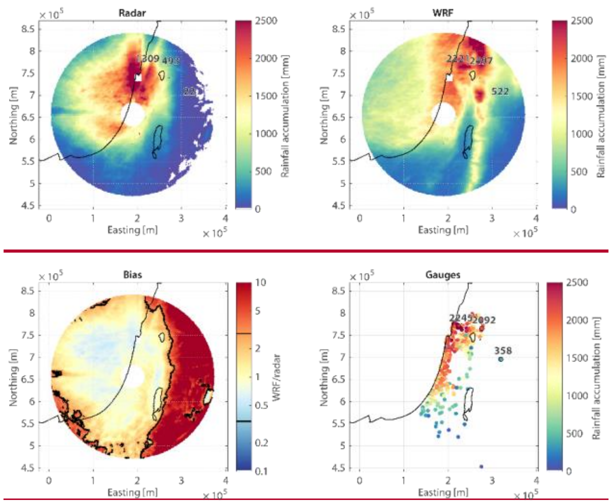

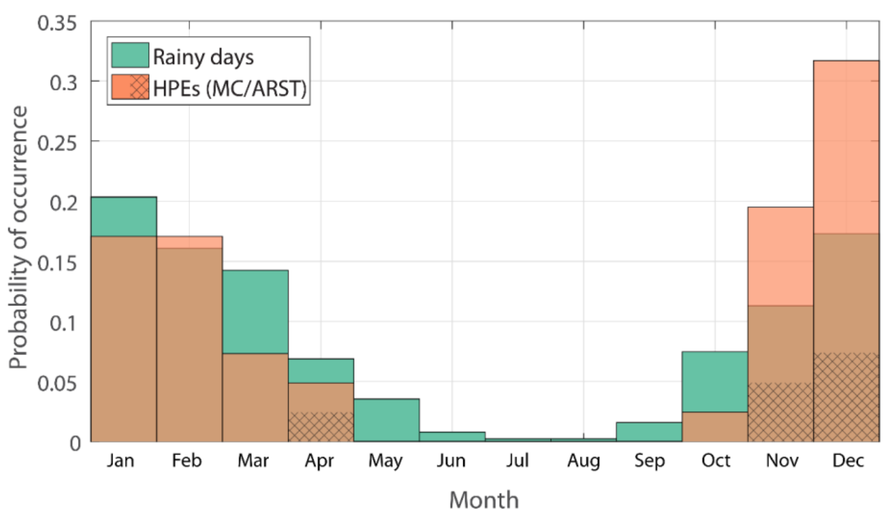

Figure 3: Monthly probability of occurrence of rainy days near the radar location (green; Bet Dagan rain gauge, 32.0°N, 34.8°E), and of HPEs from the radar archive (orange). Hatching represents HPEs classified as ARST.

Field Code Changed

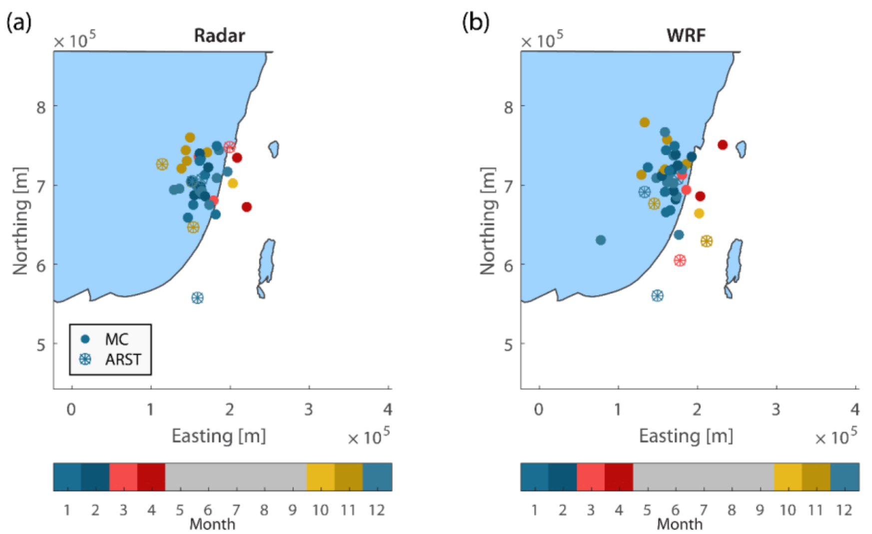

Figure 4: Centres of mass of cumulative rainfall of each of the HPEs derived from (a) radar QPE and (b) WRF. Colours represent month of occurrence. Synoptic classification according to Sect. 3.4.

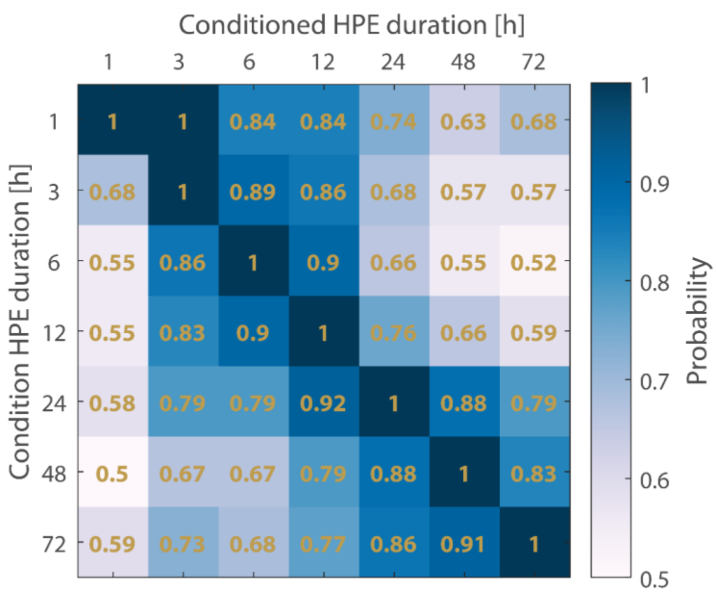

Figure 5: Probability of a HPE with a given duration listed on the x-axis conditioned on being a HPE with a duration listed on the y-axis.

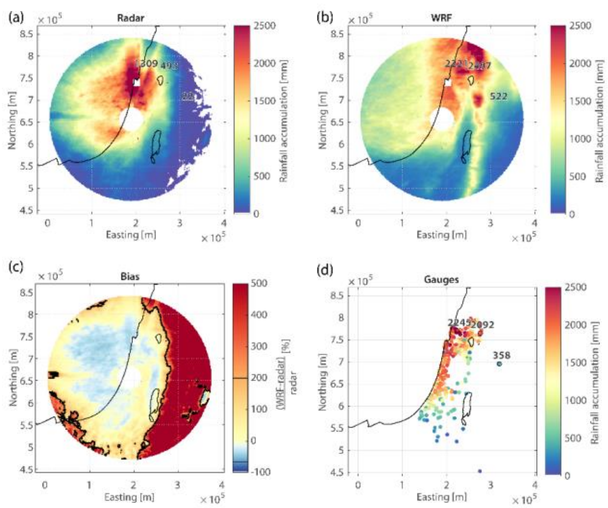

Figure 6: Total cumulative rainfall for all 41 HPEs, from (a) radar-derived QPE, (b) WRF-derived rainfall, and (d) daily rain gauges. (c) WRF~~-~~ to ~~-~~ radar rainfall accumulation ~~ratio (logarithmic colour scale).~~bias (normalised difference; Sect. 4.2). The ~~3~~200% and ~~1/3~~ -67% bias region is marked in black. Highlighted in (d) are total accumulations [mm] measured at three rain gauges from regions where radar~~-~~ QPE is considered to be inferior; corresponding radar and WRF, 9-pixel averaged values [mm] centred over the same locations, are shown in (a) and (b), respectively.

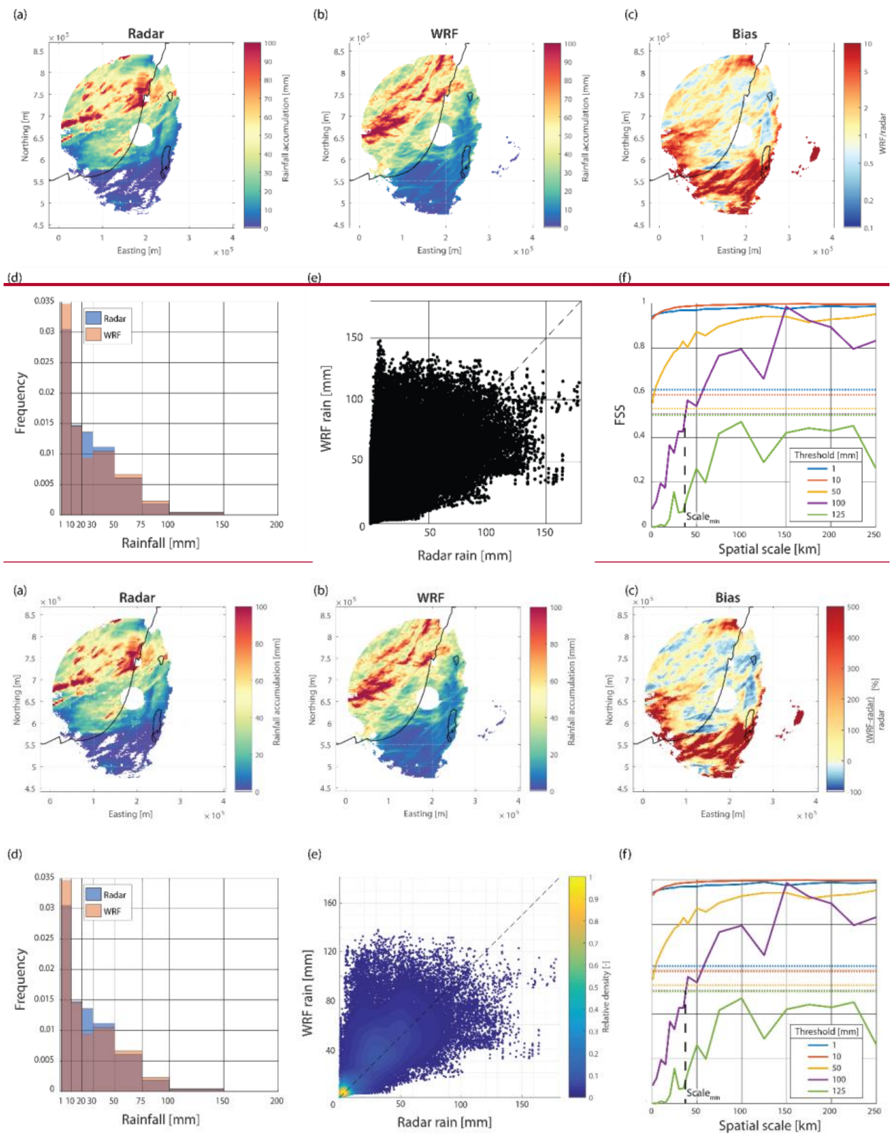

Figure ~~4:~~7: HPE #1 (02-Nov-1991 09:00 ~~-~~to 05-Nov-1991 09:00 [~~Local~~local winter time]; see Table S1). Cumulative rainfall from (a) radar-derived QPE, (b) WRF-derived rainfall, and their ratio (c; logarithmic colour scale). A pixel-based comparison between rainfall accumulations using a histogram (d; zero rainfall is omitted) and scatter plot (e). Notice that although rainfall distribution is quite well represented (d), results of a single pixel might deviate substantially from the 1:1 line (e; dashed). The fractions skill score (FSS) for the same event for various cumulative rainfall thresholds is presented in panel (f). Dashed lines are uniform FSS for the same rainfall thresholds. Also shown (dashed black line) is the minimal scale

for a valuable prediction for ~~a~~ 100 mm rain depth (at the crossing of the FSS and the uniform FSS; see details in supplementary material [S1]).

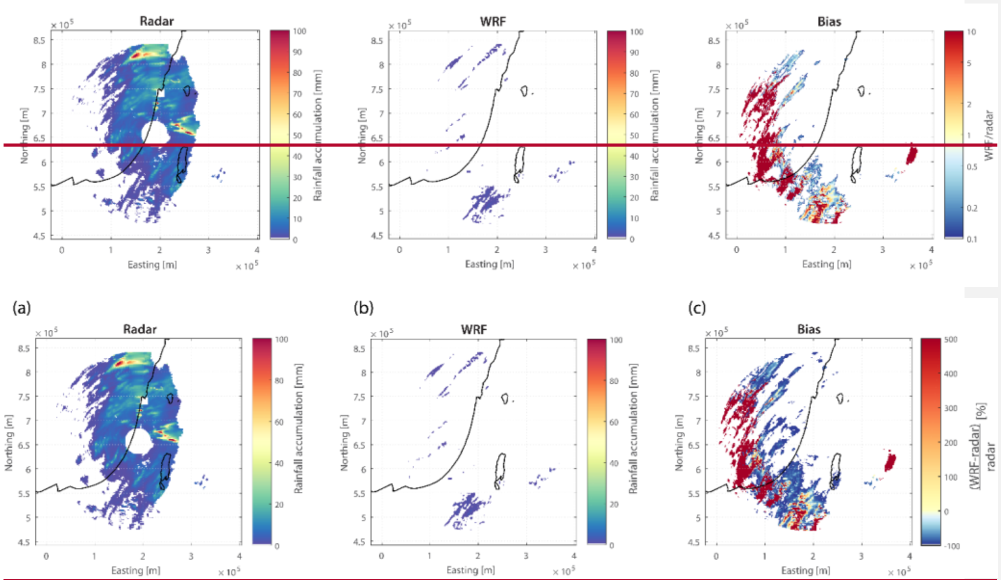

Figure ~~5:~~8: Same as Fig. ~~4 a~~7a-c~~,~~ for HPE #5 (31-Mar-1993 09:00 ~~-~~to 02-Apr-1993 02:00; Table S1).

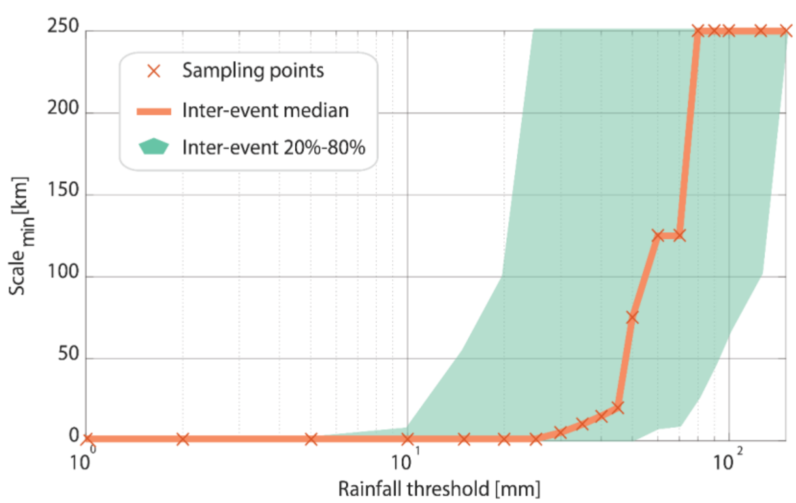

Figure ~~6:~~9: Minimal scale (see Fig. ~~4f~~7f and supplementary material [S1]) derived for all 41 events for various rainfall thresholds.

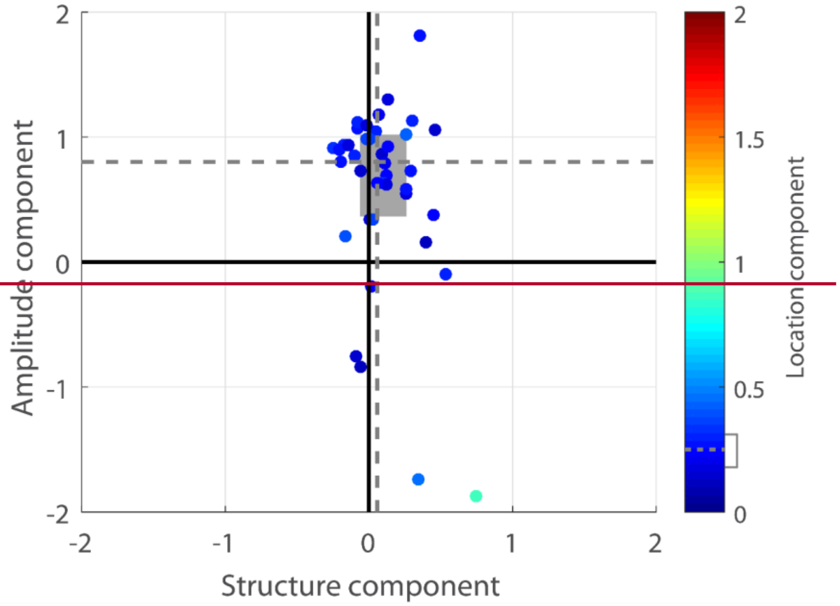

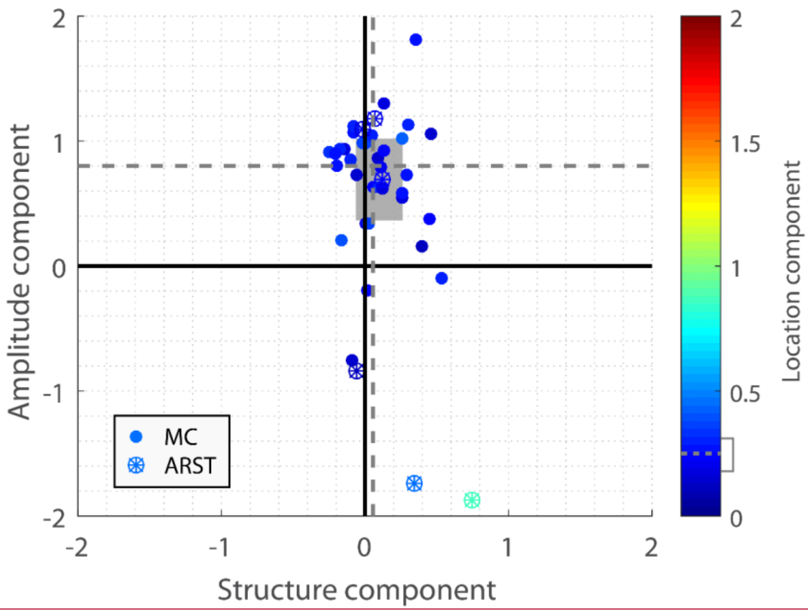

Figure ~~7:~~10: Structure-Amplitude-Location (SAL) analysis (Wernli et al., 2008). Each dot represents one event~~.~~ (classified according to Sect. 3.4). Dashed lines are median component values and the grey ~~rectangles represent~~rectangle represents the 25th – 75th percentile ranges. Location component median value is 0.25, and its 25th – 75th range is 0.18–0.31. More details are in the supplementary material (S2).

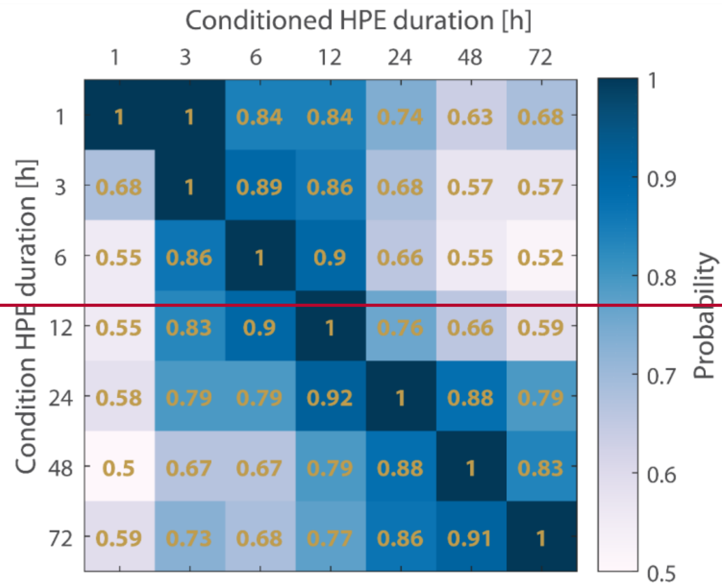

~~Figure 8: Probability of a HPE with a given duration listed on the x-axis conditioned on being a HPE with a duration listed on the y-axis.~~

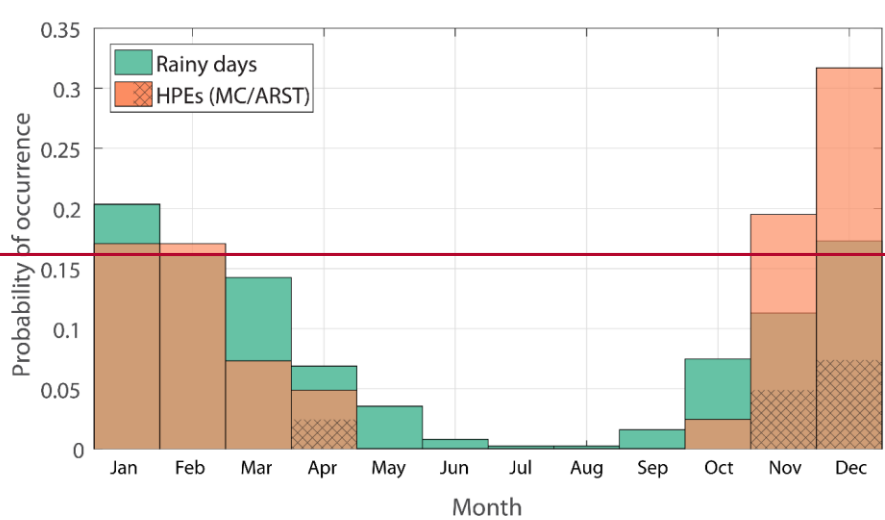

~~Figure 9: Monthly probability of occurrence of rainy days near the radar location (green; Bet-Dagan rain gauge, 32.0°N, 34.8°E), and of HPEs from the radar archive (orange). Hatching represents HPEs classified as ARST.~~

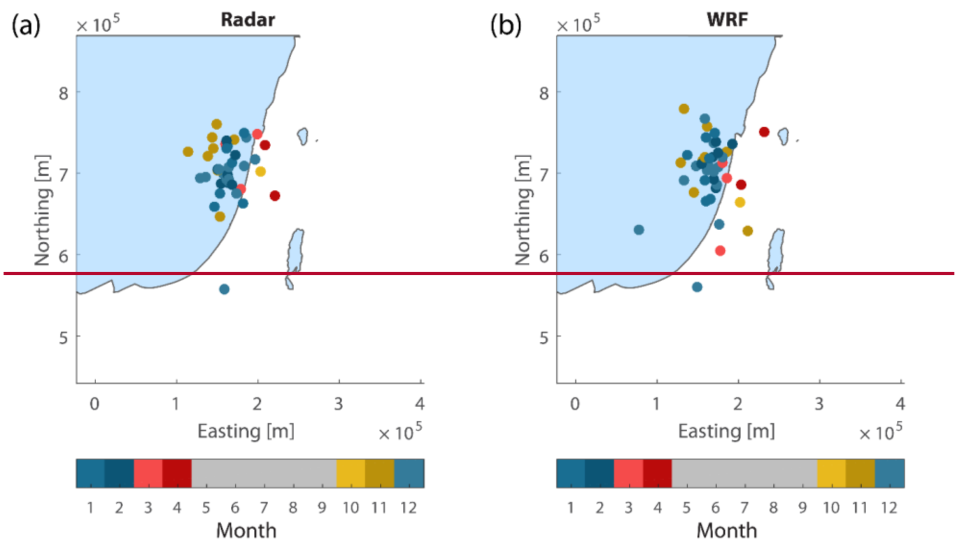

~~**Figure 10: Centres of mass of cumulative rainfall of all HPEs derived from (a) radar QPE and (b) WRF. Colours represent month of occurrence.**~~

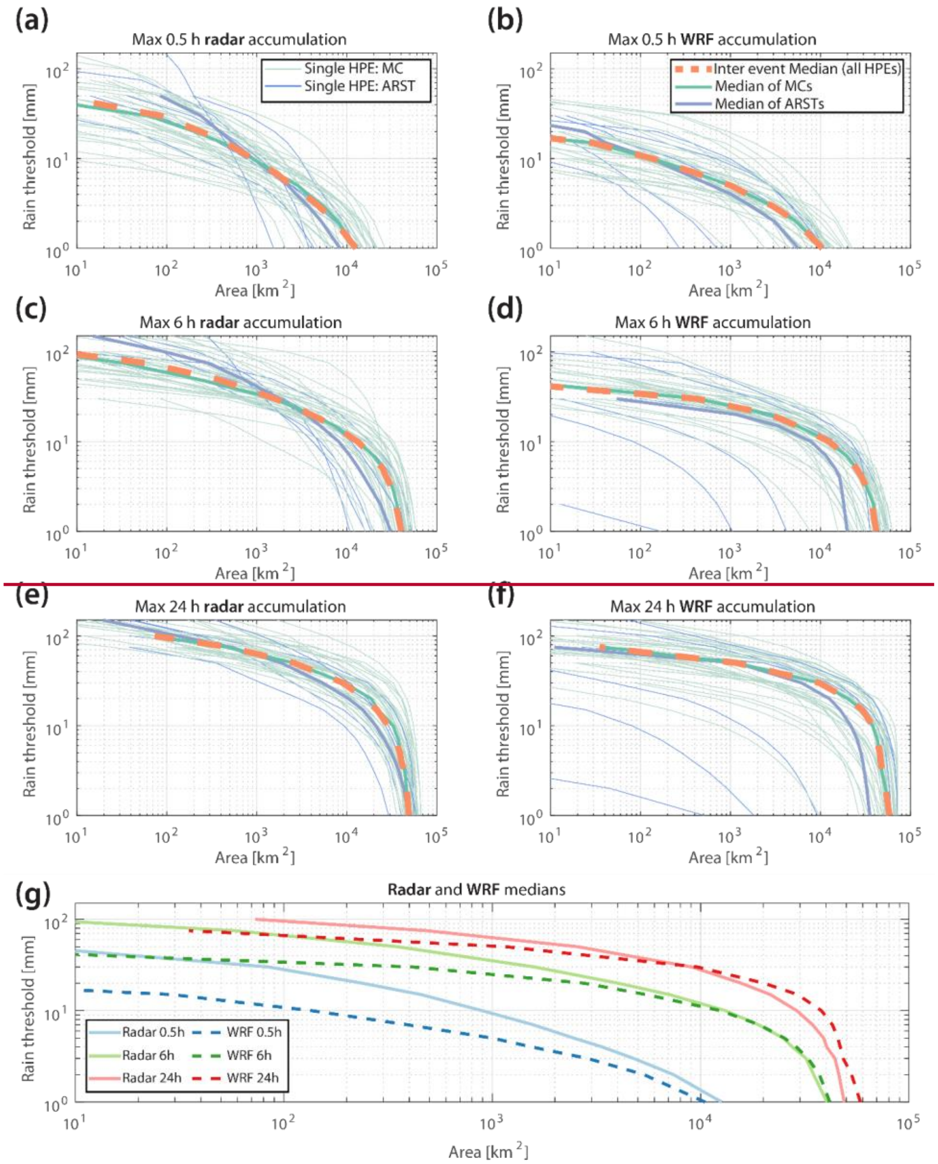
(a)
Max 0.5 h radar accumulation
Single HPE: MC
Single HPE: ARST
(b)
Max 0.5 h WRF accumulation
Inter event Median (all HPEs)
Median of MCs
Median of ARSTs
(c)
Max 6 h radar accumulation
(d)
Max 6 h WRF accumulation
(e)
Max 24 h radar accumulation
(f)
Max 24 h WRF accumulation
(g)
Radar and WRF medians
Radar 0.5h
WRF 0.5h
Radar 6h
WRF 6h
Radar 24h
WRF 24h
Rain threshold [mm]
Area [km 2]

~~Figure 11:~~

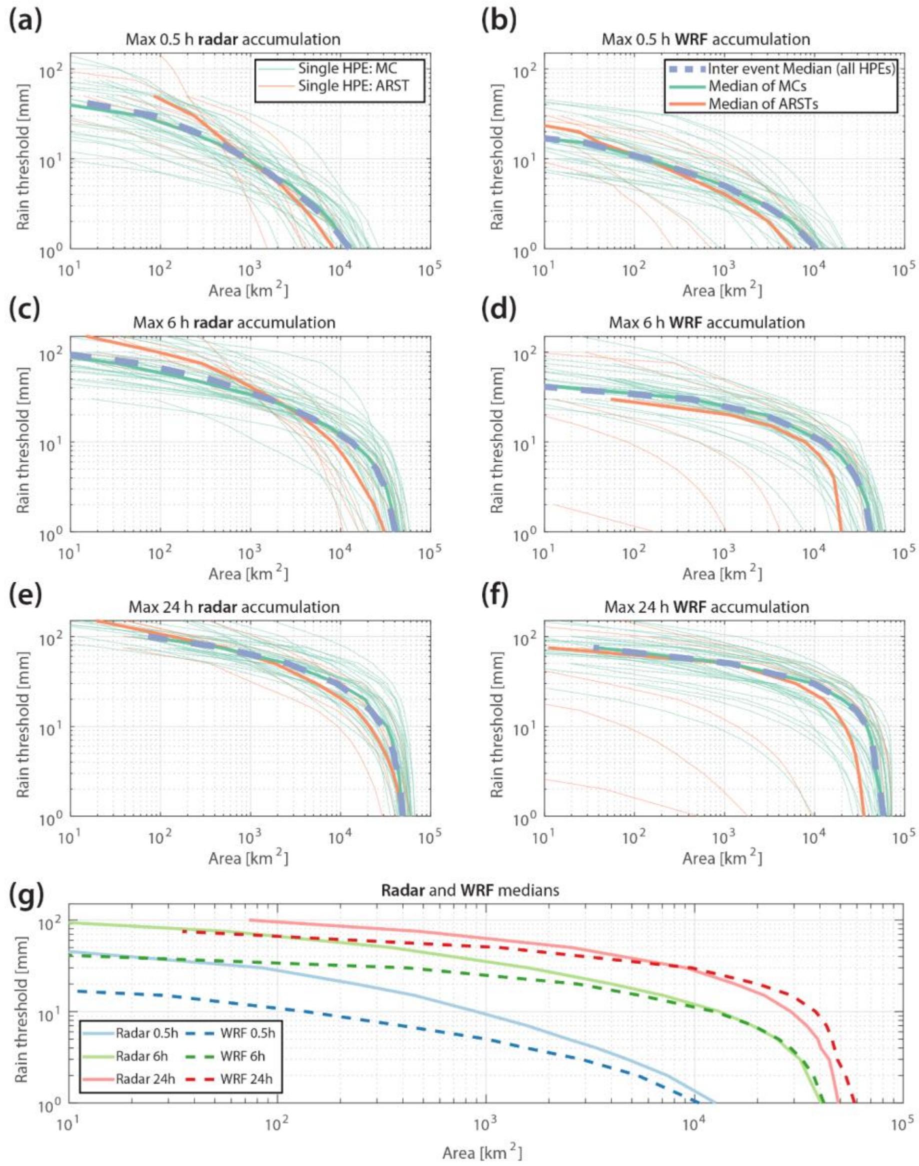

~~F~~Figure 11: Depth-Area-Duration (DAD) curves showing the maximal amount of rainfall as a function of area, derived from the radar QPE (left; a, c and e) and from the WRF model (right; b, d and f) for 0.5 h (top), 6 h (middle) and 24 h (bottom). Green and ~~purple~~orange lines represent HPEs classified as MCs and ARSTs, respectively. Thick lines represent the inter-event median. This median is compared between radar-QPE and WRF rainfall in panel g.

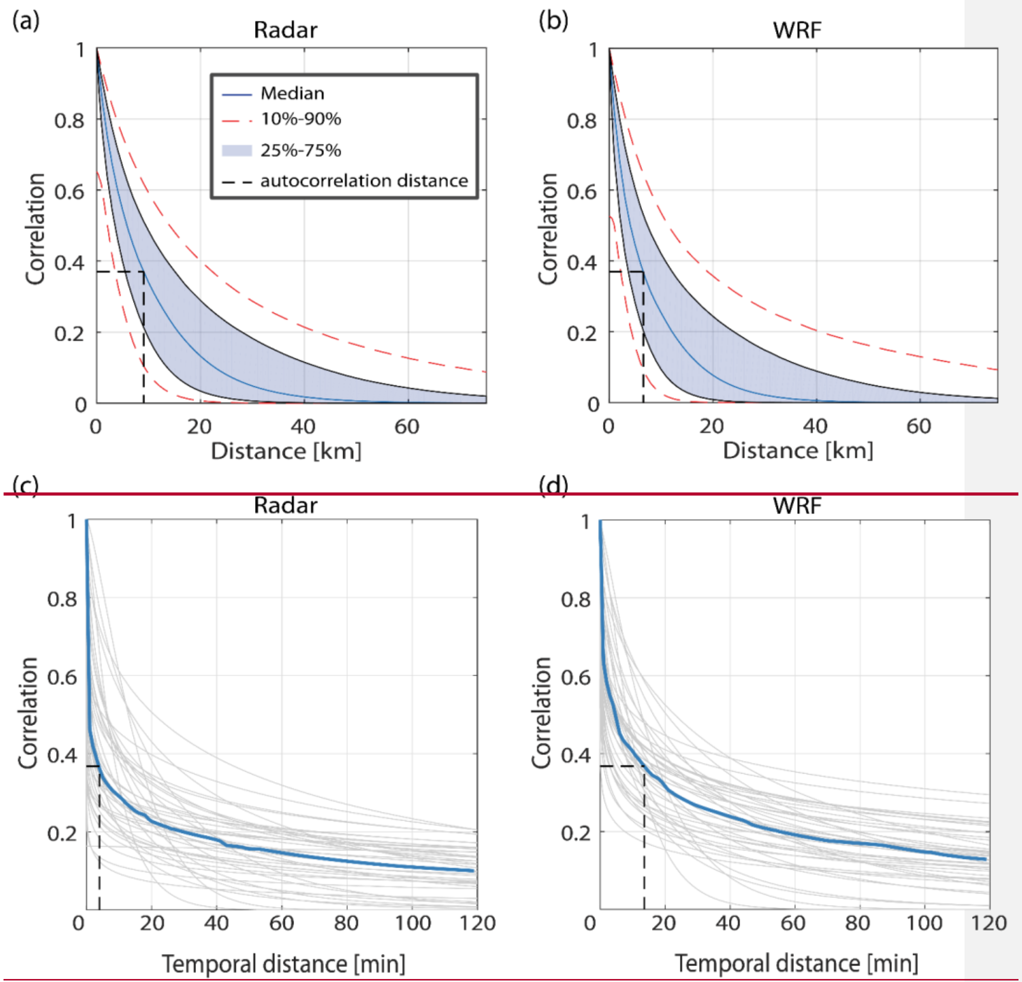

(a)
Radar
Median
10%-90%
25%-75%
autocorrelation distance
Correlation
Distance [km]
(b)
WRF
Correlation
Distance [km]
(c)
Radar
Correlation
Temporal distance [min]
(d)
WRF
Correlation
Temporal distance [min]

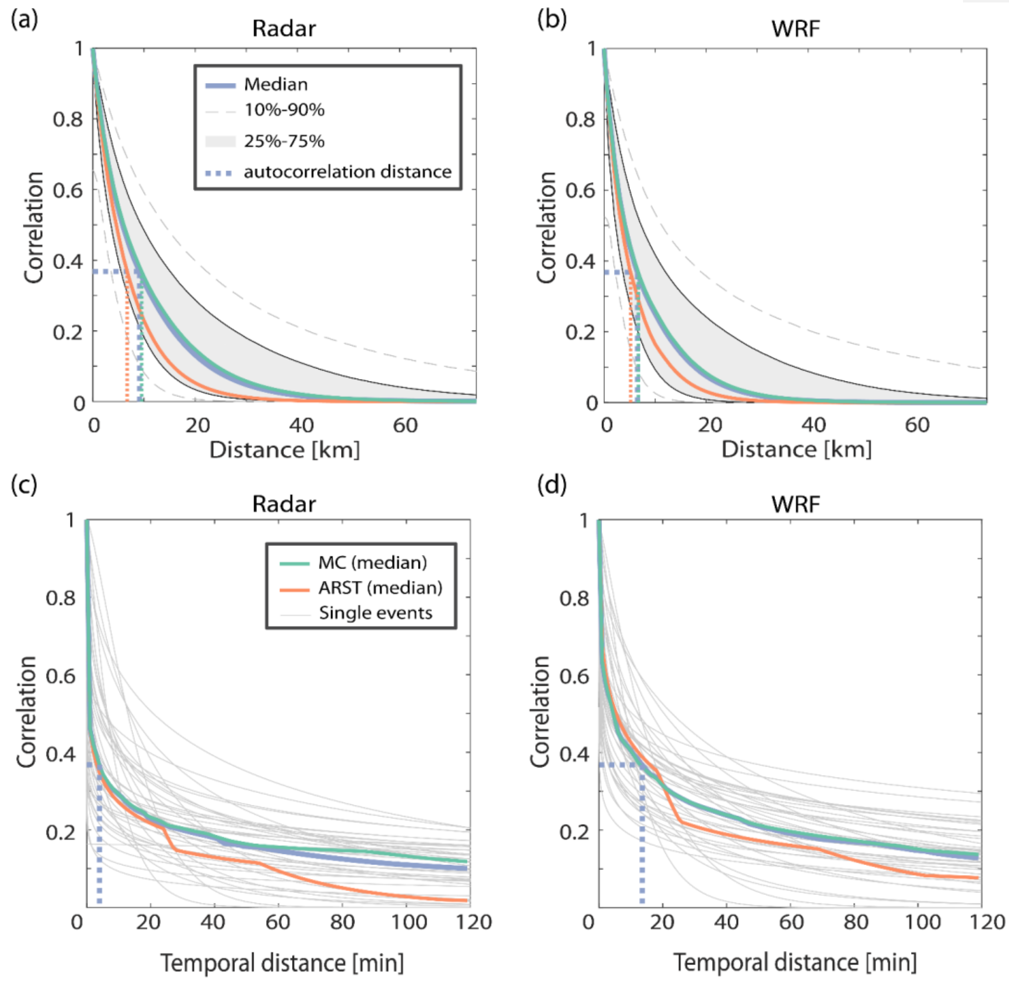

Figure ~~12:~~12: 1-D exponential fitting of rain field spatial (a, b) and temporal (c, d) autocorrelation values from radar-derived QPE (a, c) and from the WRF model (b, d). These were computed using 10~~-~~-min snapshots of rain and only for periods where convective rainfall is present. Quantiles in spatial autocorrelation (a, b) represent 11731 snapshots of radar 10~~-~~-min data~~,~~, (10,095 of which come from MC-type events), and ~~14323~~14,323 WRF rainfall snapshots~~.~~ (12,220 of which come from MC-type events). Temporal autocorrelation plots (c, d) are composed of the 41 examined HPEs (grey), and their median values ~~(blue~~for all events (purple), for MC-type only (green) and for ARST-type only (orange).

Formatted: Font: (Default) Times New Roman, 9 pt, Bold, Complex Script Font: Times New Roman, 9 pt, Bold, English (United Kingdom)

	Outer nest	Middle nest	Inner nest
Domains			
Spatial resolution [km]	2~~5X25~~25 x 25	5~~X5~~5 x 5	1~~X1~~1 x 1

Temporal resolution [s]	~100	~20	4-8
Domain size [pixels]	1~~00X100~~100 x 100	2~~21X221~~221 x 221	5~~51X551~~551 x 551
Number of vertical layers	68	68	68
Model top [hPa]	25	25	25
Physics			
Cumulus scheme	~~Tiedtke (Tiedtke, 1989; Zhang et al., 2011a)~~Tiedtke (Tiedtke, 1989; Zhang et al., 2011a)		-
Microphysical scheme	Thompson (Thompson et al., 2008)		
Radiative transfer scheme	RRTMG Shortwave and Longwave (Iacono et al., 2008)		
Planetary boundary layer scheme	Mellor–Yamada– Janjić (Janjić, 1994)		
Surface layer scheme	Eta Similarity Scheme (Janjić, 1994)		
Land surface model	Unified Noah Land Surface (Tewari et al., 2004)		

Table 1: WRF ~~Model~~model settings and specifications

Supplementary material

S1. ~~FSS~~Fractions Skill Score (FSS) statistic

The fractions skill score ~~(FSS; Roberts and Lean, 2008)~~(FSS; Roberts and Lean, 2008) statistic is defined for each rainfall threshold (q) using a binary field (I) that equals 1 wherever pixel values are $\geq q$, and 0 elsewhere. Thus, the fraction of radar-derived (observed) pixels for a given rainfall threshold over a given ~~neighborhood~~neighbourhood length n (i.e.~~,~~ spatial averaging~~)~~), termed O_n, and the similar modelled fraction derived from the Weather Research and Forecasting (WRF) model (M_n~~) is~~), are used to calculate the mean square error (MSE) as follows:

(Eq. S1) $MSE_n \equiv \overline{(O_n - M_n)^2}$,

where the overbar denotes averaging. The MSE is then used to calculate the FSS:

(Eq. S2) $FSS_n \equiv \frac{MSE_n - MSE_{(n)ref}}{MSE_{(n)perfect} - MSE_{(n)ref}} = 1 - \frac{MSE_n}{MSE_{(n)ref}}$,

where $MSE_{(n)perfect} \equiv 0$ is the MSE of a perfect forecast, and $MSE_{(n)ref} \equiv \overline{O_n^2} + \overline{M_n^2}$.

The uniform FSS is defined as ~~half of the way~~halfway between a random forecast and a perfect skill forecast:

(Eq. S3) $FSS_{(n)uniform} \equiv \frac{1+f_{(n)O}}{2}$,

where f_O is the observed frequency~~. I~~, i.e.~~,~~ the fraction of observed pixels exceeding the threshold over the entire domain using a ~~neighborhood~~neighbourhood length of size n.

S2. ~~SAL~~Structure–amplitude–location (SAL) analysis

~~The structure-amplitude-location analysis (SAL; Wernli et al., 2008) shown in the text also requires setting up a rainfall threshold (f) that enables a distinction between precipitation objects that are greater than this threshold. Following is a summary of the calculation of each of the three components of SAL:~~

The structure-amplitude-location analysis (SAL; Wernli et al., 2008) shown in the text also requires setting up a rainfall threshold (f) that enables distinguishing precipitation objects that are greater than this threshold. Following is a summary of the calculation of each of the three components of SAL.

A-component (amplitude):

(Eq. S4) $A = \frac{\overline{R_M} - \overline{R_O}}{\frac{1}{2}(\overline{R_M} + \overline{R_O})}$,

~~Where~~where R is the rainfall accumulation field and M and O denote modelled (WRF) and observed (radar) rain, respectively, and $A \in [-2,2]$.

The L-component (location) is ~~a~~the sum of two components. The first one (L_1) is a normalised measure of the distance between the ~~center~~centre of mass of the ~~modeled~~modelled and observed rain fields, and

Formatted
Formatted: English (United Kingdom)
Formatted
Formatted
Formatted
Formatted
Formatted
Formatted: English (United Kingdom)
Formatted
Formatted
Formatted
Formatted: English (United Kingdom)
Formatted
Formatted
Formatted
Formatted
Formatted: English (United Kingdom)
Formatted
Formatted
Formatted

the second (L_2) considers the average distance between the ~~center~~centre of mass of the total precipitation fields and individual precipitation objects within them, as follows:

(Eq. S5) $L_1 = \frac{|x_M - x_O|}{d}$,

where x denotes the ~~center~~centre of mass of a rain field and d is the largest possible ~~geographic~~geographical distance along the considered domain.

The second location component (L_2) ~~wheights~~weights each precipitation object using its total amount of rain (R_n) ~~using~~and a weighted average distance~~:~~ (r):

(Eq. S6) $r = \frac{\sum_{n=1}^{M} R_n |x - x_n|}{\sum_{n=1}^{M} R_n}$,

where n is an index of precipitation objects ranging from 1 to the number of objects existing (M). L_2 is computed through the difference between the modelled distance (r_M) and the observed one (r_O), calculated according to ~~eq. A7~~Eq. S7, for the modelled and observed precipitation objects, respectively.

(Eq. S7) $L_2 = 2\left(\frac{|r_M - r_O|}{d}\right)$

Finally, the L-component is simply the sum of L_1 and L_2:

(Eq. S8) $L = L_1 + L_2$

where $L \in [0,2]$.

The S-component (structure) is calculated through a scaled volume of each precipitation object (V_n):

(Eq. S9) $V_n = \frac{R_n}{R_n^{max}}$,

where R_n^{max} is the maximum rainfall value of the precipitation object n. The weighted mean of the scaled volume is ~~calculted~~calculated through:

(Eq. S10) $V = \frac{\sum_{n=1}^{M} R_n V_n}{\sum_{n=1}^{M} R_n}$,

~~Which~~which is then used to calculate the S-component:

(Eq. S11) $S = \frac{V_M - V_O}{\frac{1}{2}(V_M + V_O)}$,

where V_M and V_O represent the scaled volume calculated using the modelled and observed rain fields, respectively, and $S \in [-2,2]$.

S3. Heavy precipitation events (HPEs) identified and analysed

Table S1 – HPEs identified and analysed in this study

HPE #	Start time*	End time*	Synoptic classification#	HPE duration [h]						
				1	3	6	12	24	48	72

1	2-11-1991 9:00	5-11-1991 9:00	MC	X	X	X	X	X	X	X
2	22-2-1992 8:00	27-2-1992 21:00	MC						X	X
3	23-11-1992 9:00	26-11-1992 7:00	MC	X	X	X	X			
4	12-12-1992 14:00	18-12-1992 13:00	MC	X	X	X	X	X	X	X
5	31-3-1993 9:00	2-4-1993 2:00	ARST			X				
6	21-12-1993 12:00	23-12-1993 15:00	ARST						X	
7	21-2-1994 19:00	25-2-1994 0:00	MC		X	X	X			
8	1-11-1994 15:00	7-11-1994 13:00	ARST	X	X	X	X	X	X	X
9	14-11-1994 1:00	18-11-1994 5:00	MC	X	X	X	X	X	X	X
10	15-12-1994 12:00	20-12-1994 21:00	MC	X	X			X	X	X
11	28-12-1994 10:00	31-12-1994 23:00	MC			X				
12	4-2-1995 8:00	9-2-1995 10:00	MC					X	X	X
13	1-11-1995 11:00	3-11-1995 14:00	MC	X	X					
14	7-11-1995 10:00	10-11-1995 17:00	MC							X
15	6-3-1996 13:00	8-3-1996 4:00	MC		X	X	X	X	X	
16	11-12-1996 14:00	14-12-1996 15:00	ARST	X	X	X	X	X	X	X
17	13-1-1997 11:00	17-1-1997 7:00	MC	X	X	X	X	X	X	X
18	3-3-1997 6:00	4-3-1997 16:00	MC	X	X	X	X			
19	19-10-1997 11:00	20-10-1997 10:00	MC		X	X	X			
20	25-11-1997 10:00	27-11-1997 9:00	ARST		X	X	X	X		
21	4-4-1998 4:00	4-4-1998 17:00	MC			X	X			
22	28-12-1998 6:00	31-12-1998 21:00	MC							
23	13-12-1999 6:00	15-12-1999 8:00	MC	X	X	X	X			
24	18-1-2000 6:00	24-1-2000 2:00	MC		X	X	X	X	X	X
25	25-1-2000 15:00	28-1-2000 20:00	MC	X	X	X	X	X	X	X
26	12-2-2000 22:00	16-2-2000 16:00	MC	X	X	X	X	X	X	X
27	29-11-2000 0:00	1-12-2000 10:00	MC				X	X	X	X
28	19-12-2000 6:00	21-12-2000 17:00	MC	X	X					
29	30-4-2001 9:00	2-5-2001 17:00	MC	X	X	X	X	X	X	X
30	9-12-2002 6:00	12-12-2002 6:00	MC		X	X	X	X	X	X
31	2-1-2003 16:00	4-1-2003 12:00	MC		X	X				
32	27-1-2003 10:00	30-1-2003 13:00	MC	X	X	X	X	X		X
33	3-2-2003 0:00	5-2-2003 16:00	MC				X	X	X	
34	17-2-2003 19:00	22-2-2003 23:00	MC						X	X
35	24-2-2003 1:00	28-2-2003 2:00	MC				X	X	X	X
36	1-12-2003 14:00	5-12-2003 20:00	ARST	X	X	X	X	X	X	X
37	14-12-2003 16:00	15-12-2003 10:00	MC	X	X	X	X	X		
38	15-12-2005 15:00	18-12-2005 9:00	MC		X	X	X			
39	18-12-2007 14:00	21-12-2007 8:00	MC			X	X	X	X	
40	2-1-2008 3:00	5-1-2008 19:00	MC		X	X	X	X	X	X

Formatted
Formatted
Formatted
Formatted
Formatted
Formatted
Formatted
Formatted
Formatted
Formatted
Formatted
Formatted
Formatted
Formatted
Formatted
Formatted
Formatted
Formatted
Formatted
Formatted
Formatted
Formatted
Formatted
Formatted
Formatted
Formatted
Formatted
Formatted
Formatted
Formatted
Formatted
Formatted
Formatted
Formatted
Formatted
Formatted
Formatted
Formatted
Formatted
Formatted

41	17-1-2010 16:00	22-1-2010 6:00	MC	X	X	X	X	X	X	X

*Local winter time (UTC+2~~).~~), presented as day-month-year and hour.

#Simplified synoptic classification (Sect. 3.4 in the main text).

S4. WRF namelist.input file example

```
&time_control
 run_days                 = 0,
 run_hours                = 138,
 run_minutes              = 0,
 run_seconds              = 0,
 start_year               = 2010, 2010, 2010,
 start_month              = 01,   01,   01,
 start_day                = 16,   16,   16,
 start_hour               = 12,   12,   12,
 start_minute             = 00,   00,   00,
 start_second             = 00,   00,   00,
 end_year                 = 2010, 2010, 2010,
 end_month                = 01,   01,   01,
 end_day                  = 22,   22,   22,
 end_hour                 = 06,   06,   06,
 end_minute               = 00,   00,   00,
 end_second               = 00,   00,   00,
 interval_seconds         = 21600
 input_from_file          = .true.,.true.,.true.,
 history_interval         = 360,  180,   10,
 frames_per_outfile       = 1, 1, 1,
 restart                  = .false.,
 restart_interval         = 1440,
 io_form_history          = 2,
 io_form_restart          = 2,
```

Formatted: English (United Kingdom)

Formatted: English (United Kingdom)

Formatted: English (United Kingdom)

```
 io_form_input = 2,
 io_form_boundary = 2,
 debug_level = 0,
iofields_filename = “varsNot2Use_d01.txt”, “varsNot2Use_d02.txt”, "varsNot2Use_d03.txt",
ignore_iofields_warning = .true.,
 /
 &domains
 time_step = 8,
 time_step_fract_num = 0,
 time_step_fract_den = 1,
use_adaptive_time_step = .true.,
 step_to_output_time = .true.,
 target_cfl = 1.2, 1.2,1.2,
 target_hcfl = .84, .84,0.84,
 max_step_increase_pct = 5, 51,51,
 starting_time_step = -1, -1,-1,
 max_time_step = -1, -1,-1,
 min_time_step = -1, -1,-1,
 adaptation_domain = 1,
 max_dom = 3,
 e_we = 100, 221, 551,
 e_sn = 100, 221, 551,
 e_vert = 68, 68, 68,
 p_top_requested = 2500,
 num_metgrid_levels = 61,
 num_metgrid_soil_levels = 4,
 dx = 25000, 5000, 1000,
 dy = 25000, 5000, 1000,
 grid_id = 1, 2, 3,
```

parent_id = 0, 1, 2,

i_parent_start = 1, 28, 55,

j_parent_start = 1, 28, 55,

parent_grid_ratio = 1, 5, 5,

parent_time_step_ratio = 1, 5, 5,

feedback = 1,

smooth_option = 0,

/

&physics

mp_physics = 8, 8, 8,

cu_physics = 6, 6, 0,

ra_lw_physics = 4, 4, 4,

ra_sw_physics = 4, 4, 4,

bl_pbl_physics = 2, 2, 2,

sf_sfclay_physics = 2, 2, 2,

sf_surface_physics = 2, 2, 2,

radt = 15, 15, 15,

bldt = 0, 0, 0,

cudt = 2, 2, 2,

icloud = 1,

isfflx = 1,

ifsnow = 1,

num_soil_layers = 4,

num_land_cat = 21,

sf_urban_physics = 0, 0, 0,

surface_input_source = 1,

/

```
 &fdda
 /

 &dynamics
 w_damping                  = 1,
 diff_opt                   = 1,      1,      1,
 km_opt                     = 4,      4,      4,
 diff_6th_opt               = 0,      0,      0,
 diff_6th_factor            = 0.12,   0.12,   0.12,
 base_temp                  = 290.
 damp_opt                   = 3,
 zdamp                      = 5000.,  5000.,  5000.,
 dampcoef                   = 0.2,    0.2,    0.2
 khdif                      = 0,      0,      0,
 kvdif                      = 0,      0,      0,
 epssm                      = 0.2,    0.2,    0.2,
 non_hydrostatic            = .true., .true., .true.,
 moist_adv_opt              = 1,      1,      1,
 scalar_adv_opt             = 1,      1,      1,
 gwd_opt                    = 1,
 /

 &bdy_control
 spec_bdy_width             = 5,
 spec_zone                  = 1,
 relax_zone                 = 4,
 specified                  = .true., .false.,.false.,
 nested                     = .false., .true., .true.,
 /
```

&grib2

/

&namelist_quilt

nio_tasks_per_group = 0,

nio_groups = 1,

/

S5. Figures

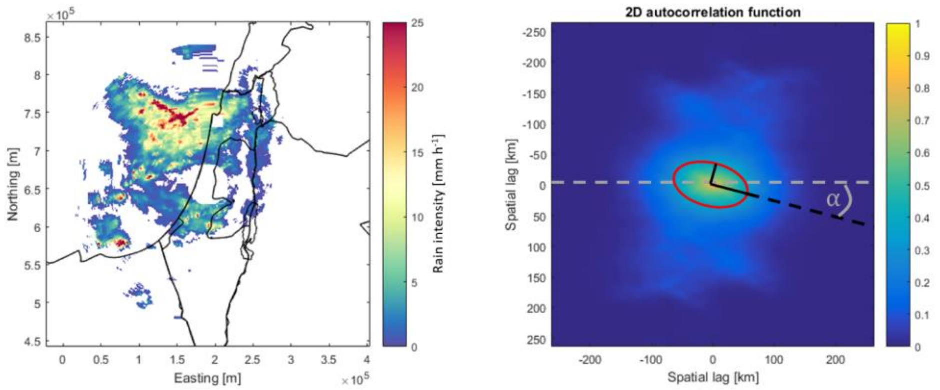

Supplementary Figure 1: An example of the spatial autocorrelation analysis (Sects. 3.5.4, 4.4.2 in the main text). The left panel shows a 10-min rainfall map based on radar data from HPE #1. The right panel shows the 2-D autocorrelation field of the same map. The red ellipse represents the approximate e^{-1} correlation region and its axes are in black. Deviation of the major axes from the east-west axis (grey) is denoted α. The short-to-long axis ratio defines the ellipticity of the autocorrelation field.

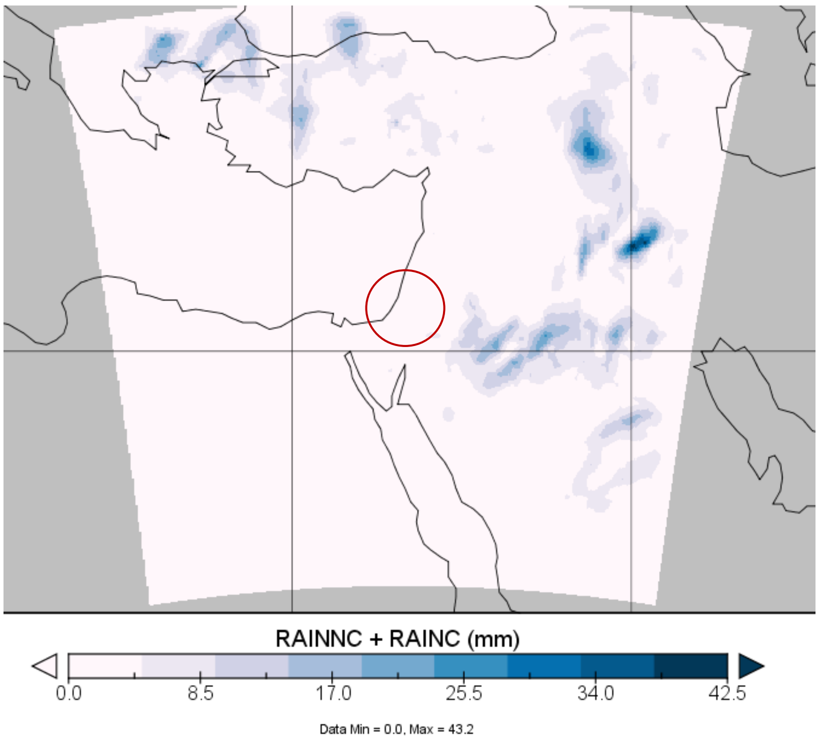

Supplementary Figure 2: Accumulated precipitation (convective [RAINC] + non-convective [RAINNC] rainfall) in the coarsest WRF domain during HPE #5 (Table S1) and the approximate range of the Shacham radar (Fig. 1 in the main text). Notice the absence of rainfall within the radar range, as opposed to the radar QPE (Fig. 8a in the main text).

Formatted: Font: Cambria, 10 pt, Font color: Accent 5, English (United Kingdom)

Formatted: English (United Kingdom)